TECTONIC EVOLUTION OF THE EASTERN YUKON-TANANA UPLAND, EAST-CENTRAL ALASKA

A thesis presented to the faculty
of the State University of New York
at Albany
in partial fulfillment of the requirements
for the degree of
Master of science

School of Arts and Sciences
Department of Earth Sciences

Grant W. Cushing
1984

THE TECTONIC EVOLUTION
OF THE
EASTERN YUKON TANANA UPLAND, ALASKA

Abstract of
a thesis presented to the Faculty
of the State University of New York
at Albany
in partial fulfillment of the requirements
for the degree of
Master of Science

College of Science and Mathematics
Department of Geological Science

Grant Cushing
1984

THE TECTONIC EVOLUTION OF THE EASTERN YUKON TANANA UPLAND, ALASKA

Grant Cushing

Field, structural, and isotopic studies in the southeastern Eagle Quadrangle reveal a complex Mesozoic history involving major metamorphism, fold development, thrusting, and igneous intrusion. These events may be related to the accretion of a terrane, possibly Stikine, to the North American continental margin.

$^{40}Ar/^{39}Ar$ incremental heating experiments on metamorphic minerals from amphibolite facies rocks reveal Late Triassic to Middle Jurassic plateau ages interpreted as the age of major metamorphism. Large scale northeast trending folds within these rocks formed after the major metamorphism and before the intrusion of an undeformed, unmetamorphased cross-cutting dike in Middle Jurassic. These folds probably developed in response to northwest-southeast compression related to terrane accretion.

A major thrust system which separates the amphibolite facies metamorphic rocks on the south from lower grade rocks to the north is characterized by complex thrust melanges, distinct faults, and shear zones between and within the two groups of rocks. There are distinct differences in the structural character of rocks on either side of this fault zone as indicated by differences in fold style and orientation of major fold generations. Thrusting involved ophiolitic material as suggested by the presence of serpentinized ultramafic rocks and silica-carbonate rocks within the thrust zone. $^{40}Ar/^{39}Ar$ data from a sample within the fault zone indicates that thrusting occurred after major metamorphism and before 187 $\pm$ 2 Ma.

$^{40}Ar/^{39}Ar$ data also show that a major batholith (Taylor Mountain) within the southern terrane was intruded just after the peak of metamorphism at about 207 $\pm$ 2 Ma and cooled at an average rate of $10^{o}C\ Ma^{-1}$ with the metamorphic rocks.

The Taylor Mountain batholith may be related to the Klotassin suite of northwestern Canada and the metamorphic terrane may be the extension of the Stikine block into east-central Alaska.

ACKNOWLEDGEMENTS

I would like to thank Drs. Helen Foster, Mark Harrison, William Kidd, Winthrop Means, Jo Laird, and Steve Delong for their guidance and their support of my research efforts for this thesis.

I am also grateful to my wife, Regina Sarkis Cushing, for her assistance in the production of this thesis, and for the support she provided with love and unyielding faith and patience throughout the process.

Grant Cushing

TABLE OF CONTENTS

GENERAL STATEMENT

Since J. Tuzo Wilson first suggested a complex tectonic evolution for the Circum-Pacific region, geologists have gained significant insight into the fundamental processes of orogeny throughout the North American Cordillera. Recent tectonic synthesis (Coney and others, 1980) and a strengthened geologic data base strongly support the concept that much of the northern Cordillera is made up of a collage of allochthonous geological provinces that were accreted to the North American cratonic margin since Paleozoic time. This hypothesis is well supported by evidence obtained from paleontological, stratigraphic, and paleomagnetic approaches, yet little is understood about the thermal, chronologic and structural character of this accretionary process. In this study, the latter questions are addressed for a field area in east-central Alaska. The study area is located in the Eagle quadrangle of the eastern Yukon-Tanana Upland (figure 1). Rocks of the Yukon-Tanana Upland are present in east-central Alaska and in the northeastern Yukon Territory of Canada and these rocks primarily consist of low to medium grade metasediments with minor meta-igneous and intrusive rocks. This metamorphic complex has been named the Yukon-Tanana Terrane (Coney and others, 1980) and is considered the innermost of the accreted or suspect terranes that comprise the northern Cordillera. This terrane is adjacent to the

Proterozoic/Paleozoic continental margin sequence that was deposited on the cratonic margin of North America. The geological evolution of the Yukon-Tanana Upland is of fundamental importance in understanding the accretionary history of the northern Cordillera as it is apparently one of the first terranes to be accreted to western North America and therefore records the initiation of this process within the region. Subsequent accretion of terranes from the south may also be recorded in the thermal and structural history of the Yukon-Tanana Upland.

FIGURE 1: The Yukon-Tanana Upland with inset map of Alaska. Quadrangles, major rivers, highways and towns are shown. The study area is in the southeastern corner of the Eagle quadrangle.

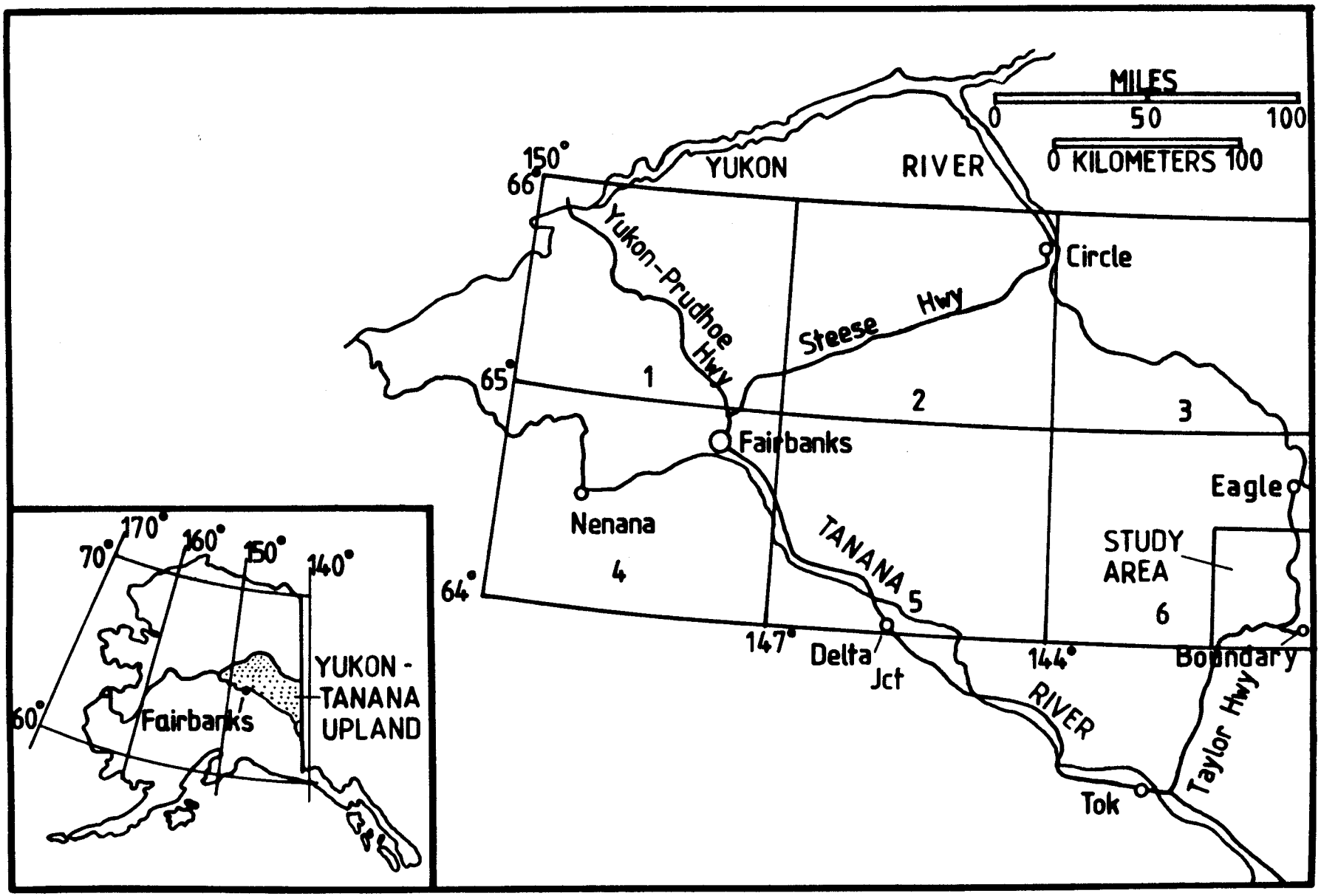
MILES
0 50 100
0 KILOMETERS 100
YUKON RIVER
150°
66°
Yukon-Prudhoe Hwy
Steese Hwy
Circle
65°
1
2
3
Fairbanks
Eagle
Nenana
4
TANANA
5
STUDY AREA
6
64°
147°
Delta Jct
144°
Boundary
RIVER
Taylor Hwy
Tok
170°
160°
150°
140°
70°
60°
Fairbanks
YUKON - TANANA UPLAND

REGIONAL GEOLOGIC SETTING

The Yukon-Tanana Upland, located in east-central Alaska, is bounded on the north by the Yukon River and on the south by the Tanana River.

The region is characterized by relatively rounded hills with gentle side slopes, but in places rugged peaks occur. The topographic relief ranges from approximately 190 m to 2130 m above sea level. The region is unglaciated except in the highest areas, where there is evidence for several episodes of alpine glaciation. Common geomorphological features in the higher altitudes include altiplanation terraces, stone polygons, stone stripes, and solifluction lobes. Stone lakes and pingos occur in the valleys. The entire region is located in the zone of discontinuous permafrost. Bedrock exposure is relatively poor (5%) due to the subarctic, tundra environment. Ridge tops and incised stream valleys provide the best exposure of bedrock.

The Yukon-Tanana Upland is primarily a region of multiply deformed metamorphic rocks which have been intruded by Mesozoic batholiths and smaller Mesozoic and Tertiary plutons. However, in the northwestern portion of the upland, there is a sequence of sedimentary or slightly metamorphosed sedimentary rocks, which are most probably related to the Proterozoic-Paleozoic continental margin rocks of North America. Thus, the Upland consists of at least two distinct geologic provinces: a metamorphic complex in the central and eastern portion and a relatively

unmetamorphosed sequence in the northwest.

The Tintina and Denali right lateral strike-slip fault systems demarcate the north and south boundaries, respectively, of the metamorphic complex that comprises most of the upland. To the northwest, a major thrust fault most probably separates the higher grade rocks of the upland from the less metamorphosed sediments. To the southeast, the metamorphic terrane extends into the Yukon territory of Canada, where it is referred to as the Yukon-Crystalline terrane (Templeman Kluit, 1976).

The metamorphic rocks in the Upland are composed primarily of quartzitic schist and gneiss, quartzite, pelitic schist and gneiss, marble, greenschist, and amphibolite. The rocks were originally layered sedimentary sequences with continental affinities and include some volcanic and plutonic material. The rocks are now regionally metamorphosed from low greenschist facies to amphibolite facies. Locally, small ultramafic bodies are infolded in the other metamorphic rocks. Cretaceous to Recent volcanic rocks of mafic to felsic compostion are also present. In the northern portion of the metamorphic terrane a relatively small dismembered ophiolite of probable Permian age is in thrust contact with the higher grade metamorphic rocks.

North and northeast of the Tintina fault is a relatively continuous record of Late Proterozoic and Paleozoic continental margin sedimentation. Depositional relationships and lithofacies show that shelf conditions and

sediment source areas existed to the northeast. Open marine conditions existed to the south and west (Payne and Allison, 1981). This geology can be correlated with Proterozoic and Paleozoic continental margin deposits in the Canadian Cordillera.

The stratigraphic environment is consistent with that expected along a rifted continental margin adjacent to a south-to-west facing depositional system (Payne and Allison, 1981).

Immediately to the south of the Denali fault system are rocks that make up a Cretaceous metamorphic belt. These rocks have a distinct geologic history from the metamorphic rocks of the upland and were emplaced in their present position by northward thrusting and/or right lateral strike slip motion.

REGIONAL TECTONIC SETTING

With the advent of the new interpretive models of accretionary tectonics or the suspect terrane concept, it has become evident that geologic provinces like the metamorphic rocks of the Yukon-Tanana Upland are probably allochthonous with respect to the North American continent. Identification of the autochthonous Proterozoic-Paleozoic continental margin sequence to the north of the metamorphic rocks of the Yukon-Tanana Upland, implies that the rocks to the south have been accreted to this margin.

In this portion of Alaska, this interpretation is complicated by the fact that the Tintina fault may separate the continental margin sequence from the metamorphic rocks. A portion of this study indicates that the Tintina fault has been active in Alaska at least since Middle Cretaceous time and probably has at least 300 km right lateral offset since that time. The accretionary history of the metamorphic rocks south of the Tintina fault is poorly understood and is, in part, the emphasis of this study. It is clear the metamorphic rocks of the Yukon-Tanana Upland have a complex structural history and in some places there is evidence that rocks with differing structural style have been tectonically juxtaposed. Little is known about the nature and timing of this juxtaposition. In the Circle quadrangle, there is evidence for pre- and post-metamorphic thrusting. In portions of the Eagle quadrangle, post-metamorphic faults have been identified. These observations imply that at least

two, but probably several, episodes of thrusting are involved in the tectonic development of the Upland. The ages of these compressional structures are not well constrained due to our poor understanding of the thermal history of the region. Some workers (Churkin and others, 1982) have subdivided the Yukon-Tanana Upland into distinct terranes based on regional map patterns and tectonostratographic environments. In general, these divisions are plausible, but there is no constraint on the age or ages of faulting and structural generations and on the age of major metamorphism.

Therefore, no interpretation can be made concerning the time or times of tectonic accretion within the Yukon-Tanana Upland and/or the time of accretion to the continental margin. It has yet to be determined whether the Yukon-Tanana Upland is a composite terrane consisting of two or more terranes that were amalgamated prior to their accretion to North America. Some writers such as Coney and others (1980) have interpreted the Upland as a composite terrane due to the complex structural and metamorphic history, but this is not yet established. Jones and others (1982) consider the Yukon-Tanana Upland as a metamorphic terrane which is defined and characterized by a regional, terrane-wide penetrative metamorphic fabric and metamorphic mineral development to such a degree that original stratigraphic features and relations are obscured. This classification is clearly applicable to the Yukon-Tanana Upland, but does not

preclude the possibility that several metamorphic terranes make up the Upland.

STUDY AREA

The study area is located in the eastern Eagle quadrangle (figure 1) which is situated in the east-central portion of the Upland and bounds the Yukon territory on the east.

Most of the field work was concentrated along the Taylor highway which runs approximately north-south through the area. The first reconnaissance geologic map (1:250,000) of the area was compiled by Dr. Helen Foster in 1976. The general geology of the region consists of greenschist to amphibolite facies metamorphic rocks that have been juxtaposed along a series of complex fault zones. Four specific geologic map units are of specific interest in this study. The biotite gneiss and amphibolite unit (PzPЄb),the quartz-mica schist and greenschist unit (Pzq), the greenstone unit (Pzg) and minor ultramafic rocks (MzPzS, MzPzSp). The biotite gneiss and amphibolite unit makes up the southern portion of the area and consists primarily of quartz-mica schist and gneiss, amphibolite, and intercalated marble. This unit has been metamorphosed to the epidote-amphibolite and amphibolite facies. Along the northern boundary of this unit, between it and the lower grade quartz-mica schist and greenschist unit (Pzq), a relatively high angle fault has been mapped Foster (1976). This fault is not mapped along the entire contact and no sense of offset is evident from the geologic map. To the north of

this fault is the quartz-mica schist and greenschist unit. These rocks have been metamorphosed to the greenschist facies. Within both of these units, but predominant within the quartz-mica schist and greenschist unit, are blocks of ultramafic rock. Their size varies from less than a meter in diameter to several kilometers across, and they show variable degrees of serpentinization. The fourth unit of interest in this study is the greenstone unit (Pzg) which in places is in contact with all the units previously described.

Quarternary deposits are also present within the field area but were not studied in detail. Sand, gravel, and silt are present along all major streams and locally contain organic silt, peat, glacial outwash and reworked glacial deposits. Intermediate and high terrace deposits flank some of the major rivers in the study area. Silt, sand, and generally unsorted gravel make up these terrace deposits and in places they lie up to 215 m above present streams and rivers.

PURPOSE AND METHOD

The aim of this study is to better understand the tectonic evolution of a portion of the Yukon-Tanana Upland so that fundamental questions can be answered regarding the nature and timing of tectonic accretion in this portion of the Cordillera. As previously stated, present tectonic interpretations place the Yukon-Tanana terrane innermost of all accreted terranes in the northern Cordillera, providing importance to an understanding of the nature and timing of significant structural and metamorphic events within the terrane. Also of interest in this study is the thermal and structural character of a complex fault zone across which are juxtaposed two distinct groups of rock. This fault zone may represent a terrane boundary within the Upland and may yield information regarding the possible composite nature of the Yukon-Tanana terrane. Detailed study of this zone may also yeild information relevant to the terrane accretion process itself.

In the study area, the two distinct groups of rock are the higher grade biotite and amphibolite gneiss unit (PzPЄb) to the south, and a lower grade quartz-mica schist and greenschist unit (Pzq) to the north. Also studied was the structural and thermal relationship of the numerous greenstone bodies within the area to the other metamorphic rock units (PzPЄb & Pzq). Field seasons in 1982-1983, totalling three months, were spent studying the structural elements within the different groups of rock so that

similarities and/or differences could be highlighted and related to the structural history/ies of the individual groups. The boundaries between these groups were studied in detail to determine the nature of the contact. Where faults are present within a unit, or at the contact between two units they were studied in detail to determine their relationship. The timing of structural events and the thermal histories of these units have been resolved using the $^{40}Ar/^{39}Ar$ age spectrum technique on metamorphic and igneous minerals. Within the higher grade unit (PzpЄb) amphibolites are widespread and were collected with emphasis on structural relationships as well as thermal history. Igneous rocks were also collected where possible so that their relationship to specific thermal events could be determined. In the northern, lower grade unit, datable samples are rare and were collected wherever possible.

Field studies were mostly resricted to the Taylor highway, although backpack and helicopter support trips were taken to points of interest. An east-west traverse along the 40-Mile River with boat support aided the field studies. Drs. Helen Foster and Jo Laird aided in some of the field work and were present for consultation and advice.

Previous Work

1. Regional Geology

The first systematic explorations of the Yukon-Tanana region took place between 1840 and 1865. The motives for these reconnaissance surveys were primarily economic and were conducted by concerns such as the Hudson Bay Company and Western Union Telegraph Company. In 1867 the ownership of Alaska changed from Russia to the United States and an era of organized scientific studies began statewide. In 1896 a scientific expedition headed by J.E. Spurr produced the first systematic classification of some of the rocks in the Yukon-Tanana Upland and description of the previously discovered gold placer deposits in the area. In 1903 the division of Alaskan Mineral Resources was organized in the U.S. Geological Survey. That same year, the first systematic study of the geology and mineral resources of the Yukon-Tanana Upland began. During the years between 1903 and 1911 geologic studies in this area were directed by L.M. Prindle and numerous geologic maps were produced at the scale of 1:250,000. In 1911, J.B. Mertie became director of these studies and was responsible for the first extensive, areal geologic studies of this area. Mertie's summary report, published in 1937, included a geologic map of the entire region at a scale of 1:500,000. This compilation is the only regional compendium published on the geology and mineral resources of the Upland as a whole. It was considered the most complete and citable publication on the

region until the latest generation of research by the U.S. Geological Survey.

Mertie (1937) subdivided what he and others considered the oldest rocks into three distinct groups. The oldest unit, called the Birch Creek Schist, was considered to form the base of the geologic section and was interpreted as Precambrian in age. This Birch Creek Schist consists principally of quartzite, quartzitic schist, quartz-mica schist, mica schist, feldspathic and chloritic schist, and a minor proportion of carbonaceous and calcareous schist and crystalline mantle. Quartzitic schist and quartz mica schist are the most common rock types. Metaigneous rocks associated with the Birch Creek Schist are primarily granitic in composition, but also include more mafic varieties, such as meta-monzonite, diorite, and gabbro. The rocks of the Birch Creek Schist were considered by Mertie to be principally of sedimentary origin and were correlated with the Archean rocks of northern Canada. No fossil data have ever been obtained from rocks of the Birch Creek Schist.

The second group of rocks that was delineated by Mertie was the Tinder Group, which are present only in the northern portion of the Upland. These rocks extend for hundreds of kilometers into Canada, and, as will be discussed later, are today considered as part of the ancient continental margin sequence of North America. The Tinder Group consists of a thick sequence of sedimentary rocks interlayered with mafic

lava flows and intruded by minor igneous masses. This sequence was considered by Mertie (1937) to be Upper Precambrian or Lower Cambrian.

The third group of rocks that Mertie (1937) described were called the undifferentiated Pre-Middle Ordovician rocks. These rocks occur in two general areas within the Upland, and their age is based on one fossil locality. The generalized geologic sequence that is found in the northwestern section includes slate, quartzite, black argillite, chert, and minor limestone. In the lower part of the section, approaching the contact with the Birch Creek Schist quartzose sandstone, graywacke and phyllite are interlayered.

In general, these three rock groups are recognized by more recent workers, although significant subdivisions have been made within each group and their structural character is better understood.

The latest generation of geologic research in this area has been directed by Dr. Helen Foster of the Branch of Alaskan Geology, U.S. Geological Survey. This work began in 1960 and is still in progress. Most of this work has been organized and funded under the Alaska Mineral Resource Assessment Program. Studies include reconnaissance geologic mapping at the scales of 1:63,360 and 1:250,000, geochemical sampling, and mineral resource assessment. Included in this research are more detailed structural analyses, examination of conditions of metamorphism, general geochronology studies, and regional tectonic analyses. Geologic maps at

the scale of 1:250,000 have now been published for every quadrangle in the Upland. Listed are the available quadrangle maps and their date of publication: Circle (Foster and others, 1983); Big Delta (Weber and others, 1978); Eagle (Foster, 1976); Livengood (Chapman and others, 1971); Tanacross (Foster, 1970); and Charley River (Brabb and Churkin, 1969).

In an early publication on the regional geology of the Yukon-Tanana Upland, Foster and others (1973) proposed that the term Birch Creek Schist be abandoned. Mertie (1937) had assigned a Precambrian age to the Birch Creek Schist based on lithologic differences and supposed stratigraphic relations to the Tinder Group to the north. Foster and others (1973) recognized that there was no stratigraphic relationship between the two units because they are bounded by the Tintina fault, and they concluded that Mertie's age assignment was based on unsound reasoning. Foster and others (1973) divided the metamorphic rocks of the Upland based on metamorphic grade and characteristic lithologies (Figure 2).

Coney and others (1980) presented the first review paper illustrating the regional significance of allochthonous terranes throughout the North American Cordillera. In this paper, the metamorphic complex of the Yukon-Tanana Upland was classified as a composite terrane, consisting of heterogeneous gneiss and schist with high level sheets of chert, basalt and ultramafic rock. This

FIGURE 2: Regional geology of the Yukon-Tanana Upland (after Foster and others, 1973).

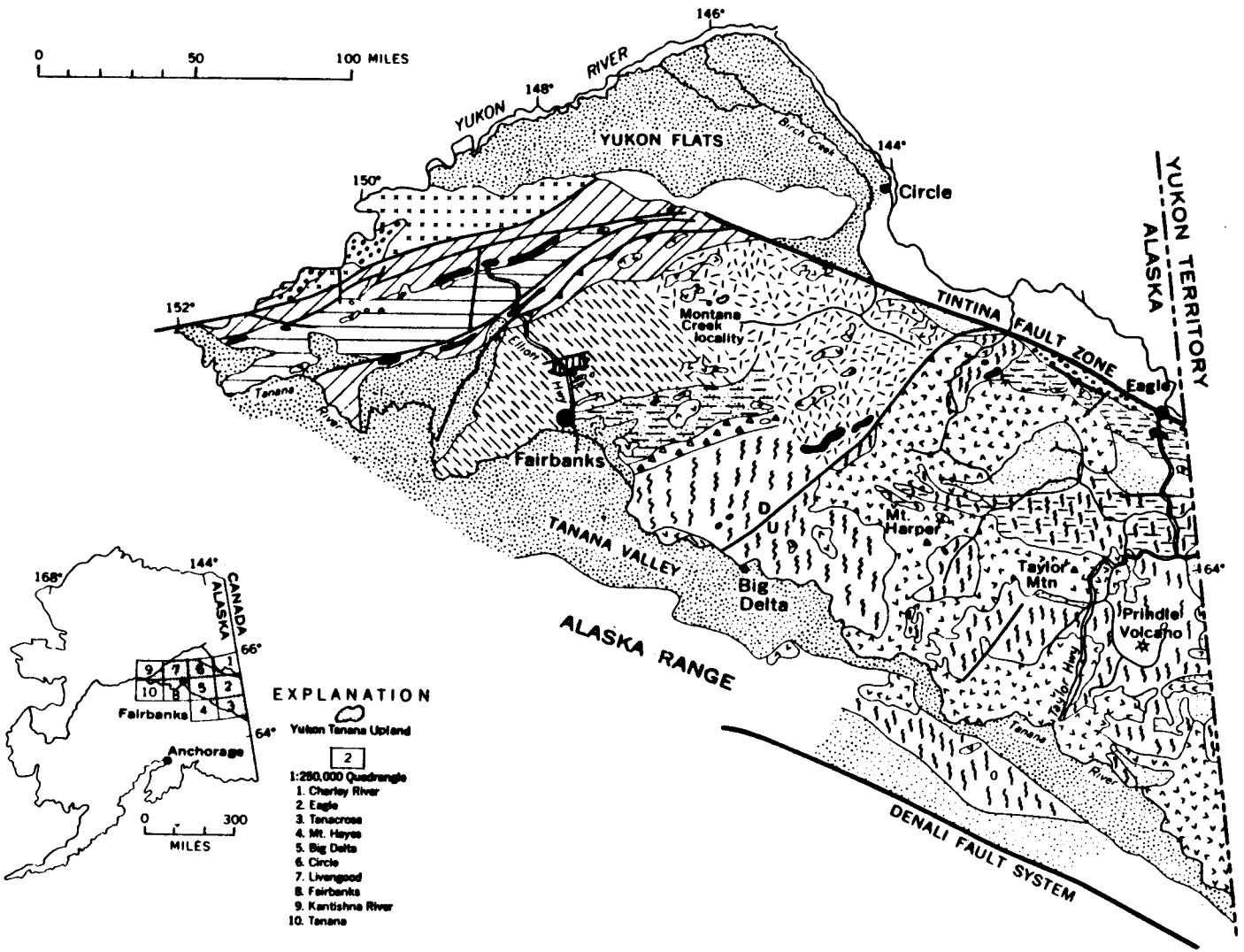
0
50
100 MILES
146°
148°
150°
152°
144°
YUKON RIVER
YUKON FLATS
Birch Creek
Circle
YUKON TERRITORY
ALASKA
TINTINA FAULT ZONE
Eagle
Montana Creek locality
Elliott Hwy
Tanana River
Fairbanks
TANANA VALLEY
Big Delta
Mt. Harper
Taylor Mtn
Taylor Hwy
Tanana River
Prindle Volcano
164°
ALASKA RANGE
DENALI FAULT SYSTEM
168°
144°
CANADA
ALASKA
66°
64°
Fairbanks
Anchorage
0
300
MILES
EXPLANATION
Yukon Tanana Upland
2
1:250,000 Quadrangle
1. Charley River
2. Eagle
3. Tanacross
4. Mt. Hayes
5. Big Delta
6. Circle
7. Livengood
8. Fairbanks
9. Kantishna River
10. Tanana

EXPLANATION

SEDIMENTARY AND METAMORPHIC ROCKS

- Alluvium (Yukon-Tanana Upland and Tanana Valley) — QUATERNARY
- Conglomerate, sandstone, shale, and tuff (nonmarine) — JURASSIC CRETACEOUS AND (OR) CRETACEOUS TERTIARY
- Conglomerate, graywacke, quartzite, shale, and siltstone — JURASSIC AND (OR) CRETACEOUS
- Quartzite, phyllite, grit, slate, chert, limestone, greenstone, dolomite, conglomerate, siltstone, and graywacke — CAMBRIAN(?) AND (OR) CRETACEOUS

METAMORPHIC ROCKS

CAMBRIAN AND (OR) PALEOZOIC

- Undifferentiated metamorphic rocks
- Quartz-mica schist, quartzite, greenschist amphibolite, and marble

Greenschist facies rocks

- Quartz-mica schist, quartzite, carbonaceous schist, chlorite, actinolite, and quartz schist, greenstone, and phyllite
- Phyllite, calc-phyllite, slate, and quartzite; carbonaceous, quartz-mica, chlorite, calcareous, actinolite, and quartz schists; marble and greenstone
- Greenschist to epidote-amphibolite facies rocks (transitional)
  Includes mica schist and quartz-mica schist

Amphibolite facies rocks

- Quartz-mica gneiss and schist (much is garnetiferous), quartzite, amphibolite, augen gneiss
- Quartz-mica gneiss and schist (much is garnetiferous), quartzite, amphibolite, and marble
- Cataclastic rocks including augen gneiss
- Eclogitic rocks interlayered with calcium-magnesium schists

IGNEOUS ROCKS

- Mostly granodiorite and quartz monzonite but includes other granitic rocks and mafic to felsic volcanic rocks — MESOZOIC AND CENOZOIC
- Diabase, diorite, gabbro, and basaltic volcanic rocks intruded into and interlayered with chert, shale, siltstone, graywacke, sandstone, and conglomerate (Rampart Group) — PERMIAN(?)
- Serpentinite, peridotite, diorite, gabbro, and meta basalt — DEVONIAN(?) AND OTHER PALEOZOIC(?)
- Geology not shown on this map (north of Tintina fault zone and in Alaska Range)

Fault
Includes buried, approximate, and doubtful segments.
U, *upthrown side*; D, *downthrown side*

Thrust fault
Teeth on upper plate

Approximate contact or isograd

configuration resulted from nappe emplacement of Upper Paleozoic oceanic assemblages thrust over the quartzo-feldspathic metamorphic complex of unknown continental affinity. The time of emplacement of this terrane to North America is not known, but based on Canadian literature, Coney and others, (1980) proposed amalgamation of the composite terrane in Triassic time. The Triassic amalgamation age is based on the work of Tempelman-Kluit (1979) in the Yukon Territory of Canada. Tempelman-Kluit's (1979) study revealed a wide zone of transported cataclasite which he interpreted as developing during arc-continent convergence in Late Triassic and Early Jurassic. This cataclasite includes sheared silicious mylonite, a dismembered ophiolite, and a sheared plutonic assemblage, which occur whithin a suture zone (Teslin Suture), and as allochthonous sheets above Upper Proterozoic, Paleozoic, and lower Mesozoic autochthonous strata that were deposited near the ancient margin of North America. In the Canadian Cordillera, the autocthonous and parautochthonous continental margin deposits make up the Omineca Belt. The extension of this belt to the northwest is nebulous due to an increase in metamorphic grade and paucity of fossil information. Coney and others (1980) Triassic amalgamation age for the Yukon-Tanana terrane is based on the interpreted extension of the Omineca Belt into Alaska and the occurence of Permian ophiolite overlying this belt. Although this is a possible interpretation (as will be discussed later), it is based on a minimal data base, and if correct, does not

apply to the entire Upland.

The Permian ophiolite that overlies the metamorphic rocks of the Yukon-Tanana terrane is located just to the north of the main field area of this study, and is called the Mt. Sorenson body (figure 3). The ophiolite has been studied in some detail by Keith and others (1981). This dismembered ophiolite sequence consists of about 47 km^2 of peridotite and serpentinized peridotite (harzburgite subtype) with slightly metamorphosed pillow basalt, cumulate gabbro, red chert, and aphanitic volcanic rocks closely associated (figure 4). The peridotite body crops out as a synformal mass trending approximately east-west with a north and south limb about 30 km and 14 km long, respectively. One occurrence of glaucophane schist is reported southeast of the ophiolite body and is most probably related to the emplacement of the ophiolite. Bordering the southern limb of the peridotite on the south is a narrow band of metasedimentary rocks consisting of fine grained quartzite, phyllite, graywacke, and argillite. A band of similar, but less metamorphosed rocks occur southeast of the northern limb. Possible equivalents of these rocks to the southeast contain Permian brachiopods. More recent studies show that chert collected just north of the ophiolite contain Mississippian radiolarians (D.L. Jones, personal communication). Based on these data, the ophiolite is most probably Mississippian? to Permian in age.

The quartzite and quartz-mica schists between the two

FIGURE 3: Location of map areas that include the peridotite at Mount Sorenson (from Keith and others, 1981).

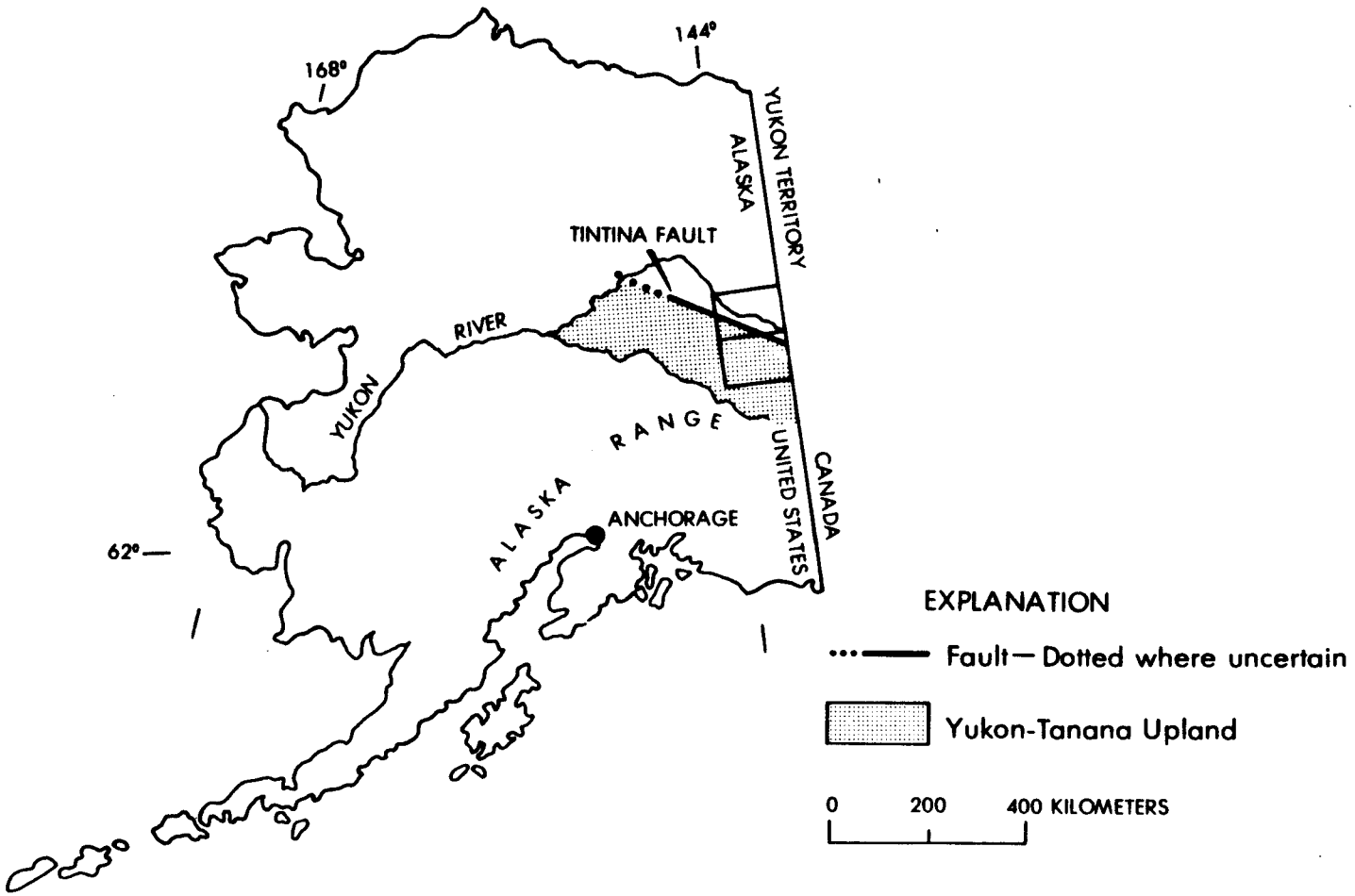
168°
144°
YUKON TERRITORY
ALASKA
TINTINA FAULT
YUKON RIVER
RANGE
ALASKA
ANCHORAGE
UNITED STATES
CANADA
62°
EXPLANATION
Fault—Dotted where uncertain
Yukon-Tanana Upland
0 200 400 KILOMETERS

FIGURE 4: Geologic map of the peridotite of Mount Sorenson (from Keith and others, 1981).

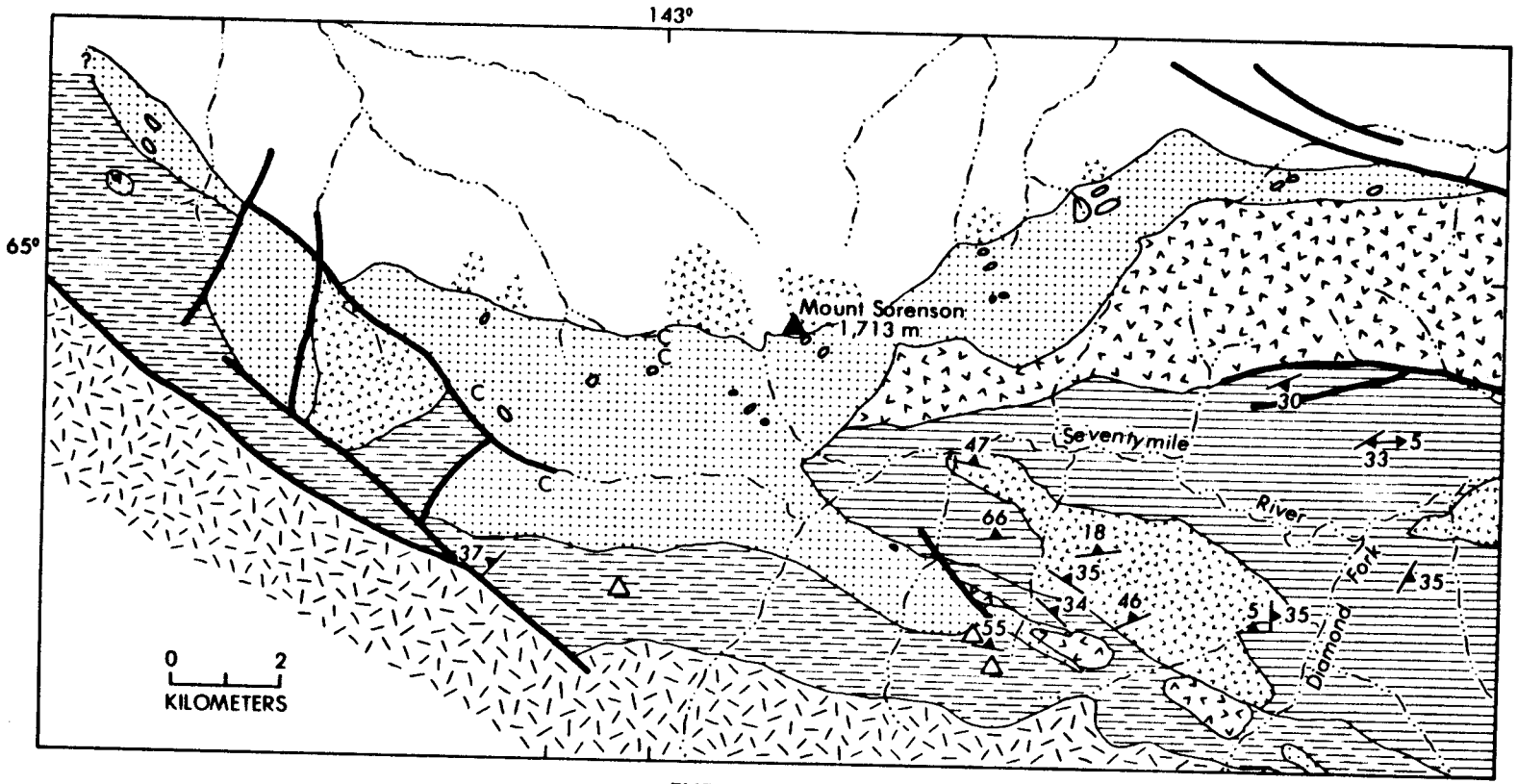

EXPLANATION

- Mesozoic granitic rocks
- Ultramafic rocks, mostly serpentinized
- Diabase pod
- Metamorphosed basalt and gabbro
- Greenstone
- Permian(?) metasedimentary rocks
- Paleozoic(?) greenschist-facies metamorphic rocks

- C — Quartz-carbonate vein
- △ — Outcrop of chert
- ——— Fault
- ———? Contact—Queried where uncertain
- 35 — Strike and dip of foliation
- →5 Bearing and plunge of lineation

limbs of the peridotite body have not been dated precisely, but are presumed to be of Paleozoic age because of crinoid columnals found in marble layers to the east.

The emplacement of the Mt. Sorenson ultramafic body remains somewhat enigmatic due to its close proximity to the Tintina fault zone. Churkin and others (1980) proposed a mantle source of the peridotite that could have been derived from a deep crustal suture, presumably a forerunner of the Tintina fault. Churkin and others, (1980) also proposed that the Tintina fault marks the boundary between the Paleozoic sediments of the ancient continental margin and metamorphic rocks of distinct origin. However, a large proportion of the metamorphic rocks south of the Tintina fault may have been derived from a similar continental source.

Keith and others (1981) suggested that the metamorphic rocks south of the Tintina fault are a slice of continental crust or remains of a small plate that moved northwestward over oceanic crust along the margin of the North American Plate. During this movement, postulated to be in Late Paleozoic time, some oceanic crust and mantle were caught up along the suture and locally obducted onto the small continental fragment.

The interpreted origin of the metamorphic rocks that make up the majority of the Upland is of fundamental importance. Certain authors suggest that they are metamorphosed equivalents of the continental margin sequence. Others consider the metamorphic rocks as a

distinct package with unknown continental affinity. Many of the regional correlations and tectonic models are based on the interpreted origin of these rocks.

To the north of the Tintina fault in east-central Alaska is a relatively continuous sequence of Late Proterozoic and Paleozoic continental margin deposits (Churkin and others, 1980; Payne and Allison, 1981). The stratigraphy in this area is well known and there is a clear correlation of units to the southeast into the Canadian Cordillera. The Upper Proterozoic and Lower Paleozoic units correlate well across the Canadian border and are both present north of the Tintina fault (Tinder Group in Alaska and Pinguicula group and MacKenzie Supergroup in northwestern Canada). These thick sequences suggest that shelf conditions and source areas existed to the northeast. Open marine conditions existed to the south and west (Payne and Allison, 1981). These stratigraphic environments are interpreted to have existed along a rifted continental margin with a south-to-west facing depositional system (Payne and Allison, 1981). Younger units (Middle and Upper Paleozoic) of continental margin affinity, in Alaska, are more difficult to correlate with Canadian units due to their suggested presence south of the Tintina fault in the Yukon Territory (Tempelman-Kluit, 1976). Specific units of concern include the outer shelf deposits of the Nasina series which may be on strike with the northern lower grade rocks south of the Tintina fault within this study area. It

is clear that there is little agreement on the distinction between autochthonous or parautochthonous continental margin deposits and distinct allochthonous terranes. This again points to the significance of the origin of the metamorphic rocks that make up the majority of the Upland. Are they of distant origin, or are they metamorphosed equivalents of the continental margin sequence?

In a more recent statewide compilation by Jones and others (1981), the Yukon-Tanana rocks were separated into three distinct terranes. The 70-mile terrane consists of the dismembered ophiolite sequence of Mt. Sorenson and other ultramafic bodies on strike with it. The ophiolite and associated rocks are considered to be of Permian age and tectonically overlie the metamorphosed sedimentary rocks of the Yukon-Tanana terrane. The two remaining subdivisions are both called the Yukon-Tanana terrane and are distinguished by their location north or south of the Tanana River. They are described together as a tectonically complex metamorphosed assemblage of continentally derived sedimentary, volcanic, and granitic rocks of Precambrian and Paleozoic age.

The most recent and slightly more detailed compilation of the terranes in east central Alaska separates the Yukon-Tanana terrane into at least four subterranes (Churkin and others, 1982) (figure 5). These authors chose to call the terrane, as a whole, the Yukon Crystalline Terrane to be in accordance with Canadian literature (Tempelman-Kluit, 1976). The subterranes are based largely on original rock types and

FIGURE 5: Terranes of east-central Alaska (after Churkin and others, 1982).

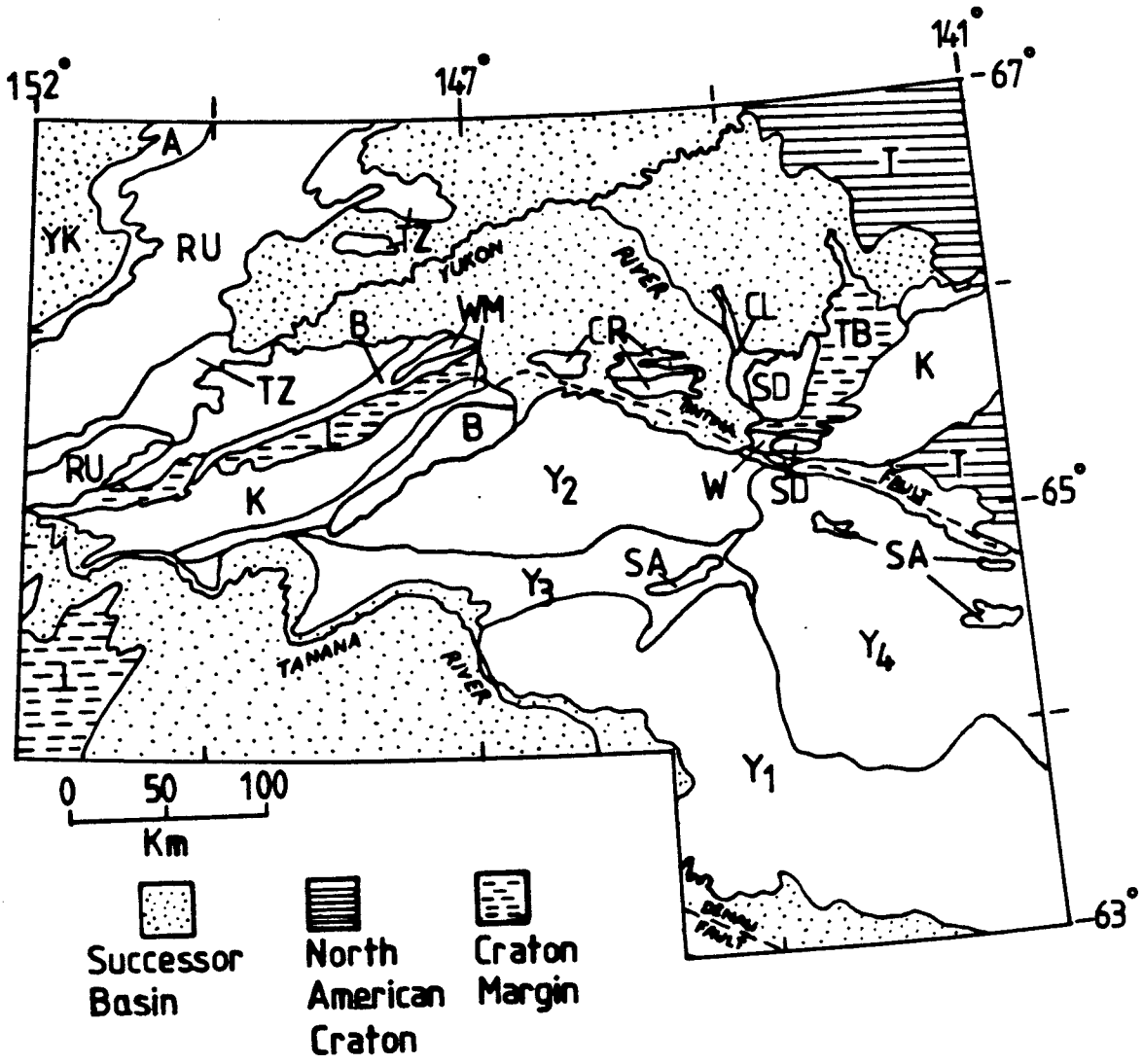
152°
147°
141°
67°
65°
63°
A
YK
RU
TZ
YUKON
RIVER
B
WM
CR
CL
TB
SD
K
TZ
B
RU
K
Y2
W
SD
SA
Y3
SA
Y4
TANANA
RIVER
Y1
0 50 100
Km
Successor Basin
North American Craton
Craton Margin

are described together in a general fashion. Metamorphic sections of the subterranes are composed primarily of quartzitic schist and gneiss, quartzite, pelitic schist and gneiss, phyllite, augengneiss, marble, greenschist, and amphibolite. The rocks were originally mostly layered sedimentary sequences with continental affinities also containing some volcanic and plutonic material. They are now regionally metamorphosed to grades ranging from low greenschist to high amphibolite facies. Locally, small masses of ultramafic rocks of unknown affinities occur within the other metamorphic rocks. The metamorphic rocks are extensively intruded by granite, particularily in the eastern part of the terrane. Mafic and ultramafic intrusions are present but cover only small areas. Cretaceous to Recent volcanic rocks of mafic to felsic compositions are also present. Because the terrane is structurally complex and relict sedimentary features and fossils are rare, it is generally not possible to reconstruct original stratigraphic successions and determine relationships between the terranes.

The above general description and accompanying metamorphic sections present the latest published account of the geology of the Yukon-Tanana Upland. The subterrane Y4 of Churkin and others (1982) includes the study area analyzed for this thesis (figure 5).

FIGURE 6: Interpretive metamorphic sequences of the Yukon-Crystalline Terrane (Y1-Y4). Thickness and statigraphic successions unknown (after Churkin and others, 1982). (see figure 5 for locations of metamorphic sequences)

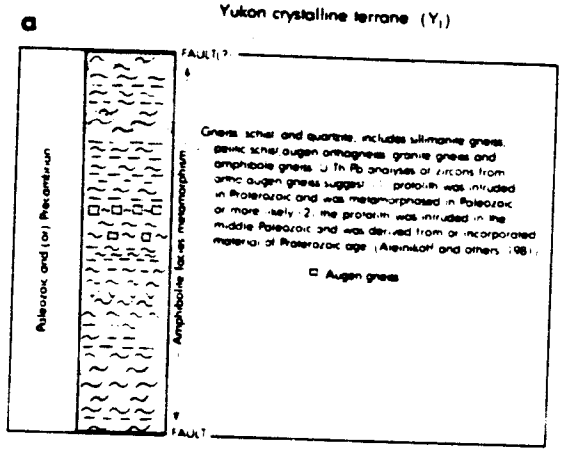
a
Yukon crystalline terrane (Y1)
Paleozoic and (or) Precambrian
Amphibolite facies metamorphism
FAULT(?)
FAULT
Gneiss, schist and quartzite, includes sillimanite gneiss, pelitic schist, augen orthogneiss, granite gneiss and amphibolite gneiss. U-Th-Pb analyses of zircons from some augen gneiss suggest that protolith was intruded in Proterozoic and was metamorphosed in Paleozoic or more likely (2) the protolith was intruded in the middle Paleozoic and was derived from or incorporated material of Proterozoic age (Aleinikoff and others, 1981).
Augen gneiss

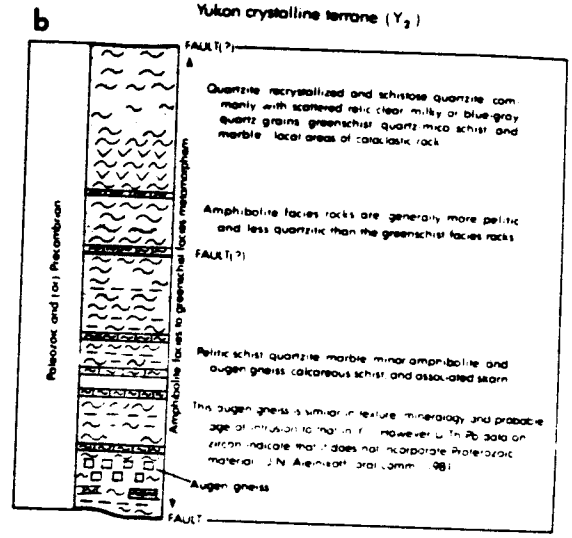
b
Yukon crystalline terrane (Y2)
Paleozoic and (or) Precambrian
Amphibolite facies to greenschist facies metamorphism
FAULT(?)
FAULT?
Quartzite recrystallized and schistose quartzite commonly with scattered relict clear milky or blue-gray quartz grains greenschist quartz mica schist and marble local areas of cataclastic rock
Amphibolite facies rocks are generally more pelitic and less quartzitic than the greenschist facies rocks
Pelitic schist quartzite marble minor amphibolite and augen gneiss calcareous schist and associated skarn
This augen gneiss is similar in texture mineralogy and probable age of intrusion to marble (1) However U-Th-Pb data on zircon indicate that it does not incorporate Proterozoic material (J.N. Aleinikoff oral comm., 1981)
Augen gneiss

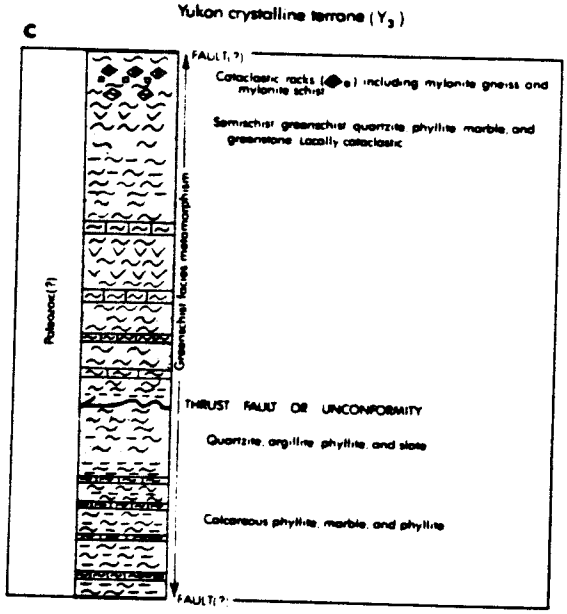
c
Yukon crystalline terrane (Y3)
Paleozoic(?)
Greenschist facies metamorphism
FAULT(?)
Cataclastic rocks including mylonite gneiss and mylonite schist
Semischist greenschist quartzite phyllite marble, and greenstone Locally cataclastic
THRUST FAULT OR UNCONFORMITY
Quartzite, argillite phyllite, and slate
Calcareous phyllite, marble, and phyllite
FAULT(?)

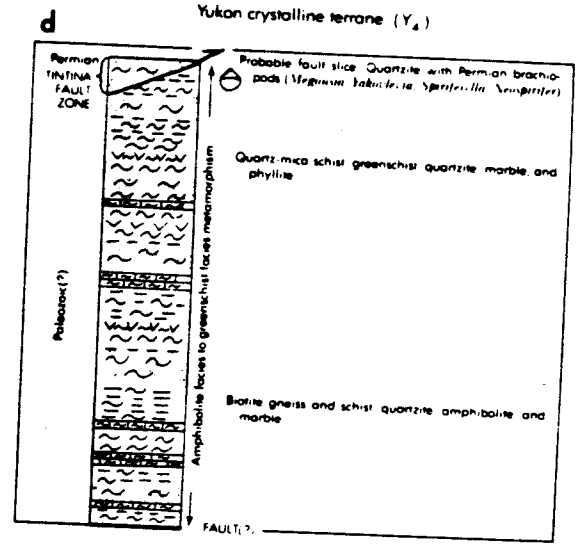
d
Yukon crystalline terrane (Y4)
Permian TINTINA FAULT ZONE
Paleozoic(?)
Amphibolite facies to greenschist facies metamorphism
Probable fault slice Quartzite with Permian brachiopods (Waagenoconcha labrador...)
Quartz-mica schist greenschist quartzite marble, and phyllite
Biotite gneiss and schist quartzite amphibolite and marble
FAULT(?)

2. Geochronology

Geochronologic studies in the Yukon-Tanana Upland began with Pb-alpha work in the late 1950's (Matzko and others, 1958; Jaffe and others, 1959; Gottfried and others, 1959). These dates have long been considered invalid although the numbers are relatively close to many of the potassium-argon dates. The first K-Ar and Rb-Sr dates were produced by Wasserburg and others (1963) from a variety of metamorphic and igneous rocks primarily from the Circle quadrangle.

The great majority of dates in the Upland are K-Ar and have been obtained under the auspices of the ongoing Alaska Mineral Resource Assessment Program. More than 120 K-Ar age determinations on plutonic and metamorphic rocks have now been compiled by Dadisman (1980). Most of these dates were obtained from igneous rocks collected during the course of reconnaissance geologic mapping in particular quadrangles. Regional potassium-argon studies have also been conducted on rocks from the adjacent Yukon Territory in Canada (Tempelmen-Kluit and Wanless, 1975) and culminated in a review paper. Forty-four new ages were obtained from igneous and metamorphic rocks within the Yukon-Crystalline Terrane (Tempelman-Kluit, 1976) and compiled with previously published data to analyze significant thermal events. Least squares fitted isochron plots for micas and amphiboles show three distinct age groupings at 168 Ma, 95 Ma and 54 Ma.

A similar review of the K-Ar dates in Yukon-Tanana

Upland, Alaska, has been written by Wilson and others (in press). In this paper over 120 K-Ar dates on metamorphic (50) and igneous (70) rocks are compiled and grouped in histogram form. Wilson and others (in press) suggest that clear distinctions can be made between igneous and metamorphic events, and that the Upland can be divided into specific age domains based on the K-Ar data. The histogram for the igneous rocks indicates two dominant events, at 50-70 Ma and 85-105 Ma. There is also a suggestion of an igneous event at approximately 180 Ma (figure 7). Wilson and others (in press) grouped the igneous dates areally on the basis of a series of northeast trending lineaments. They noted that ages greater than 120 Ma are from a region east of the Mt. Harper lineament (figure 9). This lineament trends through the Eagle quadrangle and delineates an area that includes the study area of this thesis. Igneous rocks yielding ages between 50 and 70 Ma are distributed throughout the terrane. The 85 to 105 Ma igneous event is widespread, but is not evident in the Circle quadrangle.

The histogram of the metamorphic ages shows two distinct groupings at about 180 Ma and between 100 Ma and 125 Ma (figure 8). The rocks yielding the younger metamorphic ages (100-125 Ma) are interpreted by Wilson and others (in Press) to be dominant west of the Tok lineament (figure 9). This includes the area studied in this thesis. It was concluded by the authors that deviations from the two age groups could be attributed to argon loss due to proximity to intrusive rocks.

FIGURE 7: Histogram showing potassium-argon ages of igneous rocks from the Yukon-Crystalline Terrane. Mineral dated is indicated as follows: b = biotite, h = hornblnde, w = whole rock, m = muscovite, a = amphibole, s = sanidine.

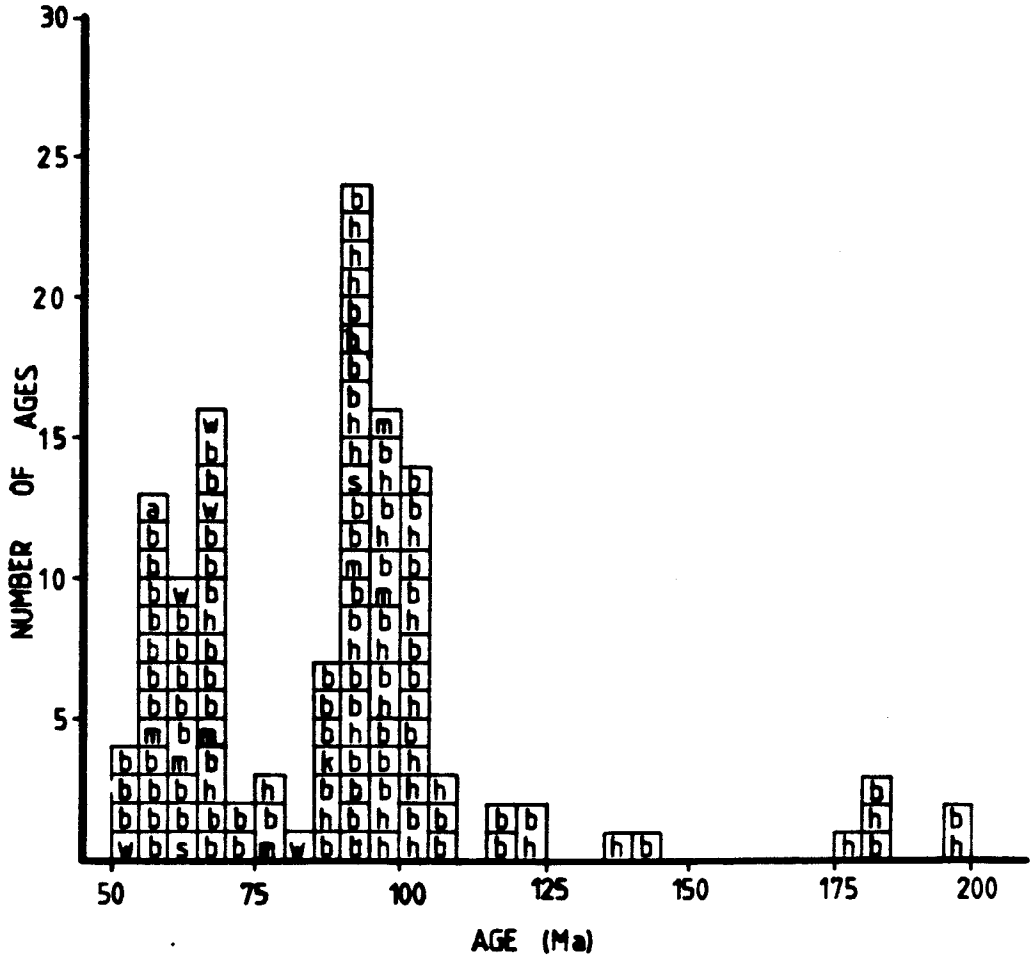
30
25
20
15
10
5
NUMBER OF AGES
50
75
100
125
150
175
200
AGE (Ma)

FIGURE 8: Histogram showing potassium-argon ages of metamorphic rocks from the Yukon-Crystalline Terrane. Mineral dated is indicated as follows: b = biotite, m = muscovite, h = hornblende, a = amphibole.

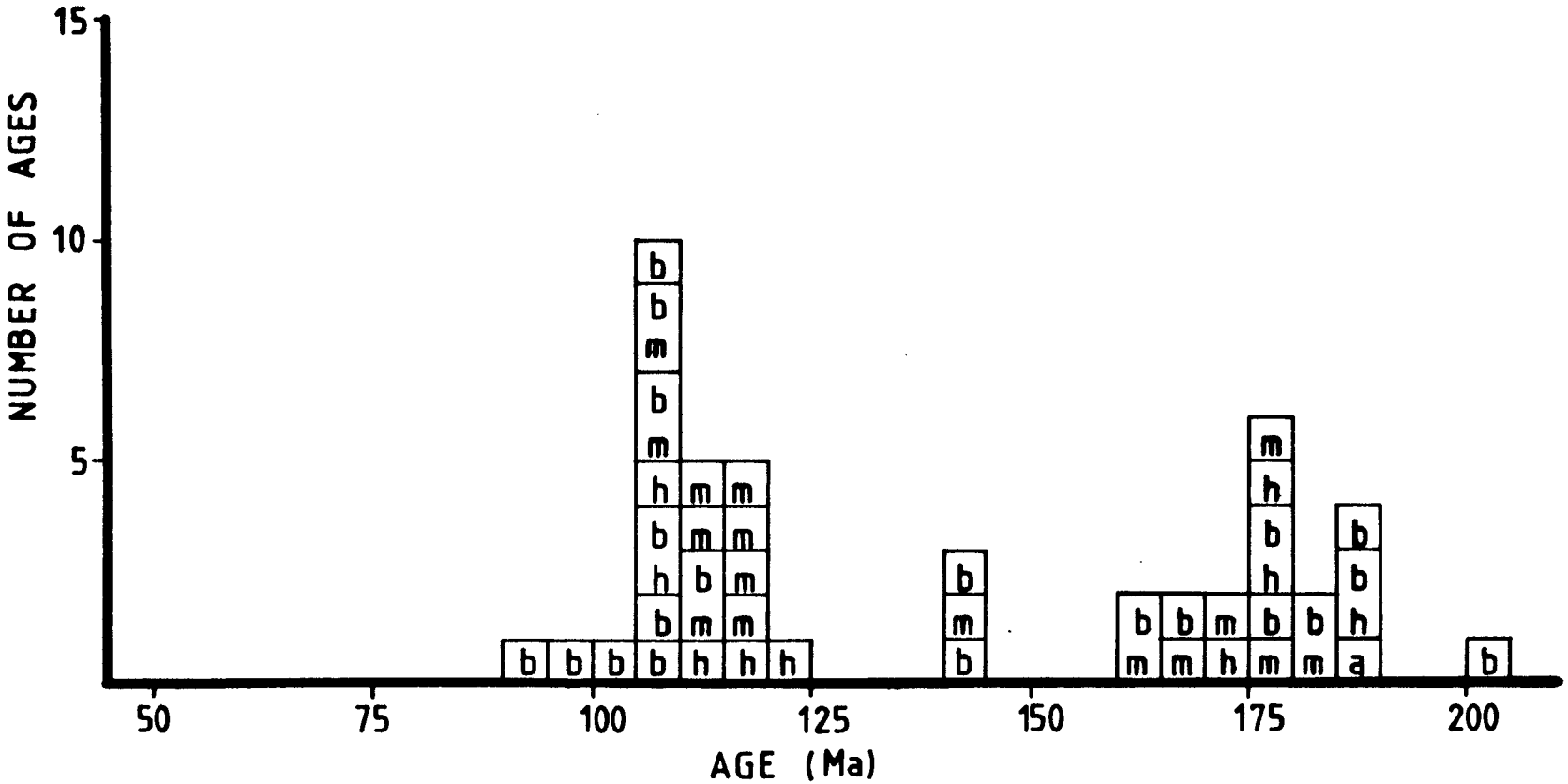
NUMBER OF AGES
15
10
5
50
75
100
125
150
175
200
AGE (Ma)

FIGURE 9: Map of the Yukon-Crystalline Terrane showing major lineaments, major faults and quadrangle names (after wilson and others, in press).

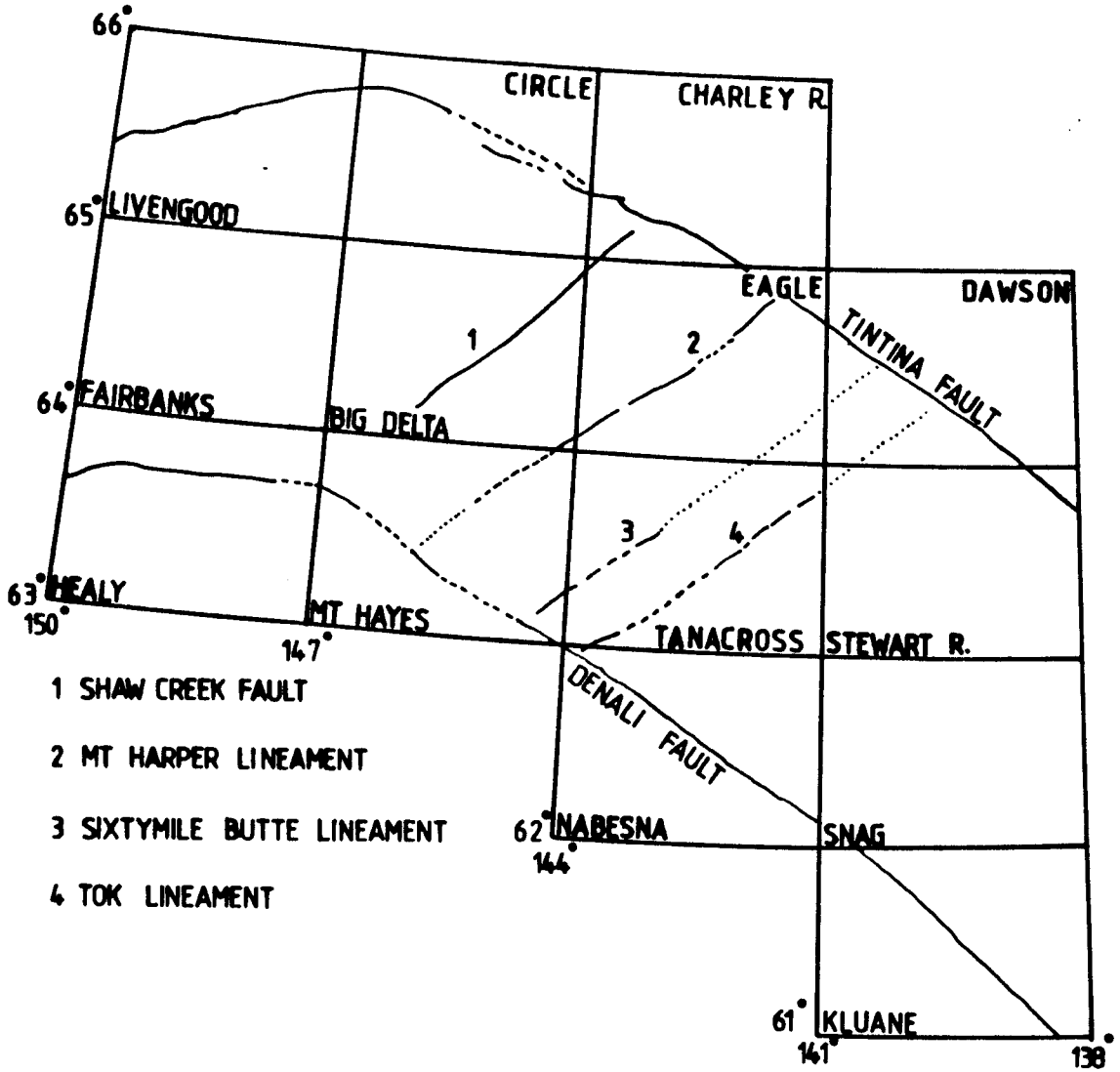
66°
CIRCLE
CHARLEY R.
65°
LIVENGOOD
EAGLE
DAWSON
1
2
TINTINA FAULT
64°
FAIRBANKS
BIG DELTA
3
4
63°
HEALY
150°
MT HAYES
147°
TANACROSS
STEWART R.
DENALI FAULT
62°
NABESNA
144°
SNAG
61°
KLUANE
141°
138°
1 SHAW CREEK FAULT
2 MT HARPER LINEAMENT
3 SIXTYMILE BUTTE LINEAMENT
4 TOK LINEAMENT

Other isotopic studies in the Yukon-Crystalline Terrane include recent U-Th-Pb, Sm-Nd, and Rb-Sr analyses of igneous and metamorphic rocks. Aleinikoff and others (1981 a, b and in press), using U-Th-Pb and Sm-Nd methods, suggest a Proterozoic history for some of the rocks in the Upland. An initial U-Th-Pb study of an orthoaugen gneiss in the Big Delta quadrangle gave upper and lower concordia intercepts of 2.3 Ga and 345 Ma, respectively. Aleinikoff and others (1981b) presented two possible interpretations: (1) the protolith was intruded during the Proterozoic and was metamorphosed in the Paleozoic, or, (2) the preferred interpretation that the protolith was intruded in the Paleozoic and in part was derived from pre-existing Proterozoic material. A Sm-Nd whole rock model age of 1.9 Ga on the augen gneiss was used as additional evidence for a Proterozoic protolith.

Aleinikoff and others (1981a,b) also attempted to constrain the age of major metamorphism by U-Th-Pb dating of zircon and sphene from the oldest (Rb/Sr biotite, Wasserburg and others, 1963) unmetamorphosed pluton in the region (Taylor Mountain batholith). The zircon analyses from this sample plotted on a cord subparallel to concordia and were not used for any significant interpretation regarding the batholith. A sphene analyzed from Taylor Mountain gave a concordant age of 212 Ma and was interpreted as the age of intrusion. This age correlates well with the age of the Klotassin batholith in the Yukon territory of Canada, which

Tempelman-Kluit (1976) considers equivalent to the Taylor Mountain batholith. Integrating the augen gneiss and Taylor Mountain studies, Aleinikoff and others (1981a,b) constrained the time of major metamorphism in the Upland to between 210 Ma and 345 Ma.

A recent U-Th-Pb follow up study by Aleinikoff and others (in press) shows that intercept ages for the same augen gneiss body can be better defined by using additional size fractions and abraded zircons. New calculated intercept ages are 344 ± 7 Ma and 2,281 ± 76 Ga. Also analyzed in that study were zircons from unmetamorphosed aplite sills that cross-cut the augen gneiss body. These sills are interpreted as late stage differentiates and were analyzed (U-Th-Pb) in order to place a maximum limit on metamorphism. The results did not yield a linear plot on a concordia diagram and were attributed to a combination of Paleozoic inheritance and Mesozoic and/or Cenozoic lead loss.

The age of metamorphism within the augen gneiss body was also examined by Rb-Sr whole rock and mineral isochron age determinations. Results of the mineral isochron study yield an age of 115 ± 4 Ma, which is in good agreement with much of the K-Ar data. The whole rock isochron gives an age of 333 ± 26 Ma, with an initial $^{87}Sr/^{86}Sr$ ratio of 0.728± .002. This age is interpreted as the age of amphibolite facies metamorphism.

Wilson and others (in press) in a reevaluation of Aleinikoff and others (1981b) U-Th-Pb interpretations have

suggested the possibility of continuous lead loss. If continuous lead loss has occurred, then the lower intercept age for the augen gneiss (341 ± 3 Ma) is fictitious.

Wilson and others (in press) have also questioned the U-Th-Pb interpretations of Aleinikoff and others (in press) on the Taylor Mountain batholith. If all of the data of Aleinikoff and others (1981a) are plotted, a linear array results, with upper and lower intercept ages of 345 and 161 Ma respectively. Wilson and others (in press) interpret these data to indicate that the Taylor Mountain batholith was derived from, or incorporated zircons from, rocks of the same age (Devonian or Mississippian) as the augen gneiss.

RESULTS

Description of Units

1. Lithology

The lithologic units discussed in this section have previously been described by Foster (1969, 1976) for regional mapping projects. The three units of specific interest have been broadly delineated and described on the Reconnaissance geologic map of the Eagle quandrangle (1976). The same three unit names will be used in this thesis for simplicity and correlation, although descriptions are less general (figure 10).

The quartz-mica schist and greenschist unit (Pzq) is the northernmost group of rocks studied. Within the study area the unit consists mostly of medium dark to dark gray quartz-graphite schist and quartzite with minor phyllite. Interlayered light and medium gray quartz-muscovite schist and quartzite is present. The dark gray quartzite and schist commonly have distinctive layers of cream to white colored quartz a few millimeters to several centimeters in thickness. These layers are commonly tightly folded and discontinuous. Most samples contain quartz and muscovite ± graphite with garnet and/or biotite rarely present. The most distinctive feature of this unit is its graphitic nature.

Minor interlayers of quartz-chlorite schist and

quartzite are present.

Present only locally is a distinctive light green calcareous talc schist and phyllite with minor quartz and sericite. Minor medium to light tan, massive, quartz-carbonate (magnesite) rocks occur usually as large unfoliated blocks, one to several meters across.

Serpentinite blocks or lenses also occur locally from one to several hundred meters across. Most commonly they occur as antigorite and can include associated rocks such as talc, magnesite, and rarely dolomite. The serpentinite was derived mostly from harzburgite and dunite (Foster, 1976).

The biotite gneiss and amphibolite unit (Pzp€b) makes up the southern portion of the study area. This unit consists primarily of medium gray biotite gneiss and medium-dark green amphibolite. Light tan to cream coarse crystalline marble is common usually as discontinuous outcrops that cannot be traced as layers into the biotite gneiss and amphibolite. These outcrops can occur as isolated fold hinges, several to 100 meters in length, or as larger blocks with seemingly less folded internal structure, up to several hundred meters thick. Minor associated rocks include quartz-biotite gneiss and schist, medium gray quartzite with muscovite, and feldspathic gneiss. The pelitic rocks commonly contain observable biotite + muscovite + garnet and the mafic rocks consist of amphibole + plagioclase ± epidote ± carbonate.

Observed locally, usually in the northern portion of this unit, are lenses or blocks or serpentinite from less

than a meter to several meters across.

The third unit studied is a greenstone unit (Pzg) which occurs as large bodies (several kilometers across) in contact with both units previously described. The northern greenstone body (figure 10) studied is a dark green, fine grained mafic rock with rarely observed epidote and amphibole. Amygdules are present locally and commonly filled with calcite. Pillow structures occur locally. This northern body is generally unfoliated, although highly fractured fine grained greenstone is present, usually near contacts with other rocks. In one occurrence, a serpentinized ultramafic lens over 100 meters across occurs at the contact between the greenstone unit and the quartz mica schist unit. The southern greenstone body, (figure 10), consists of similar mafic rocks, although no definite pillow structures were observed. Other rocks associated with this southern unit include chert, limestone, and quartzite, but occur these only in minor amounts.

2. Age of Units

Very little is known about the age of the rocks within the study area. The biotite gneiss and amphibolite unit (Pzpϵb) was formally included in the Precambrian Birch Creek schist by Mertie (1937). Poorly preserved crinoid columnals were found in crystalline marble within the mapped unit (Foster, 1976). The age, therefore,is uncertain but probably mostly Paleozoic, and could include rocks of

FIGURE 10: Map showing location of units within the study area (after Foster, 1976).

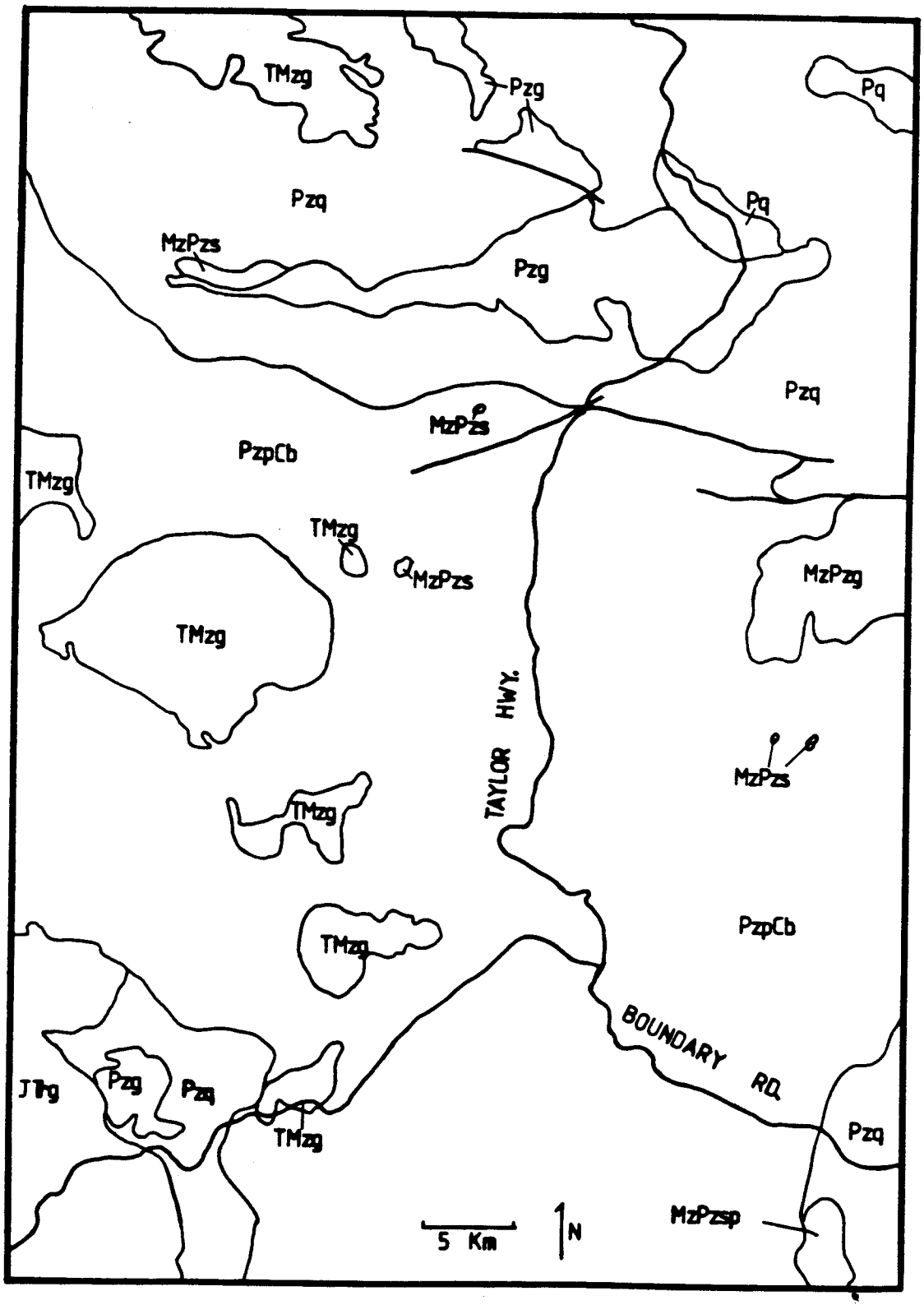
TMzg
Pzg
Pq
Pzq
Pq
MzPzs
Pzg
Pzq
MzPzs
PzpCb
TMzg
TMzg
QMzPzs
MzPzg
TMzg
TAYLOR HWY.
MzPzs
TMzg
TMzg
PzpCb
BOUNDARY RD.
JTrg
Pzg
Pzq
TMzg
Pzq
5 Km
N
MzPzsp

Precambrian and/or Mesozoic age.

The quartz-mica schist unit (Pzq) was partly included in a group of undifferentiated Devonian rocks by Mertie (1937). Poorly preserved crinoid columnals were found in marble at several localities within the unit as mapped by Foster (1976). None of the above localities are within the study area for this thesis. Therefore, the age of the unit is uncertain, but it is likely that it is mostly Paleozoic, and could include Precambrian and/or Mesozoic strata.

The age of the greenstone unit (Pzg) is also unknown. No fossils have ever been recovered from sedimentary rocks directly associated with the greenstones. The northern greenstone body is in contact with only slightly metamorphosed sedimentary rocks that have been correlated with Permian rocks to the northwest (Foster, 1976). The identified Permian rocks include two localities of fossiliferous quartzite with well preserved brachiopods. These localities are just south of the Seventy Mile River and have been associated with the ophiolite at Mt. Sorenson (Keith and others, 1981). It is therefore possible that the northern greenstone body within the study area and the related sedimentary rocks are of Permian age.

3. Metamorphic Grade

The conditions of metamorphism have not been analyzed in detail for this study. During the course of general petrographic studies, significant mineral assemblages and textures were noted and used to interpret the metamorphic

grade of the various units. Pelitic rocks within the quartz-mica schist unit (Pzq) primarily contain quartz + muscovite + plagioclase + chlorite + graphite. This assemblage in pelitic rocks is generally considered stable in the chlorite zone of the greenschist facies (Miyashiro, 1973). At one locality, possibly within a fault slice, the assemblage quartz + muscovite ± plagioclase + garnet + biotite + minor chlorite was observed. This assemblage is generally considered stable in the almandine zone of the epidote-amphibolite facies (Miyashiro, 1973). Therefore, within the study area, the rocks of the quartz-mica schist unit (pzq) have been metamorphosed to the greenschist facies except for the possible fault slice mentioned above.

The biotite gneiss and amphibolite unit (Pzpєb) contains pelitic rocks with the primary assemblage quartz + muscovite + plagioclase + biotite + garnet + opaques. This assemblage is stable in the epidote-amphibolite and amphibolite facies (Miyashiro, 1973). The general absence of chlorite suggests the assemblage is stable in the upper epidote-amphibolite facies and amphibolite facies. The mafic rocks in this unit contain the primary assemblage quartz + amphibole + plagioclase ± muscovite ± chlorite ± epidote ± biotite ± garnet. When observed, chlorite is commonly intergrown with biotite and/or garnet and may represent later replacement or retrogradation. Epidote is present in minor proportions in some samples and is completely absent in others. Amphibole generally displays blue-green to pale brown pleochroism and is most probably hornblende. These assemblages are

characteristic of mafic rocks metamorphosed to the upper epidote-amphibolite to amphibolite facies (Miyashiro, 1973).

The greenstone unit (Pzg) consists almost entirely of mafic rocks with the metamorphic assemblage quartz + epidote + chlorite + actinolite + carbonate. Relict igneous textures and minerals are commonly present. This mineral assemblage is characteristic of the greenschist facies.

All of the facies discussed above are considered to be in the medium pressure facies series (Miyashiro, 1973).

Structure

1. General Statement

The structural elements within each unit were studied on a regional scale primarily along two major traverses within the study area. A north-south traverse along the Taylor Highway was the longest and most detailed. an east-west traverse by boat along the Forty Mile River aided the structural analysis greatly due to the good exposure. A second phase of the structure study was a detailed analysis of a complex series of faults between and within the biotite gneiss unit (Pzpeb) and quartz-mica schist unit (Pzq) (figure 11). The regional structural elements within each unit will be described first. Based on overprinting relationships, a relative sequence of structural generation development has been worked out and the structures are described here from oldest to youngest.

2. Structural Elements: Quartz-Mica Schist Unit

This unit has a well developed foliation that is defined in the schist by the planar orientation of muscovite and chlorite. In the more quartzitic rocks, this foliation takes the form of a fracture cleavage defined by closely spaced fractures that divide the rock into a series of tabular or planar bodies. This foliation is very well developed locally and defined by closely spaced (1-20 mm) fractures with a concentration of graphite on the foliation

FIGURE 11: Map showing locations of studied faults within the field area.

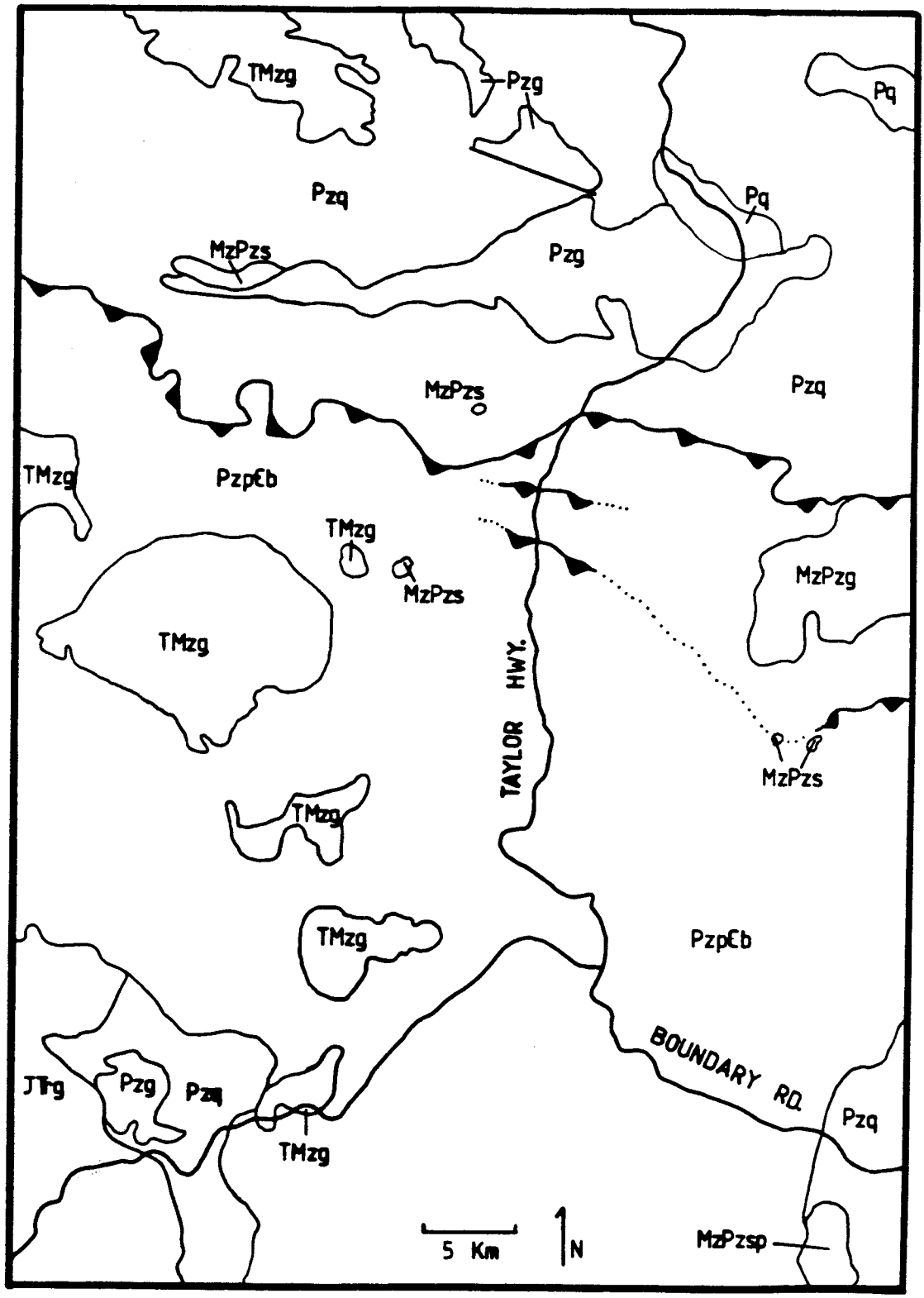
TMzg
Pzg
Pq
Pzq
Pq
MzPzs
Pzg
MzPzs
Pzq
TMzg
PzpCb
TMzg
MzPzs
MzPzg
TMzg
TAYLOR HWY.
MzPzs
TMzg
TMzg
PzpCb
BOUNDARY RD.
JTrg
Pzg
Pzq
TMzg
Pzq
5 Km
N
MzPzsp

surface. This foliation is commonly parallel to compositional layering where discernable. No sedimentary structures are evident, so the relationship between bedding and compositional layering is not known. Poles to this foliation are plotted on a stereogram and they display a well defined north-south girdle representing approximately east-west striking foliations (figure 12). The girdle is symmetric about the equator, representing foliation planes dipping to the north and south generally from about 60° to horizontal.

The first generation of folds (F_1) observed in this unit are tight to isoclinal, and they fold compositional layering and the prominent foliation. Folds are inclined to recumbent and range in wavelength and amplitude from a few millimeters to several meters. Fold closures are generally rounded. Characteristic of this unit are small (1-10 cm amplitude and wavelength), asymmetric, rootless folds, defined by cream to white colored, fine grained, polycrystalline quartz (plate 1). These rootless folds are rarely truncated by an axial planar fracture cleavage. In a single outcrop, these distinctive quartz bands can be variably folded from lens shaped structures to asymmetric sigmoids, to complex refold structures (figure 13). In most cases, such structures are confined between two fracture cleavage surfaces, but rarely, they are cut by the cleavage.

The trend and plunge of the first generation folds (F_1) and related fold axis lineations are plotted on a stereogram

FIGURE 12: Stereogram - quartz-mica schist unit. Poles to foliations (81)

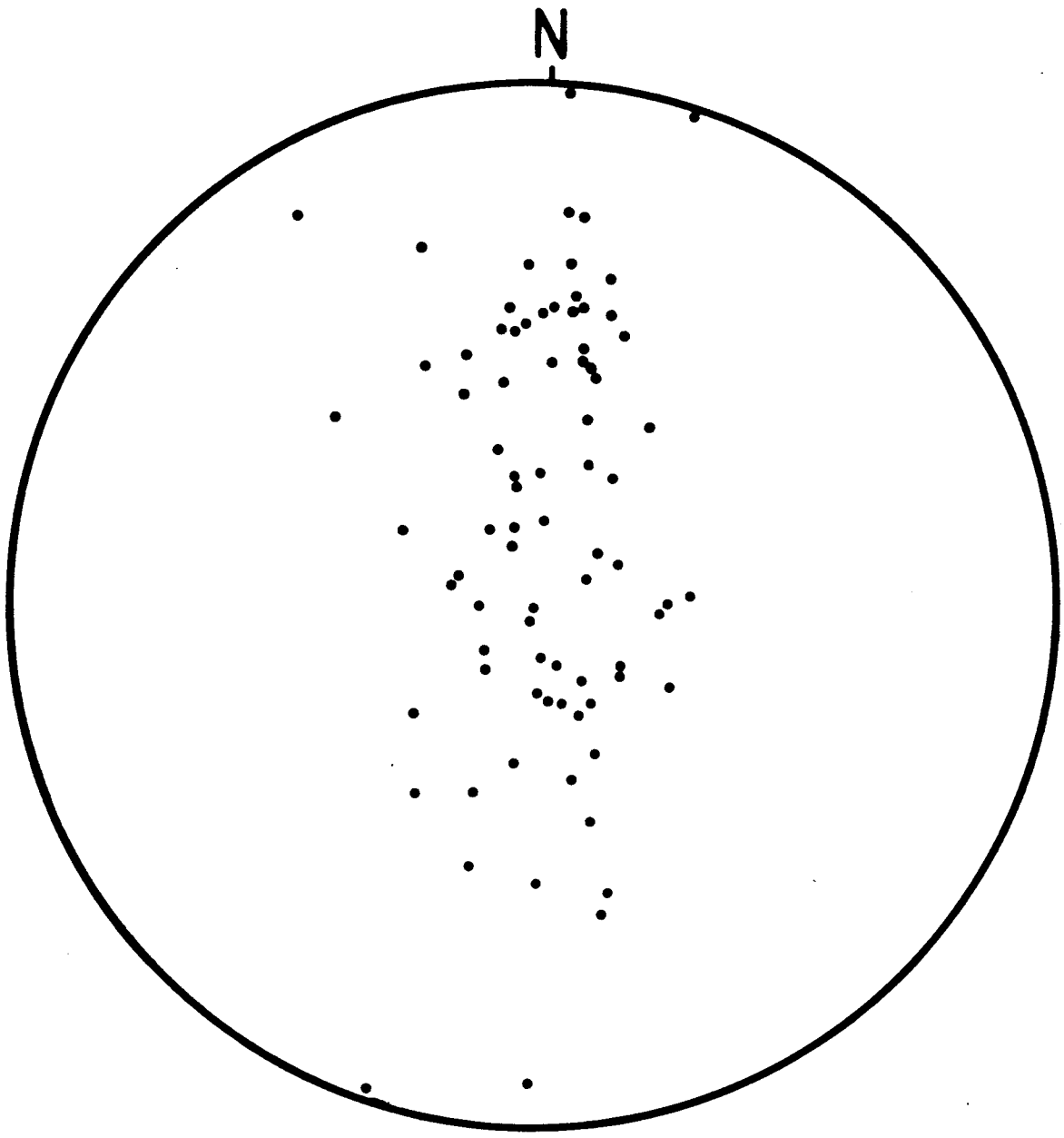
N

PLATE 1: Photograph of asymmetric, rootless folds, defined by cream colored polycrystalline quartz.

PLATE 1: Photograph of asymmetric, rootless folds, defined by cream colored polycrystalline quartz.

FIGURE 13: Diagramatic sketch of the variation in deformed quartz bands: 1-4 progressive deformation of quartz bands (drawn to scale).

1

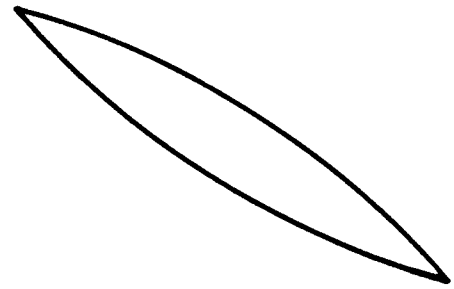

2

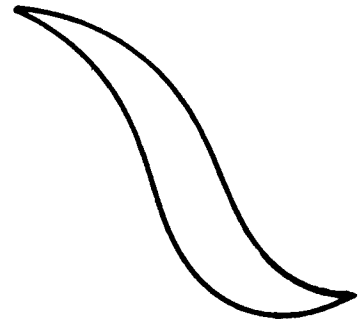

3

4

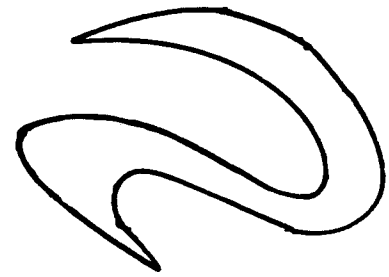

in figure 14. This plot shows two concentrations, one in the west-northwest quadrant, and the other in the east-southeast quadrant. This pattern represents shallowly plunging fold axes (0-20o) that trend in an east-southeast - west-northwesterly direction (average trend N68W). The two maxima are probably the result of the later folding event (F_1).

The second fold generation (F_2) is recognized as a very gentle open folding of all previous structures. These folds are generally symmetric with rounded fold closures. The wavelength of these folds is on the order of 0.5 meters with an average amplitude of about 10 centimeters. The trend and plunge of fold axes and fold axis lineations are plotted on a sterogram in figure 15. It is evident that the average lineation strikes approximately N5-10W and plunges a few to 25o to the southeast and northwest. An axial plane cleavage is rarely observed, but where present, its average strike is about north-south (figure 15). There is some scatter in the points to the east and west, representing the fanning of cleavage around fold hinges. Cleavage fans have been observed within a single fold hinge in the field.

3. Structural Elements: Biotite Gneiss and Amphibolite Unit

The prominent foliation in this unit (S_1) is defined by preferred orientation of micas in the schist and hornblende in the amphibolites. There is little evidence in the field

FIGURE 14: Stereogram - Quartz-mica schist unit - Tight folds (F1): Fold axes and fold axis lineations (124).

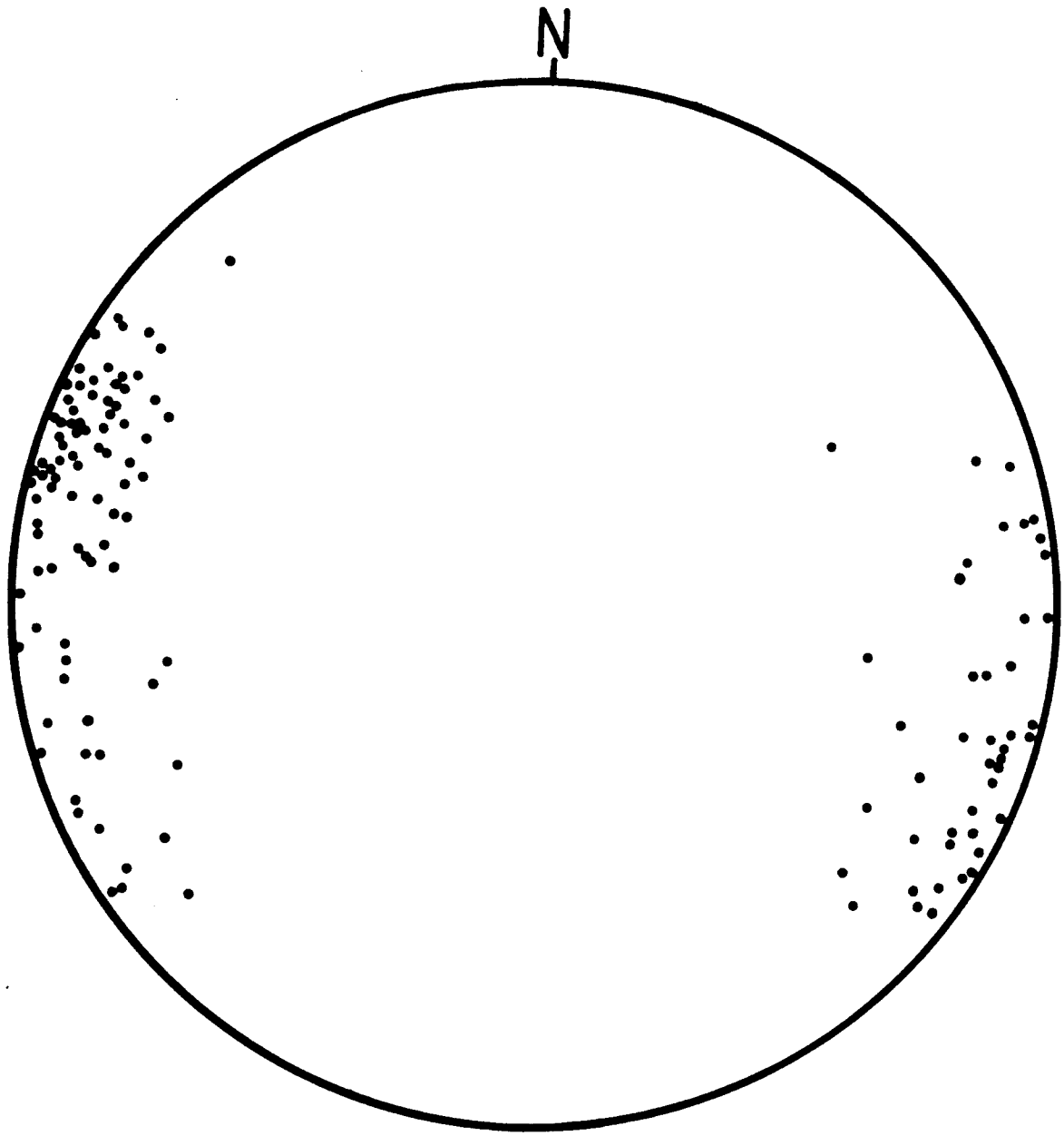
N

FIGURE 15: Stereogram - quartz-mica schist unit. open fold generation F2.

. = Fold axes and fold axis lineations (18)

+ = Axial plane cleavage (22)

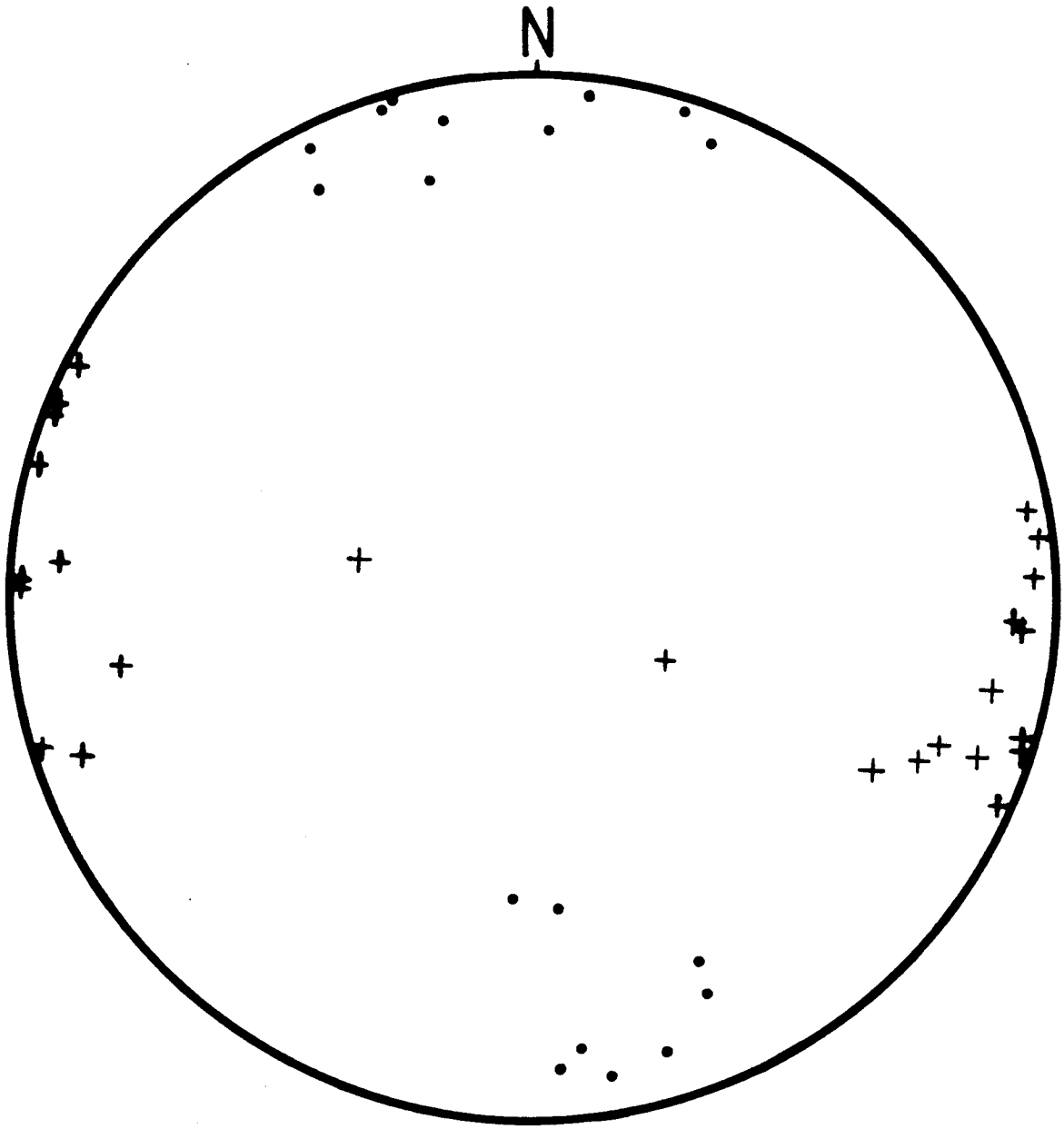
N

that this foliation is an axial planar foliation. In a few localities, small rootless folds (F^1) have been observed with the prominent foliation axial planar. These occurrences are seen in the amphibolites and the folds were defined by discontinuous plagioclase layers. Poles to this foliation (S^1) are plotted on a stereogram in figure 16. Two dominant concentrations are observed; one in the northwest quadrant, and the other in the southeast quadrant. There is some suggestion of a girdle across the center of the stereogram although the two maxima dominate the pattern on the stereogram. The greater number of points observed in the southeast quadrant represents the asymmetric nature of the second generation folds (F^2) in this unit.

The second generation folds (F^2) in this unit are asymmetric, tight, and vary in wavelength and amplitude from approximately 0.5 to several hundred meters. These structures fold compositional layering and the prominent foliation. These folds (F^2) are upright (vertical axial plane) to inclined and have rounded closures. Generally, there is no axial planar fabric developed but, rarely, in fold hinges, there is the incipient development of such an axial planar structure. The trend and plunge of fold axes and fold axis lineations of this generation are plotted on the stereogram in figure 17. Two concentrations are evident from the plot; one in the northeast quadrant, and the other in the southwest quadrant. It is clear that the fold axes plunge only gently in the two directions; generally from 0^o to 20^o. The average trend of these folds is about N35E as

FIGURE 16: Stereogram - Biotite gneiss and amphibolite unit: poles to foliations (S1) (189).

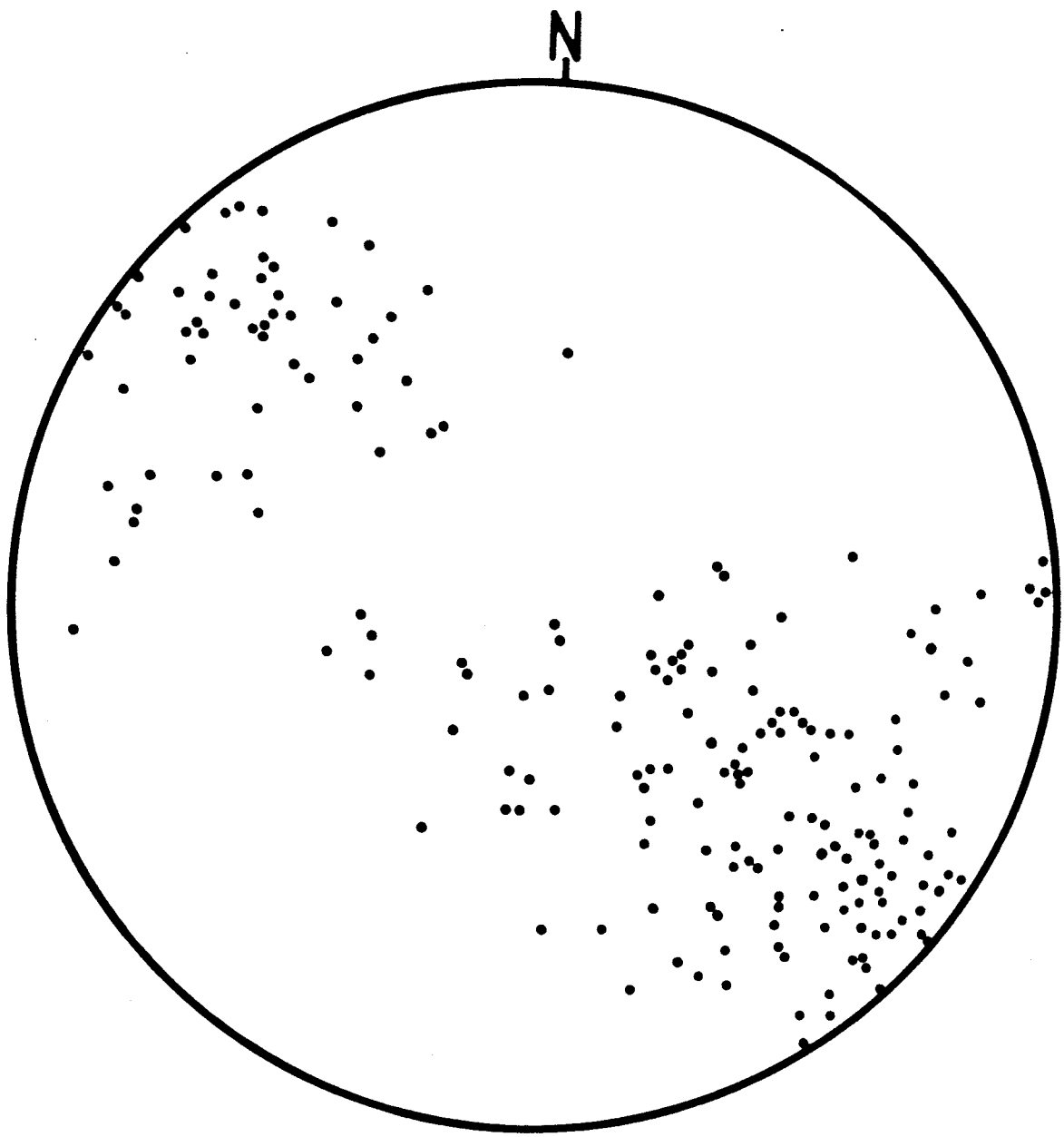
N

FIGURE 17: Stereogram - Biotite gneiss and amphibolite unit: Tight folds F2: Fold axes and fold axis lineations (115).

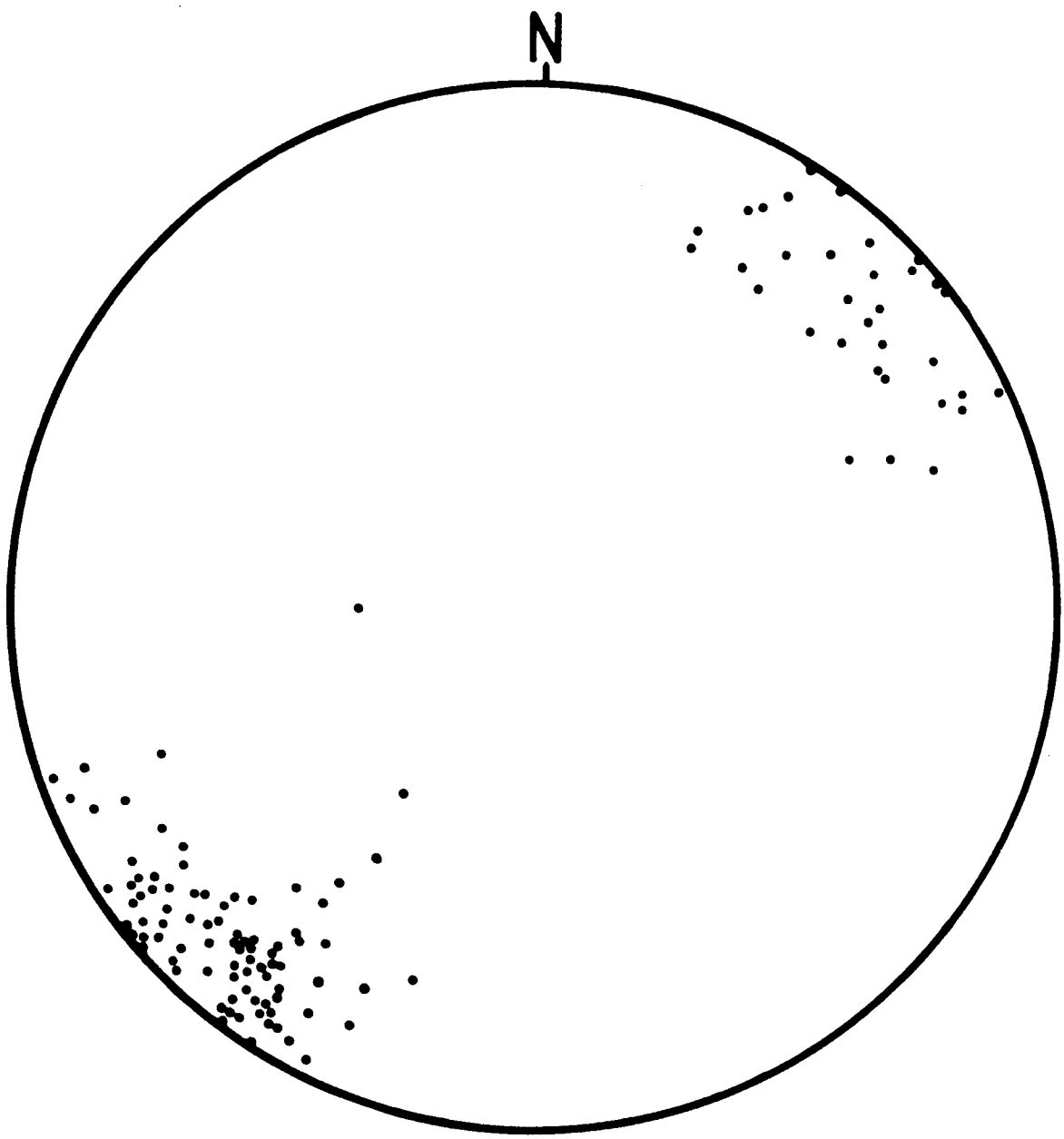
N

suggested by the stereogram in figure 17.

The third generation of folding (F_3) in this unit is recognized as a gentle open folding of all previous structures. The wavelength of these folds is about 0.5 meters with an average amplitude of about 10 centimeters. The folds are symmetric with rounded closures. The trend and plunge of fold axes and fold axis lineations of this generation are plotted on a stereogram in figure 18. The average lineations strikes approximately north, as can be seen on the stereogram. The plunge of these fold axes is gentle, ranging from about horizontal to 25°. An axial planar cleavage is rarely observed, but where present, it strikes about north-south (figure 18). The scatter in the poles to the axial planes is attributed to the cleavage fanning around the fold hinge.

4. Structural Elements: Greenstone Unit

The greenstone unit in general is apparently much less deformed than the other two units previously discussed. In general, no prominent foliation is observed. Large outcrops of greenstone show at least two widely spaced (0.5 to 3 m) joint patterns. Other indications of strain are preserved pillow structures that appear deformed, yet have maintained their basic configuration. Although a prominent foliation was not observed throughout the greenstone units, locally such a structure is present and occurs as a subhorizontal fabric. At two localities, there is a closely spaced (1-5

FIGURE 18: Stereogram - Biotite gneiss and amphibolite unit: Open folds F3.

. = Fold axes and fold axis lineations (43)

+ = Axial plane cleacage (17)

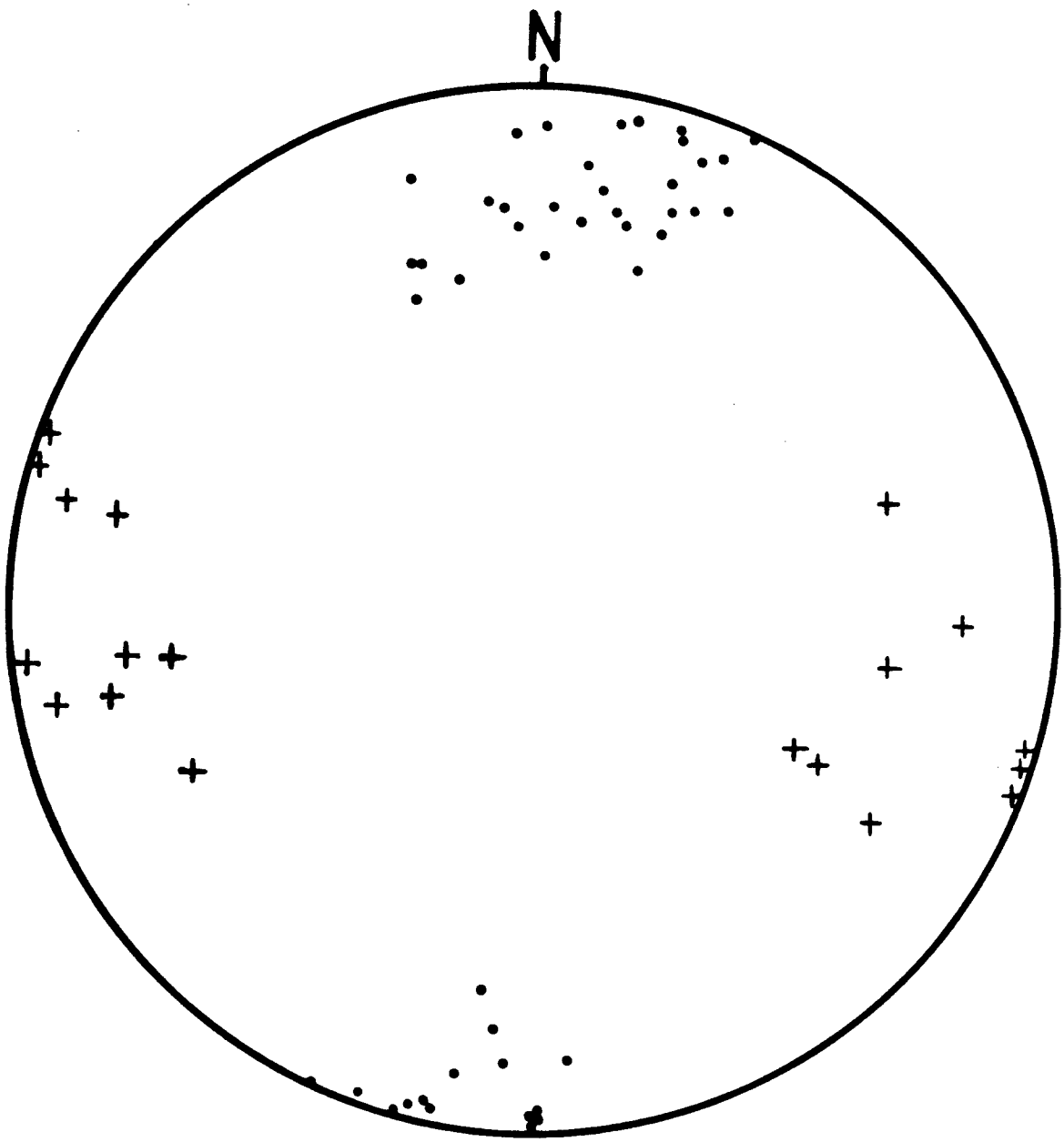
N

cm) fracture cleavage developed in the greenstone; this fabric seemed to progressively intensify near the contact with the country rock. A general gradation was observed from relatively massive greenstone to fissile, well cleaved greenstone.

5. Fault Zones

(a) General Statement

A series of faults between and within the biotite gneiss and amphibolite unit and the quartz-mica schist unit were studied to determine their significance. Three major fault zones were selected for detailed study. The northernmost fault is at the contact between the two units and is exposed along the Taylor Highway for over 260 meters (plate 2). The central fault zone is located approximately 3 kilometers south of the northern fault zone and is also exposed along the Highway. The third fault zone studied, the southern fault zone, is located 3 kilometers south of the central zone. There were numerous other faults observed within each of the units although the three described above were the largest and the best exposed.

(b) Northern Fault Zone

The northern fault zone contains slices of both the gneiss and schist units. The fault zone is best exposed along a north-south portion of the Highway and strikes approximately east-west. Graphitic fault gouge has washed down over much of the exposure making individual rock types difficult to identify from a distance (plate 2). On the south side a fairly continuous section of quartz-biotite gneiss with minor amphibolite can be traced up to the fault zone. Within the fault zone, individual blocks or slices of

FIGURE 19: Map of studied fault zones.

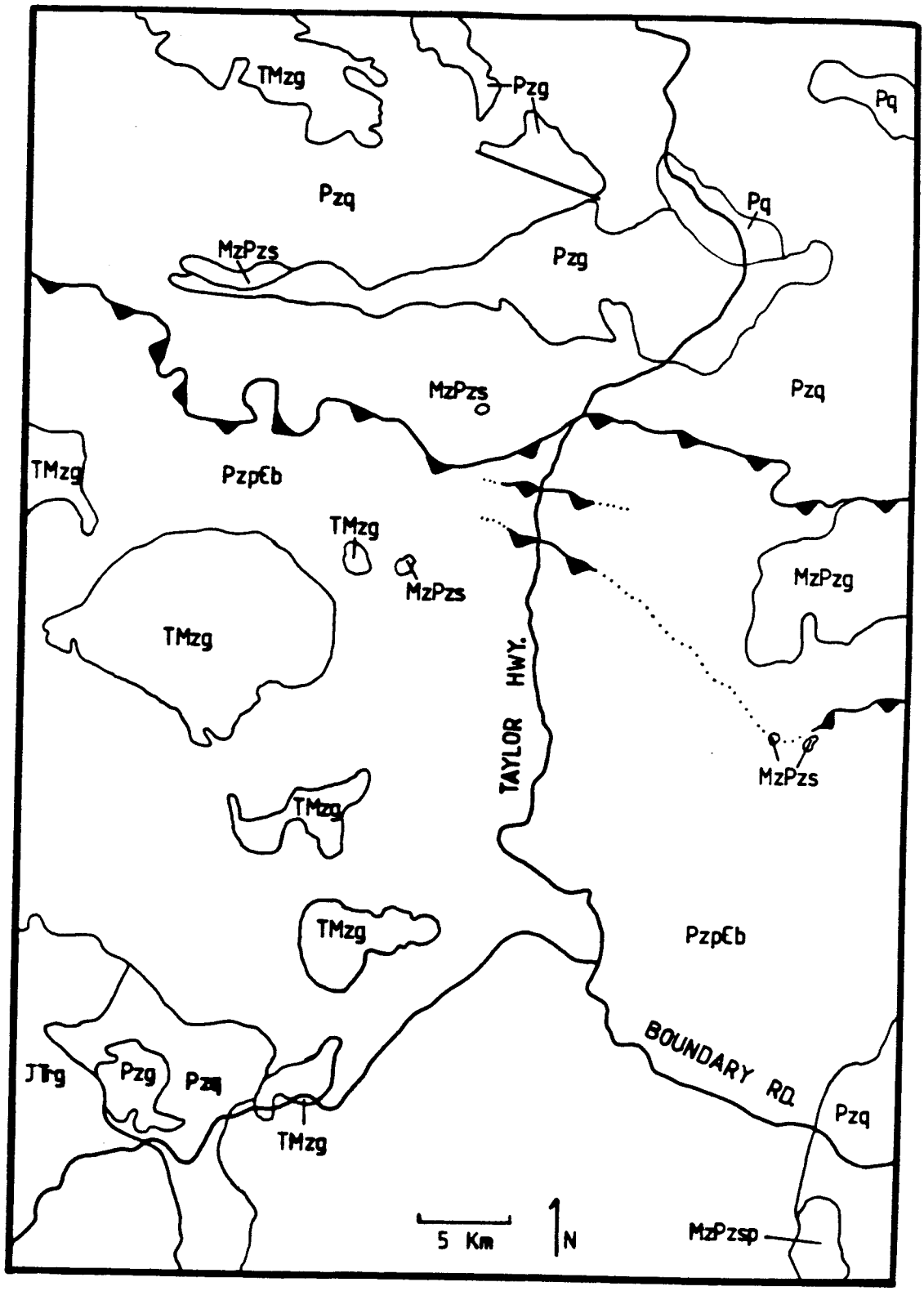
TMzg
Pzg
Pq
Pzq
Pq
MzPzs
Pzg
MzPzs
Pzq
TMzg
PzpEb
TMzg
MzPzs
MzPzg
TMzg
TAYLOR HWY.
MzPzs
TMzg
TMzg
PzpEb
BOUNDARY RD.
JTrg
Pzg
Pzq
Pzq
TMzg
5 Km
N
MzPzsp

PLATE 2: Northern fault zone along Taylor Highway (highway is oriented north-south): Gouge has washed down over much of the exposure.

PLATE 2: Northern fault zone along Taylor Highway (highway is oriented north-south); Gouge has washed down over much of this exposure.

the two units are identified and range in size from a few centimeters to several meters across. Most of the slices consist of the typical lithologies observed within the two units. Quartz-biotite gneiss and quartzite, amphibolite ± biotite and garnet are the most common fault slices of the gneiss unit. Medium dark gray to dark gray graphitic quartzite and schist make up the fault slices of the quartz-mica schist unit. In addition to the above rock types, blocks of silicified metamorphic rocks are common in the fault zone. These rocks rarely contain a recognizable foliation and generally consist almost entirely of silica (plate 3). These blocks are surrounded by a foliated or cleaved matrix of gouge and lensoid microlithons. A relatively small (0.5 - 1 m), well foliated (fractured) zone of serpentinite was observed at one locality. The gouge in this zone is soapy and weathered a distinctive light olive green. Also observed was one distinctive block of silica-carbonate rock. This block is several meters long and contains silica, carbonate (magnesite/dolomite) and possible fuchsite. At the northern end of the exposed fault zone is a slice of garnetiferous graphitic schist that may be a higher grade equivalent of the typical graphitic schist member.

Between single fault slices and/or blocks are gouge zones, unconsolidated breccia zones, and foliated or fracture cleaved gouge or breccia zones. These zones range in width from a few centimeters to several meters (plate 4). The foliated gouge and breccia zones consist of poorly

PLATE 3: Northern fault zone: Block of silicified metamorphic rock in matrix of unconsolidated fault gouge.

PLATE 3: Northern fault zone; Block of silicified metamorphic rock in matrix of unconsolidated fault gouge.

PLATE 4: Northern fault zone: Fault zone containing unconsolidated fault gouge.

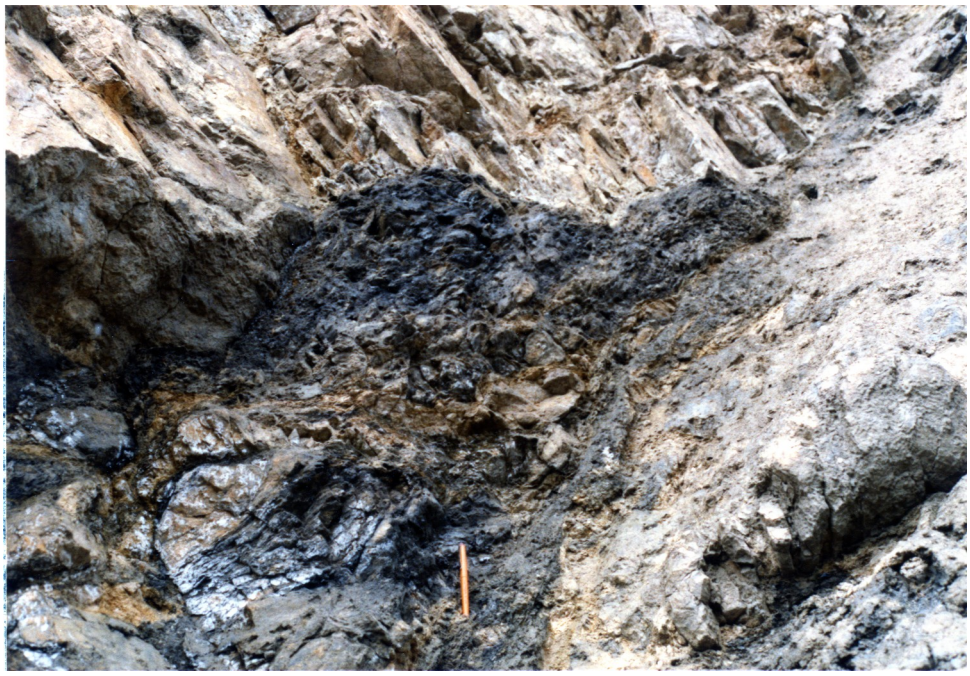

PLATE 4: Northern fault zone; Fault zone containing unconsolidated fault gouge.

consolidated material that is fractured into discontinuous lensoid shaped pods. These zones also contain small (one to several centimeters long) lensoid shaped microlithons. These microlithons can generally be identified as belonging to one of two distinct units. These foliated zones commonly contain fold closures and fold axes in a wide variety of orientations. The occurrence of these fault slices and blocks in a highly deformed matrix classifies this zone as a fault related melange.

Prominent zones of dislocation between specific fault slices were studied to determine the orientation of major fault planes. Foliations or fracture cleavage orientations in the matrix between these fault slices are plotted on a stereogram in figure 20. This stereogram shows two general populations of points. The larger set of points plot in the north-northeast quadrant and represent west-northwest - east-southeast striking foliations that dip from about 60 to 85 degrees to the south. A second population, with about one half as many points, plot in the south-southwest quadrant and represent west-northwest - east-southeast striking foliations that dip from about 40 to 80 degrees to the north. The orientations of these specific fracture surfaces probably represent the orientations of major fault planes in this zone.

Also plotted on a stereogram (figure 21) are foliations measured within massive slices and blocks in the fault zone. The specific unit from which a foliation was measured is

FIGURE 20: Stereogram - Northern fault zone: Poles to foliations or cleavage orientations in matrix between distinct fault slices.

. = Biotite gneiss and amphibolite unit (30)

+ = Quartz-mica schist unit (7)

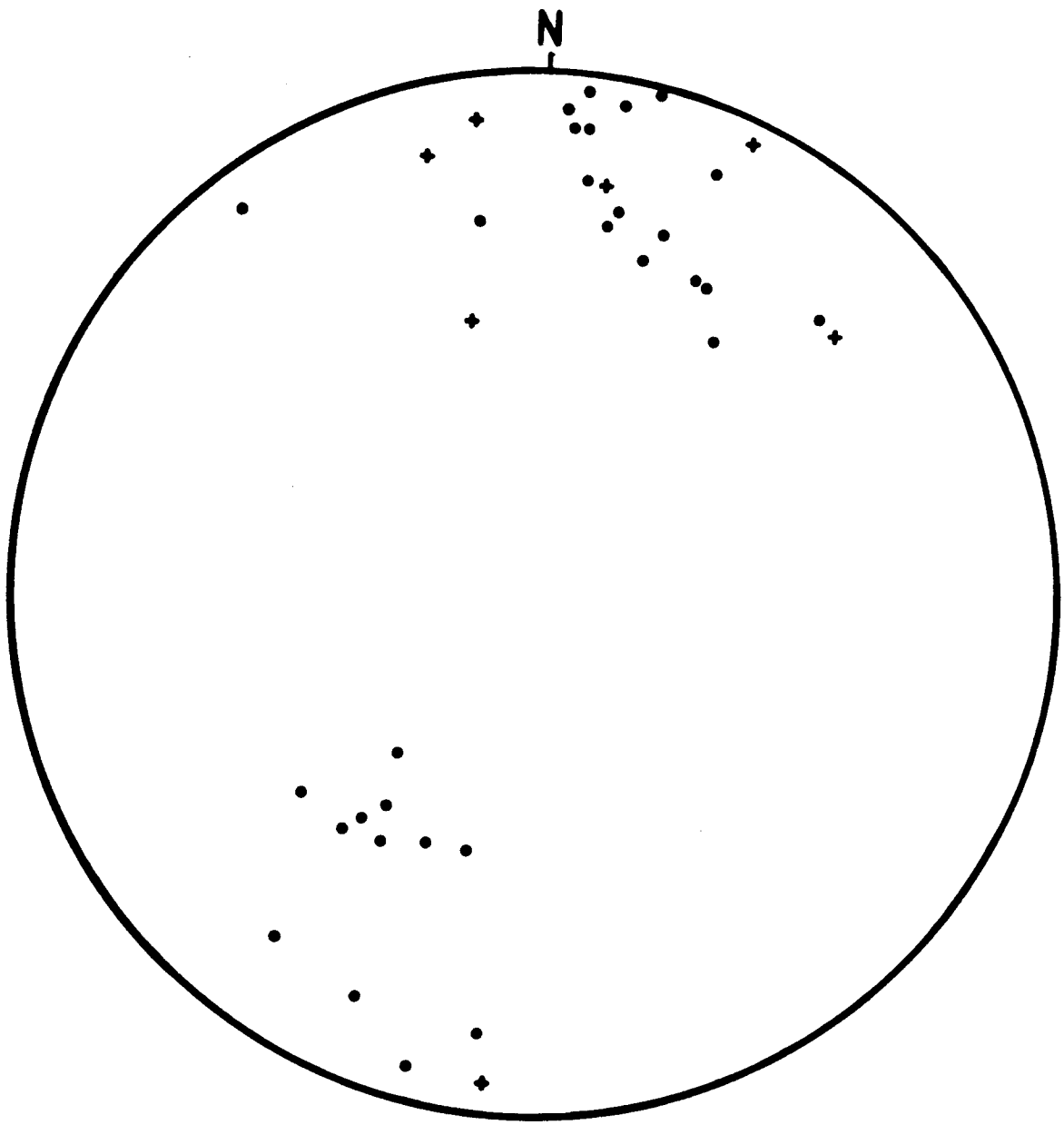
N

FIGURE 21: Stereogram - Northern fault zone: Poles to foliations within massive slices in the fault zone.

. = Biotite gneiss and amphibolite unit (32)

+ = Quartz-mica schist unit (25)

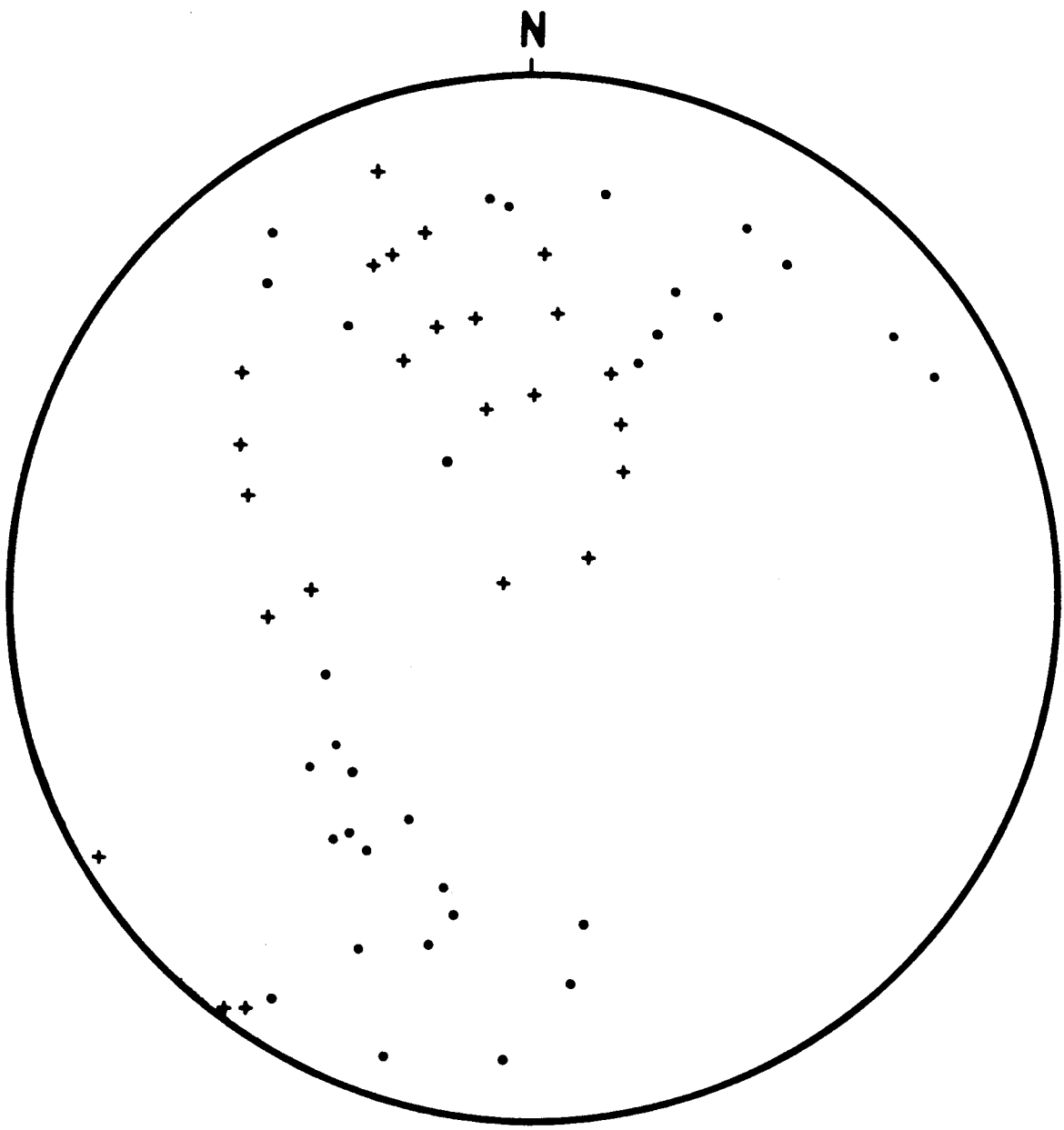
N

specified on the stereogram and the individual patterns overlap. These foliations show the same general pattern as do the foliations measured in the matrix between fault slices (figure 20).

Fold axes observed within the massive rock units are plotted on a stereogram in figure 22. The two units are again differentiated by different symbols on the stereogram and their individual patterns are indistinguishable. The main concentration of points is in the southeast quadrant and represent northwest-southeast trending axes. Many of the folds in this group fold both massive rock and highly fractured zones (plate 5). This may suggest a cogenetic relationship between folding and faulting in this melange.

(c) Central Fault Zone

The central fault zone primarily consists of rocks of the biotite gneiss and amphibolite unit, although there are blocks or slices of highly graphitic schist with garnet that may be a higher grade equivalent of the graphitic member of the quartz-mica schist unit. This fault zone is exposed along a steep cut parallel to the highway for several hundred meters. This zone is much more coherent than the other two fault zones in terms of the identification of individual faults, their orientations, and directions of apparent offset.

The best exposed fault in this zone is characterized by a 1 to 3 meters wide fractured gouge zone, which separates

FIGURE 22: Stereogram - Northern fault zone: Fold axes orientations obtained from massive rocks within the fault zone.

. = Biotite gneiss and amphibolite unit (17)

+ = Quartz-mica schist unit (16)

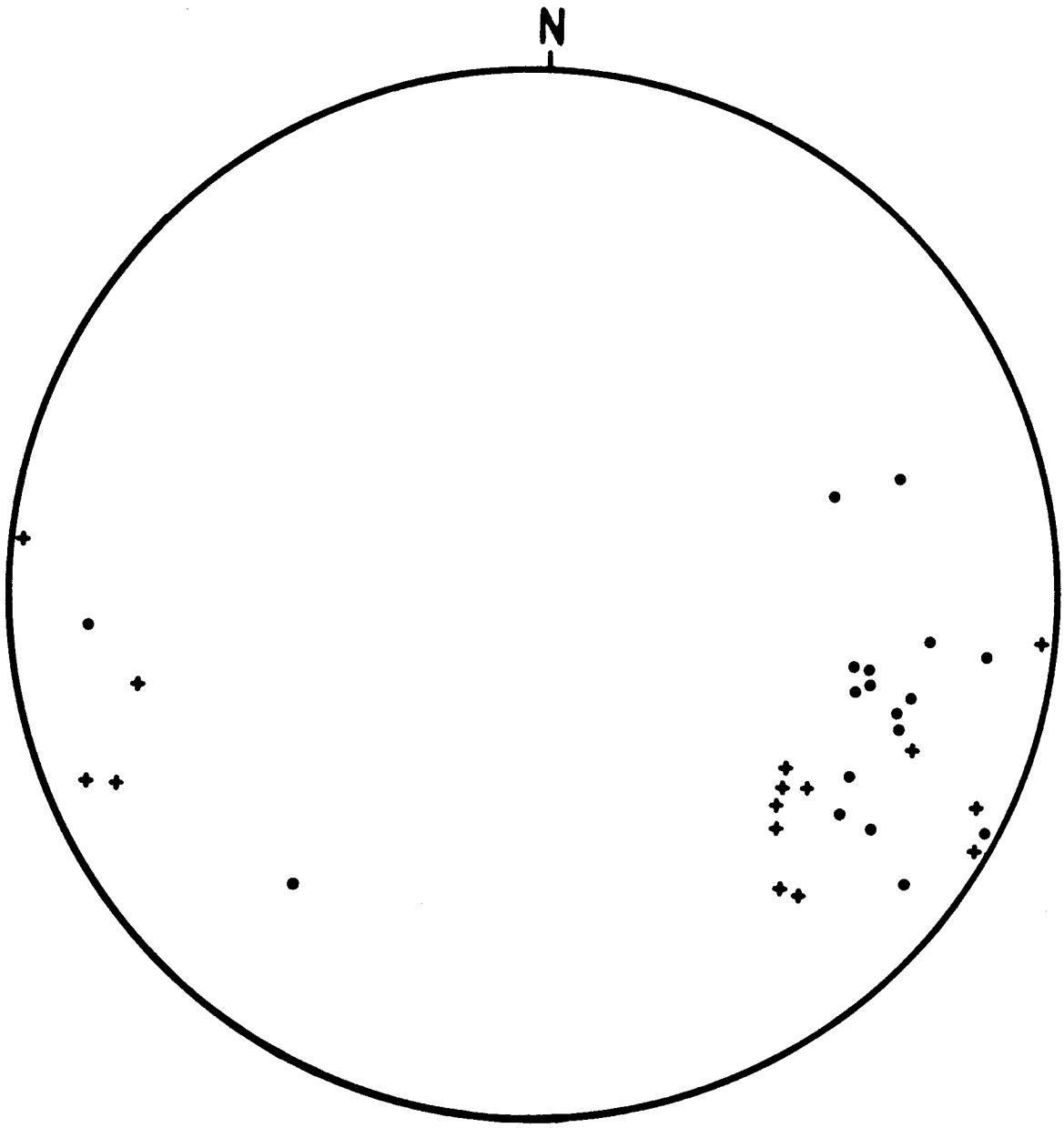
N

PLATE 5: Fold of both massive biotite quartzite and highly fractured, unconsolidated, fault gouge.

PLATE 5: Fold of both massive biotite quartzite and highly fractured, unconsolidated, fault gouge.

two slices of quartz-biotite gneiss (plate 6). This fault is parallel or subparallel to the near horizontal foliation in the gneiss at the base of the outcrop. The fault steepens to almost vertical at the top of the exposure (see plates 6 & 7). The orientation of the fault plane varies from N85 - 30E, with southeast dips ranging from 85 to 15°. The foliation in the gneiss on either side of the fault plane is near horizontal, except close to the fault, where a large bend fold is evident (plate 8). This large fold appears to be divided or cut by the fault plane, and may be genetically related to it. The two end member interpretations for such folds are: (1) the fold formed by "drag" along the fault plane, or, (2) the fault plane developed along a zone of weakness within the fold structure. Also evident at this one fault locality are conjugate faults that intersect the main fault plane at a high angle.

Fold axis orientations in the massive rock were measured within the fault zone for comparison with typical axes in the biotite gneiss unit. These fold axes were measured from rocks within this fault zone, but not from rocks that were obviously disturbed by the individual faults. These axes are plotted in figure 23, and show a widely scattered pattern. The one line plotted on the stereogram represents the entire set of 115 fold axes typical of the gneiss unit. It is evident that the fold axes in the fault zone are not all typical of the gneiss unit.

Fold axes within one of the major gouge zones were

PLATE 6: Central fault zone: Fault separates two slices of quartz-biotite gneiss.

PLATE 7: Central fault zone: Fault plane parallel to sub-parallel to foliation at base of outcrop.

PLATE 6: Central fault zone: Fault separates two slices of quartz-biotite gneiss.

PLATE 7: Central fault zone: Fault plane parallel to sub-parallel to foliation at base of outcrop.

PLATE 8: Central fault zone: Large bend fold associated with fault.

PLATE 8: Central fault zone: Large bend fold associated with fault.

analyzed to determine their significance. A particular series of fold axes could be traced within the gouge zone from the hanging wall block towards the center of the zone. These fold axes are plotted on a stereogram in figure 23 and are numbered progressively from the hanging wall towards the center of the gouge zone. Also plotted on the stereogram is the line representing the fault plane. The fold axes in the gouge fall close to a great circle that intersects the fault plane at the first fold axis. This relationship may indicate a progressive rotation of the fold hinges into the thrusting direction.

Most of the rock types juxtaposed in this fault zone are easily classified as members of the biotite gneiss and amphibolite unit. Across the more steeply dipping faults, like the one previously described, well foliated pelitic, psammitic, and mafic rocks of epidote-amphibolite to amphilbolite facies grade are observed. Near the base of the exposed outcrop are several subhorizontal faults, which juxtapose highly graphitic schists, some of which contain garnets. Although highly interpretative, it is possible that the garnetiferous graphitic schists are higher grade equivalents of the graphitic member of the quartz mica-schist unit.

FIGURE 23: Stereogram - Central fault zone.

. = Fold axis orientations

o = Fold axis orientations in foliated (fractured) fault material.

_____ Set of 115 fold axis orientations of the gneiss unit.

+# Progression of fold axes in foliated (fractured) fault material from hanging wall (+1) to center of fault zone (+5).

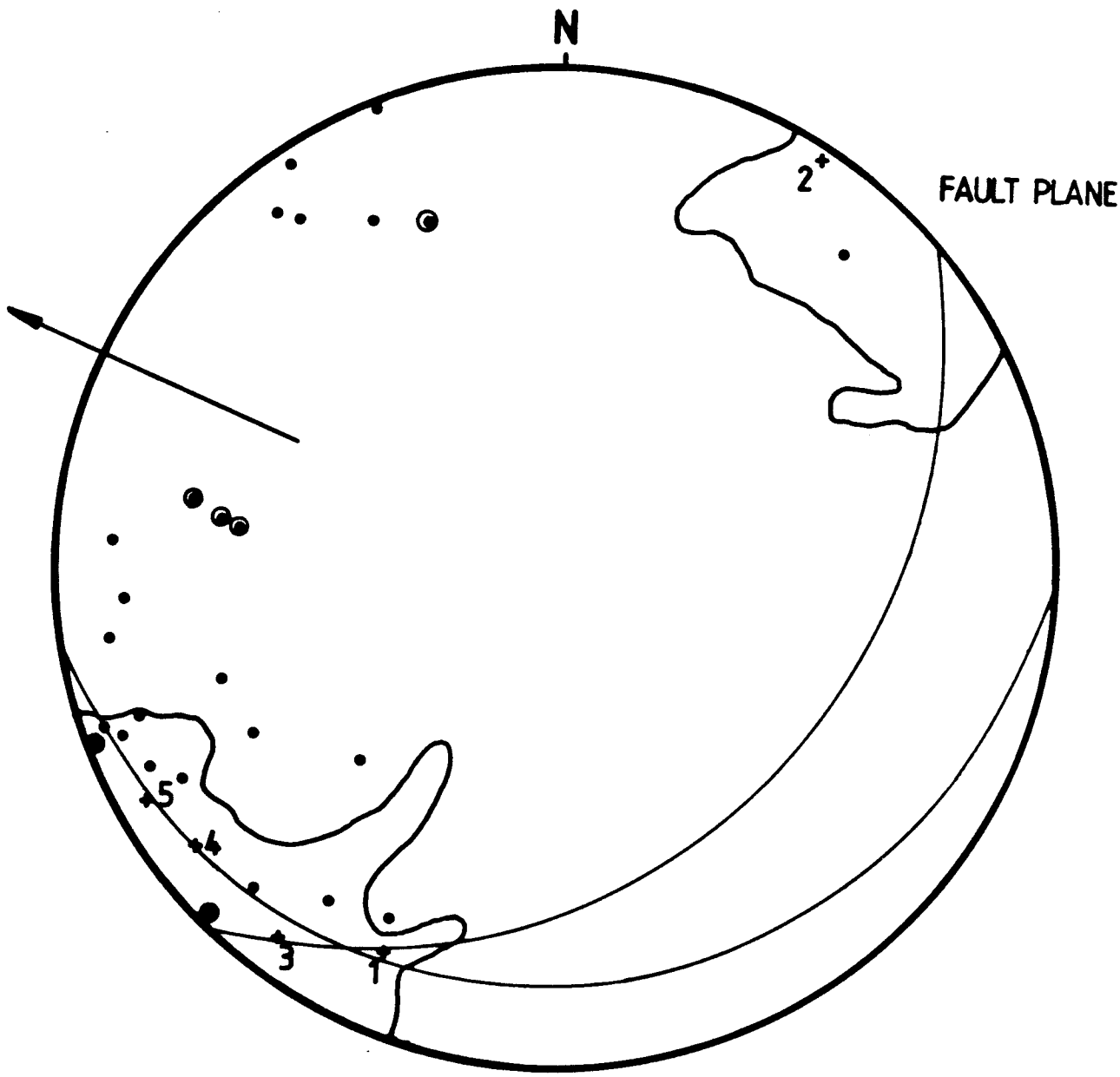
N
FAULT PLANE
2+
5
4
3
1

(d) Southern Fault Zone

The southernmost fault zone is the smallest of the three studied and is the most chaotic. It consists primarily of blocks ranging from a few centimeters to several meters across that lie in a cleaved matrix. This zone clearly classifies as a fault-related melange. The largest block in this zone is a (3 to 5 meters across) silicified tan-white marble block with minor sulphides and white mica (plate 9). The edges of the block consists of silica + white mica + sulphide + minor carbonate. This block is completely surrounded by the highly fractured, loosely consolidated matrix. Smaller blocks and much of the matrix consist of fractured, brecciated, and ground-up metamorphic rocks, typical of the biotite gneiss unit.

A more continuous outcrop exposure is present on either side of this zone than at the other two zones. Therefore, a study of fold axis orientations was undertaken for comparative purposes. Fold axis orientations taken from both sides of the fault zone are plotted in figure 24. The stereogram also shows the two maxima representing fold axes typical of the biotite gneiss and amphibolite unit.

It is evident that the fold axis orientations close to the fault zone form a pattern on the net extending from the typical maxima of the gneiss unit into the northwest and southeast quadrants. Also plotted are fold axis orientations obtained within the highly foliated matrix.

Although meager, these data show the same general pattern as the fold axes in the massive rocks.

PLATE 9: Southern fault zone: Large tan-white marble block in a highly foliated (fractrued), poorly consolidated fault gouge.

PLATE 9: Southern fault zone: Large tan-white marble block in a highly foliated (fractured), poorly consolidated fault gouge.

FIGURE 24: Stereogram - Southern fault zone: fold axis orientations obtained from both sides of fault zone.

. = Fold axis orientations - massive rock (26).

o = Fold axis orientations from foliated (fractured) fault material (8).

_____ Set of 115 fold axes typical of gneiss unit.

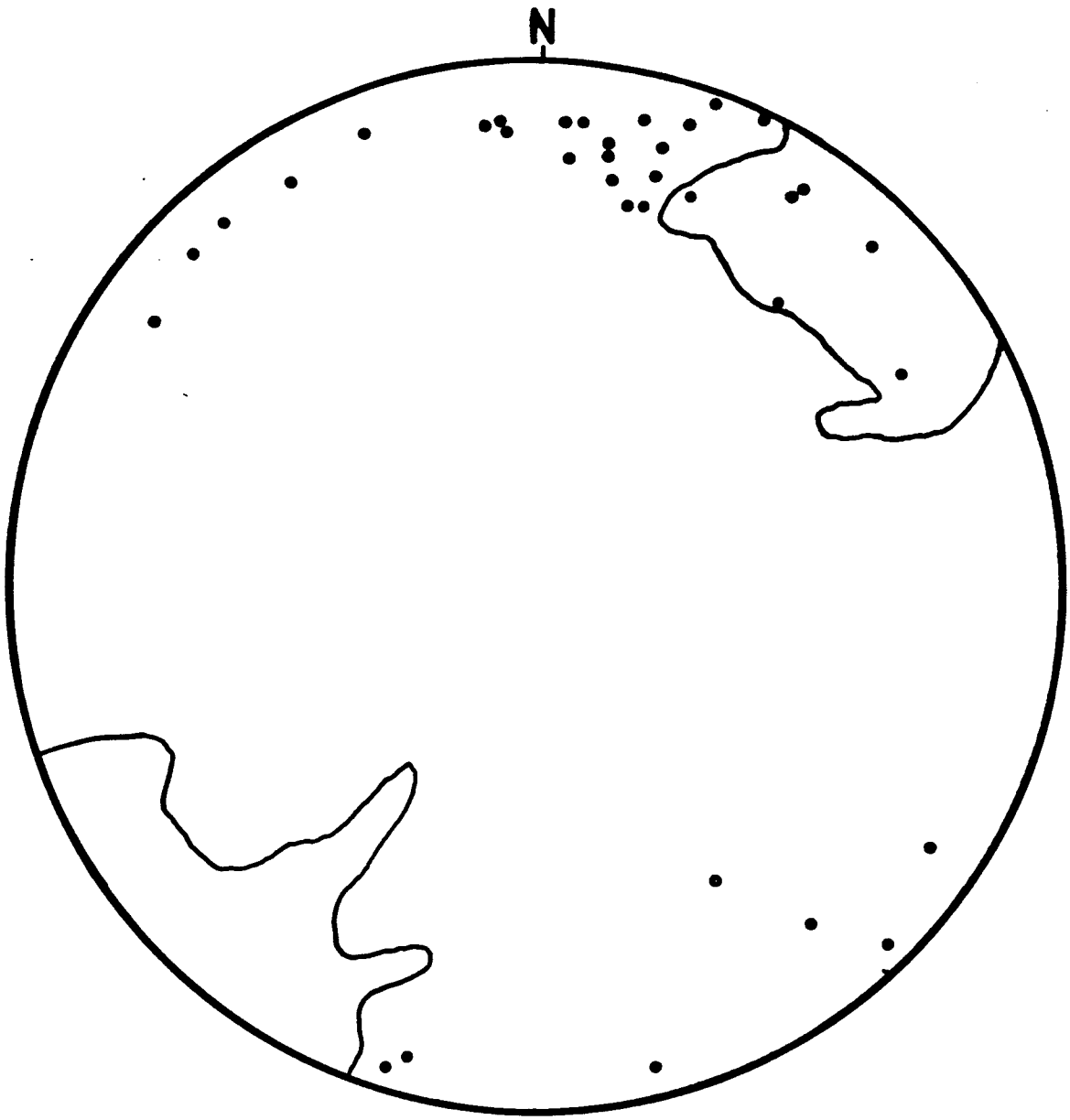
N

Geochronology - Thermal History

1. General Statement

The $^{40}Ar/^{39}Ar$ age spectrum approach has the potential to resolve non-uniform distributions of radiogenic ^{40}Ar that are related to thermal disturbances (e.g. Turner, 1968; Huneke, 1976; Albarede, 1978; Harrison and McDougall, 1980; Harrison, 1983). With the first published age spectrum on a disturbed chondrite, Turner and others (1966) presented a model based on diffusion theory that corresponded well to empirical results. The model (Turner, 1968) indicated that the first infinitesimal increment of gas extracted form a mineral in the laboratory represents the age at which a relatively brief episodic thermal disturbance of the chondrite terminated. Continued gas extractions in the laboratory would sample fractions of gas from the more interior portions of a given crystal. Therefore, this model suggested that the age spectrum represented a general internal distribution of radiogenic 40Ar within a sample.

Several implications of this model were presented by Huneke (1976) and can be used interpreting an age spectra. Although many age spectra from non-terrestrial samples have corresponded well to a diffusive loss model, terrestrial samples were slow to reveal unambiguous results. This, in part, may be due to more complex thermal histories, but is also the result of specific mineralogical characteristics of

earthly samples (Harrison, 1983). Recent studies of the response of terrestrial samples to complex thermal histories have significantly helped refine the interpretation of $^{40}Ar/^{39}Ar$ age spectra (e.g., Hanson and others, 1975; Harrison and McDougall, 1980, 1981, 1982; Harrison, 1981; Harrison and Bé, 1983).

In Turner's (1968) model, it was demonstrated that the age of an episodic gas loss could be determined from the first gas released from a given sample. The model also indicated that an age spectrum was unique to a given amount of outgassing, and that the grain-size distribution also affected the shape of the age spectrum. It was also demonstrated that for large outgassings (greater than approximately 10 to 15%), the terminal or plateau age of a sample could be less than the original cooling age. Numerous studies of terrestrial samples have taken advantage of these various aspects of the technique and determined the age of re-heating and crystallization of thermally disturbed samples. Other studies (e.g. Harrison and McDougall, 1980) have used gas-loss information from the age spectra in conjunction with experimental data to determine the temperature of the sample during a thermal event. These temperature calculations are based on mathematical expressions which represent the distribution of a diffusant in various geometric forms. For a spherical geometry, the radial distribution of a diffusant can be represented as follows (Crank, 1975):

$$\frac{C-C_1}{C_0-C_1} = 1 + \frac{2a}{\pi r} \sum_{n=1}^{\infty} \frac{(-1)^n}{n} \sin \frac{n\pi r}{a} \exp -\left(Dn^2 \pi^2 \frac{t}{a^2}\right.$$

where the surface concentration is kept at constant zero concentration, c_o, and yields an equation for the concentration, c, as a function of the radial distance from the center, r, and where c_1 in our case, represents the initial uniform concentration of radiogenic ^{40}Ar.

The above equation can then be solved in terms of fractional loss, f, by integrating between r = 0 and r = a and comparing to the original concentration:

$$f = 1 - \frac{6}{\pi^2} \sum_{n=1}^{\infty} \frac{1}{n^2} \exp -\left(Dn^2 \pi^2 \frac{t}{a^2}\right)$$

With the above fractional loss equation, the diffusivity, D, can be determined for a particular outgassing. The calculated diffusivity can then be used, with specific experimental data, to estimate the temperature required for a particular reheating event. The Arrhenius equation can be solved for temperature, T, with experimental activation energy, E, and frequency factor, Do:

$$T = -\frac{E}{\left(R \ln \frac{D}{D_o}\right)}$$

where R is the gas constant.

Although it has been demonstrated that the age of a single episodic reheating event can be indicated by an age

spectrum, multiple reheating events may yield ambiguous results. Harrison (1983) studied the problem of multiple episodic loss in hornblende and showed that a sample that has undergone more than one reheating event did not produce an age spectrum which accurately displayed the complex thermal history. It is therefore unclear how to interpret accurately age spectra of samples that have experienced several episodes of gas loss.

Harrison and McDougall (1982) first recognized that age spectra with linear gradients rather than convex ones may result in a lower intercept that does not accurately represent the age of a reheating event. Harrison and McDougall (1982) recognized this characteristic from age spectra of K-feldspar, and were able to demonstrate that the lower intercept age did not represent the time of a thermal event. Turner (1969) noted that samples cooling very slowly through their partial radiogenic ^{40}Ar retention region would develop some sort of gradient. Harrison and McDougall (1982) related the gradient to the slow accumulation of radiogenic Ar during cooling and suggested that the lower intercept represented the time at which the sample cooled below approximately 110°C. On independent grounds, the cooling rate of these rocks was estimated to be approximately $5°C\text{-}Ma^{-1}$, which supports the slow cooling interpretation.

Dodson (1984) calculated age spectra resulting from slow cooling of spherical, cylindrical, and plane sheet

geometries. He was able to show that the form of the resulting age gradient was highly dependent upon the diffusion geometry. For a given slow cooling history, the sphere portrayed the steepest and largest age gradient with little or no age plateau. The shape of the gradient was convex upwards. For the same cooling history, the cylindrical and plane sheet geometries showed less pronounced age gradients with better plateau development. The shape of the age gradients were increasingly more linear in the sphere, cylinder, and plane sheet, respectively. These observations indicate that there are numerous complications in interpreting slow cooling age gradients. Harrison (1983) states that without sufficient geochronological information, it is possible to misinterpret the significance of apparent age gradients in spectra for samples that have cooled slowly through the temperature region of partial radiogenic ^{40}Ar accumulation.

In this study, three major priorities were considered when collecting samples for analysis. The most significant question addressed in this study concerning the thermal history was the age of major metamorphism in this region. This question was addressed by collecting and analyzing samples, primarily amphibolites, from areas distant from intrusive bodies and structurally disturbed zones. A second question of regional importance is the timing of significant intrusive events in the area and their influence on the thermal history of the metamorphic rocks. This problem was addressed by dating the oldest (based on K-Ar) unfoliated

major igneous intrusion in the area. The third problem of interest is the relationship of structural events to thermal events. This relationship was analyzed by collecting and dating samples that could constrain the timing of specific structural events.

Fourteen mineral separates were analyzed in all and included hornblende, muscovite, biotite, and potassium feldspar. Nine samples were analyzed from metamorphic rocks; eight were hornblendes and one was a biotite separate. Five samples from igneous rocks were analyzed and included two amphibole, two muscovite, and one K-feldspar separate.

Sample preparation was conducted in the labs at the State University of New York at Albany. Samples were crushed by jaw and roller crushers, then sieved to various size fractions ranging from -35 to +200 mesh. Mineral separates were done by standard heavy liquid and magnetic separation techniques. Samples were hand picked to remove any impurities, resulting in separates that were 99% pure.

Samples were irradiated both in the TRIGA research nuclear reactor of the U.S. Geological Survey; and the University of Michigan reactor. For details on mineral separations and irradiation procedures, see Appendices.

2. Metamorphic Rocks

Sample 82AFr4033 is an amphibolite collected 11.3 miles west on Boundary Road from the Canadian border (figure 25). Several large outcrops of amphibolite occur here on both the north and south sides of the road. These rocks are mapped as part of the biotite gneiss and amphibolite unit. This sample was collected because it is several kilometers from any mapped intrusive bodies and is a considerable distance from a contact between the gneiss unit and other units. In outcrop, these rocks appear well foliated, defined by the alignment of hornblende and plagioclase. Minor intercalcated pelitic rocks are present as layers of quartz + biotite + plagioclase + muscovite ± garnet gneiss. The foliation is gently dipping to the north except where folded around rare, tight, inclined to recumbent folds. Observed wavelenghths and amplitudes of these folds is on the order of 20-30 centimeters. Late open folds deform all other structures in these outcrops.

In thin-section, this sample consists of green, blue-green, to light brown pleochroic hornblende, quartz, plagioclase, white mica, and minor biotite. Sphene, zircon, and opaques occur as minor phases (plate 10). Minor chlorite occurs after biotite and minor white mica (sericite) occurs after plagioclase. The average hornblende grainsize is approximately 1 millimeter in length and they are weakly aligned parallel to the foliation. The hornblende is optically homogenous suggesting a simple

FIGURE 25: Map showing locations of smaples dated by $^{40}Ar/^{39}Ar$.

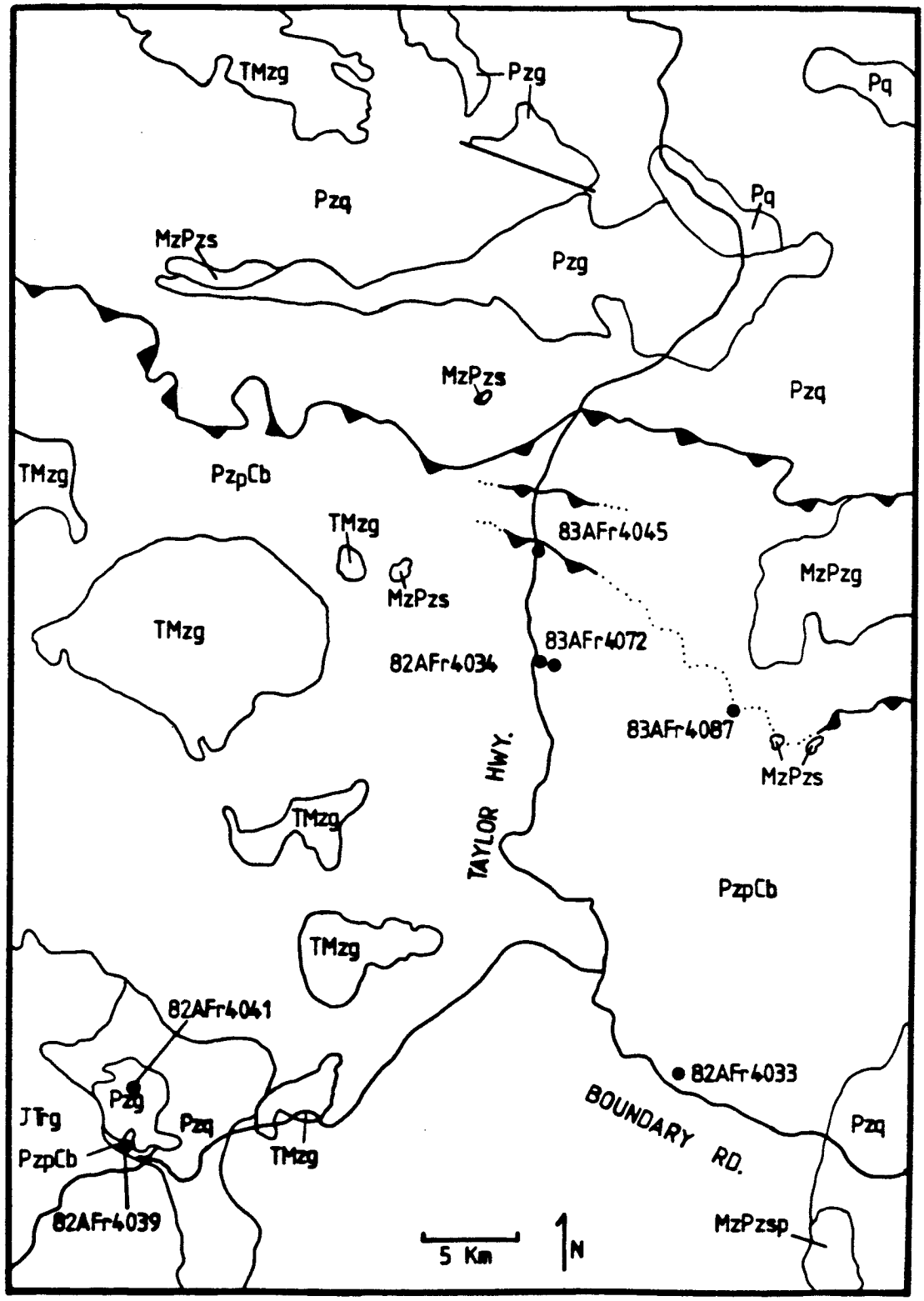
TMzg
Pzg
Pq
Pzq
Pq
MzPzs
Pzg
MzPzs
Pzq
TMzg
PzpCb
TMzg
83AFr4045
MzPzs
MzPzg
TMzg
83AFr4072
82AFr4034
83AFr4087
MzPzs
TAYLOR HWY.
TMzg
PzpCb
TMzg
82AFr4041
82AFr4033
Pzg
JTrg
Pzq
PzpCb
TMzg
BOUNDARY RD.
Pzq
82AFr4039
MzPzsp
5 Km
N

PLATE 10: Photomicrograph of sample 82AFr4033.

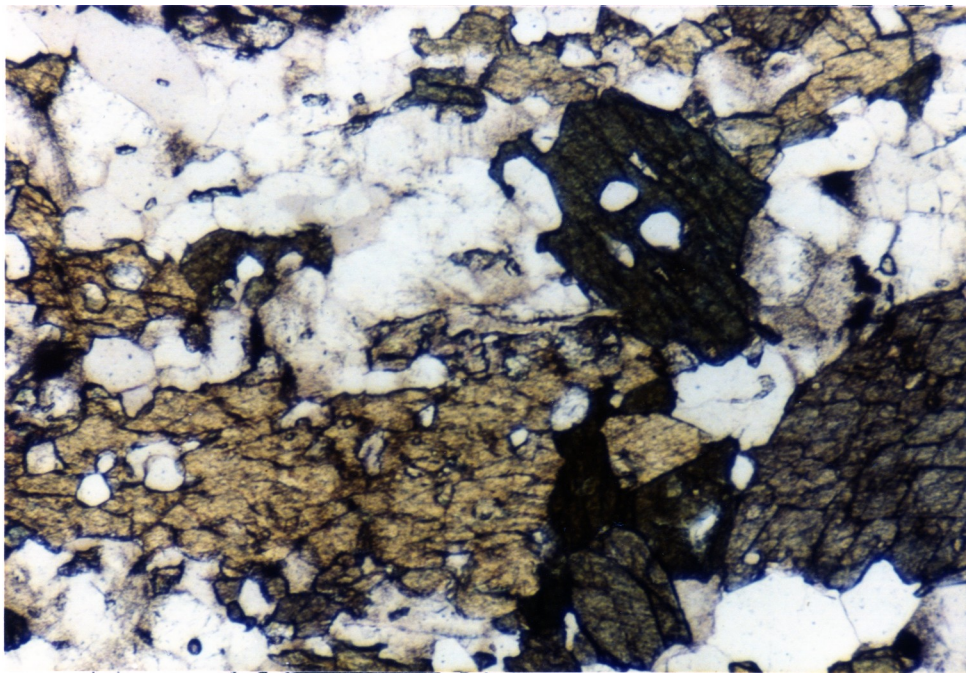

PLATE 10: Photomicrograph of sample 82AFr4033.

growth history and is poikilitic containing minor inclusions of plagioclase, quartz, and very minor biotite and chloritized biotite. The lack of primary chlorite and epidote suggests this rock is stable in the amphibolite facies. The mineral separate is very pure, containing very minor quartz and sphene composites. The hornblende is dark green and generally euhedral. The size fraction used for analysis was -35 to +60 mesh.

The age spectrum for this analysis is shown in figure 26. The first two gas fractions show some inherited radiogenic ^{40}Ar as indicated by the high initial ages. The following several steps (3-14) yield a range of ages from 163 ± 3 Ma to 230 ± 9 Ma and cannot be simply interpreted in terms of a thermal history. The integrated plateau age is 194 ± 2 Ma as defined by steps 15-16, which consists of 42.7% of the gas released. The isochron plot in figure 27 shows the gas (15-16) fractions that lie on a single line between atmospheric composition ($^{36}Ar/^{40}Ar$) and the age of the sample ($^{39}Ar/^{40}Ar$). The last two steps (17-18) at temperatures of 1090°C and 1250°C yield ages of 204 ± 4 Ma and 201 ± 2 Ma, which are about 4% higher than the plateau age. These gas fractions do not plot on the isochron represented by the plateau age. The K_2O content of these amphiboles as estimated from the ^{39}Ar released is 0.25%.

Sample 82Afr4039 is an amphibolite that was collected on a backpack trip near Chicken (figure 25). Several small outcrops of this amphibolite occur as knolls forming a small

FIGURES 26&27: Age spectrum and isochron plot: sample 82AFr 4033 (hornblende).

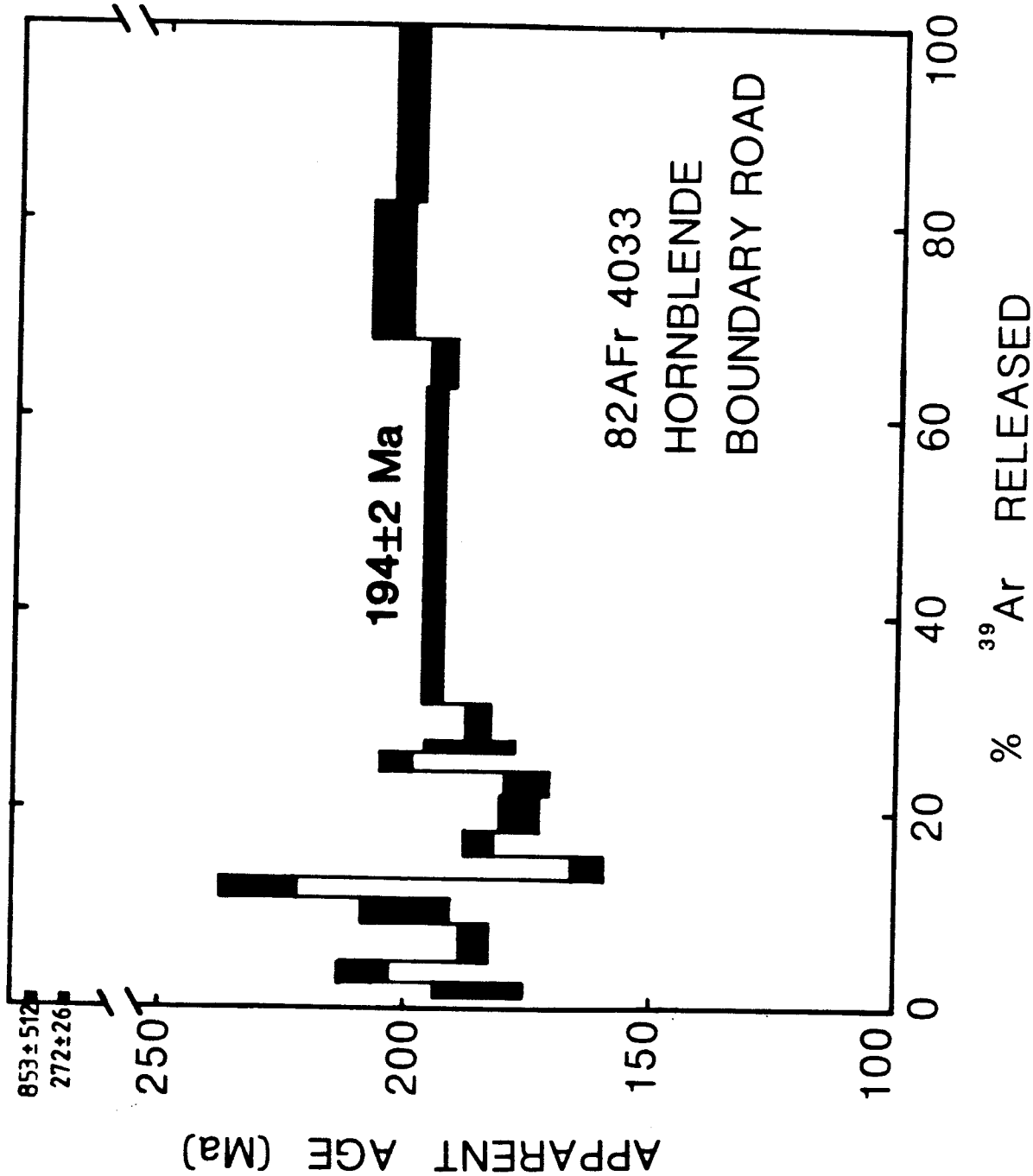
853±512
272±26
250
200
150
100
0
20
40
60
80
100
194±2 Ma
82AFr 4033
HORNBLENDE
BOUNDARY ROAD
APPARENT AGE (Ma)
% ^{39}Ar RELEASED

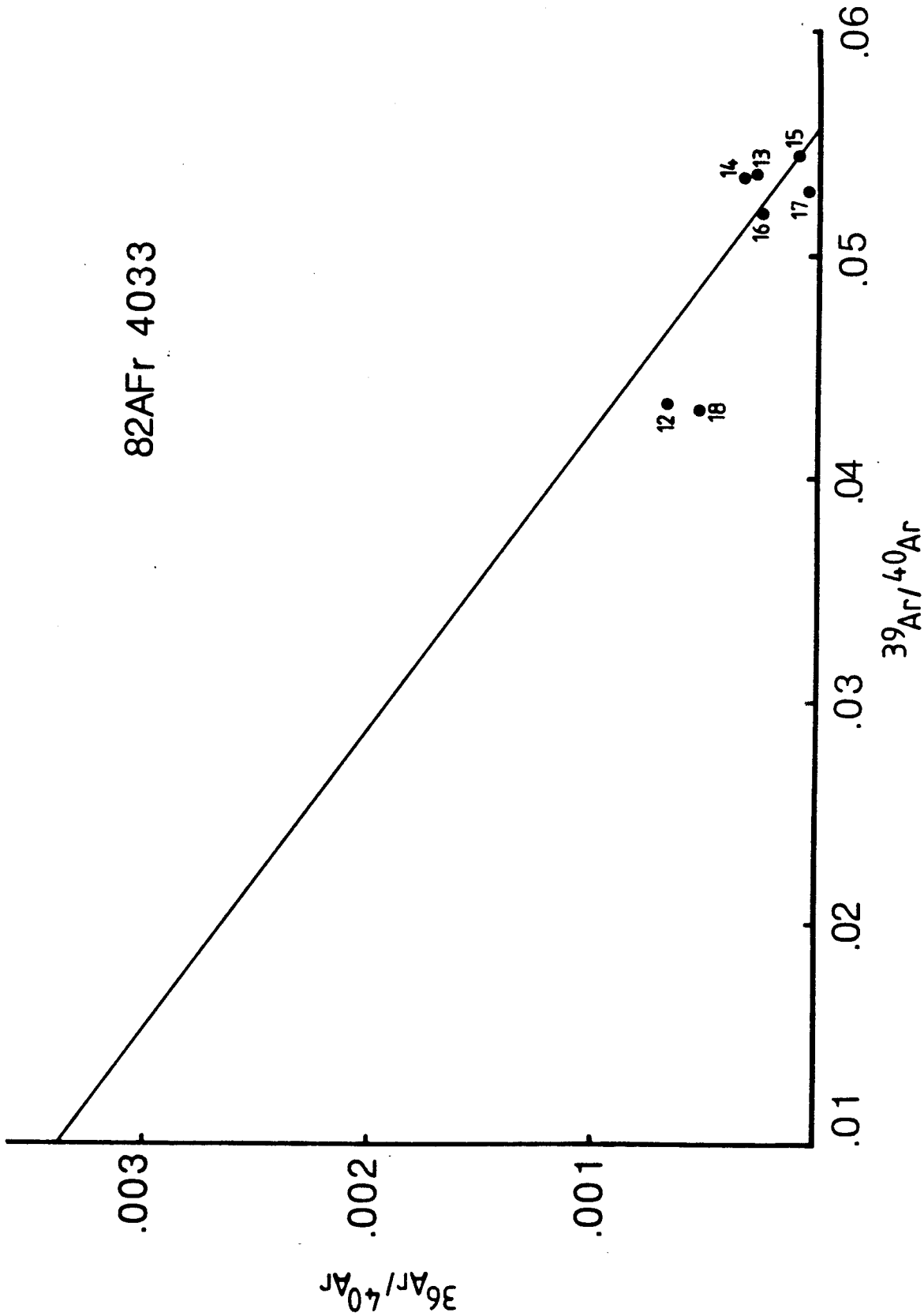
82AFr 4033
$^{36}Ar/^{40}Ar$
.003
.002
.001
.01
.02
.03
.04
.05
.06
$^{39}Ar/^{40}Ar$
12
18
16
17
14
13
15

SAMPLE #: 82AFr4033
MINERAL: Hornblende
J= .006422

TEMPERATURE (Degrees Centigrade)	(1) 40Ar/39Ar	(1) 37Ar/39Ar	(1) 36Ar/39Ar	39ArK x 10e-14 Moles	Cumulative 39Ar (%)	(2) 40Ar*/40Ar(t) (%)	40Ar*/39ArK	Apparent Age (Ma)	(3) Standard Dev. (Ma)
400	279.90	0.000	0.373100	0.04	0.01	55.0	167.590	853.0	512.2
500	39.78	2.279	0.049510	3.20	1.10	63.2	25.365	272.3	4.1
560	40.79	0.890	0.081300	4.26	2.60	41.0	16.841	185.3	8.8
620	47.50	1.650	0.096700	5.22	4.40	39.9	19.070	208.4	3.9
670	29.17	0.842	0.041670	10.90	8.20	5.8	16.924	186.1	2.5
690	21.44	0.153	0.010650	6.96	10.60	84.8	18.301	200.5	8.7
720	57.59	0.623	0.123600	5.91	12.70	36.6	21.131	229.6	7.4
750	19.19	1.096	0.015400	7.75	15.40	76.1	14.724	163.0	2.4
780	18.31	1.215	0.005388	8.00	18.30	91.2	16.822	185.1	1.8
810	18.16	1.728	0.007689	7.67	21.40	87.6	16.032	176.8	3.5
850	18.49	2.621	0.009496	7.01	23.60	85.2	15.910	175.5	4.2
890	22.40	11.706	0.018810	5.02	25.60	79.0	18.433	201.8	2.4
920	18.61	6.381	0.007274	4.43	27.10	90.0	17.023	187.2	8.4
960	18.67	5.592	0.007578	130.00	30.70	89.8	16.927	186.2	2.4
1020	18.28	5.931	0.003456	93.50	63.00	96.9	17.784	195.1	0.4
1060	19.15	6.434	0.006945	28.80	73.40	91.7	17.675	194.0	2.0
1090	18.88	6.430	0.002647	24.70	82.00	98.3	18.678	204.4	3.2
1250	21.52	6.779	0.013010	51.00	100.00	84.6	18.382	201.3	0.5

1) Corrected for mass discrimination, machine background, orifice discrimination, and blank.
2) Total Ar includes blank.
3) Error values are for analytical error only (quoted at 1 sigma level).

north-south striking ridge. This amphibolite is not delineated on the geologic map (Foster, 1976) of the quadrangle because of its small size. These outcrops are located approximately 300 meters from a mapped portion of the Taylor Mountain batholith, although granitic rubble was found very close to the amphibolite suggesting the presence of dikes and/or sills in the area. This small ridge of amphibolite can be traced within about 100 meters of the mapped greenstone unit Pzg. The greenstone unit forms the tops of several hills in the area and is topographically and probably structurally above the amphibolite.

In outcrop, this amphibolite shows a strong foliation, which is defined by the alignment of hornblende and plagioclase. There were no visible folds in these outcrops, and the foliation is dipping gently to the southwest. No pelitic rocks were observed in this section.

In thin-section, the gneissic foliation is also well defined by the alignment of hornblende and plagioclase (plate 11). The primary assemblage in this sample is hornblende + plagioclase + quartz + white mica + carbonate + opaques with very minor epidote, chlorite, and sphene. Some white mica (sericite) alteration of the feldspar was observed. The average hornblende length varies from approximately 0.2 to 1 millimeter and they appear optically homogenous. The lack of abundant chlorite and epidote suggests this sample was metamorphosed to the amphibolite facies. The mineral separate was very pure containing minor quartz composites. The size fraction used for analysis was

PLATE 11: Photomicrograph of sample 82AFr 4039 (amphibolite).

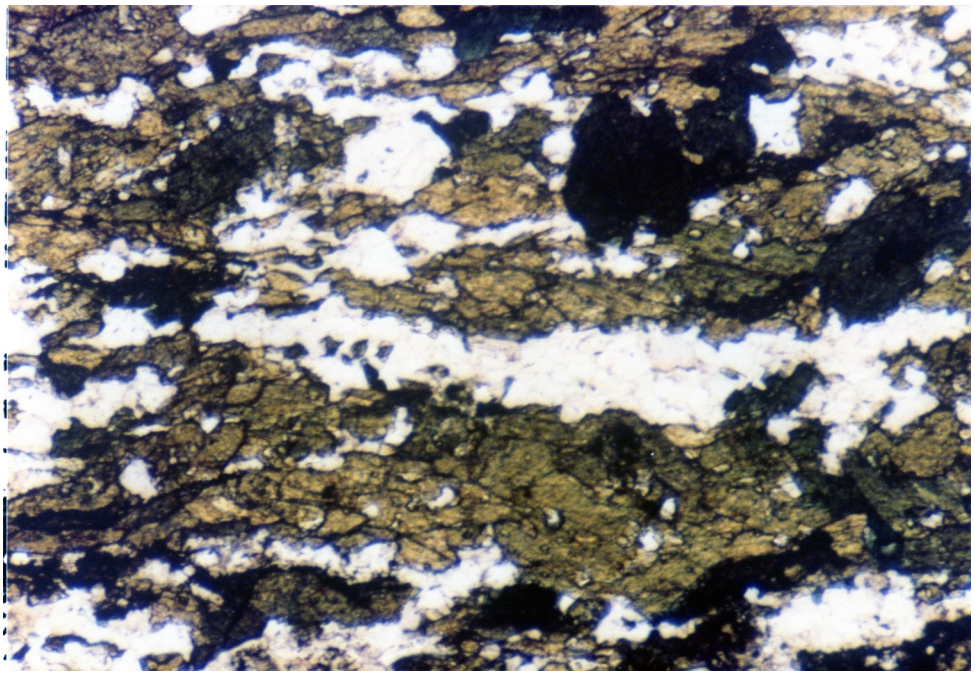

PLATE 11: Photomicrograph of sample 82AFr 4039 (amphibolite).

-60 +100 mesh.

The age spectrum for this analysis is shown in figure 28. The first two gas fractions show anomalously high ages which are the result of inherited radiogenic ^{40}Ar near the edges of the crystals. The following 9 steps (3-11) show a general progressive increase in age from 162 ± 8 Ma to 216 ± 3 Ma. This type of age spectrum is typical of a sample that has experienced gas loss (approximately 6% in this sample) due to an overprinting thermal event. The estimated lower intercept is about 100 Ma which may broadly represent the age of the overprinting thermal event.

The integrated plateau age for this sample is 213 Ma as defined by steps 12, 13, and 16 (950°C, 980°C, and 1040°C respectively) which consist of 53.1% of the gas released. The isochron plot in figure 29 shows the gas fractions (12, 13, 16) that lie on the line between the plateau age and atmospheric composition. Steps 14, 15, and 17 through 19 yield ages ranging from 222 ± 3 Ma to 232 ± 3 Ma, which are about 5% higher than the plateau age. These steps represent the high temperature fractions (1010°C to 1250°C) of the analysis and do not plot on the isochron in figure 29. The K_2O content of this sample is calculated to be 0.26%.

Sample 82AFr4041 is a greenstone collected approximately 1 kilometer north of the amphibolite sample (82AFr4039) previously described (figure 25). It is mapped as part of the Paleozoic greenstone unit (Pzg) by Foster (1976). This unit, in the area where the sample was collected, consists

FIGURES 28 & 29: Age spectrum and isochron plot: Sample 82AFr 4039 (hornblende).

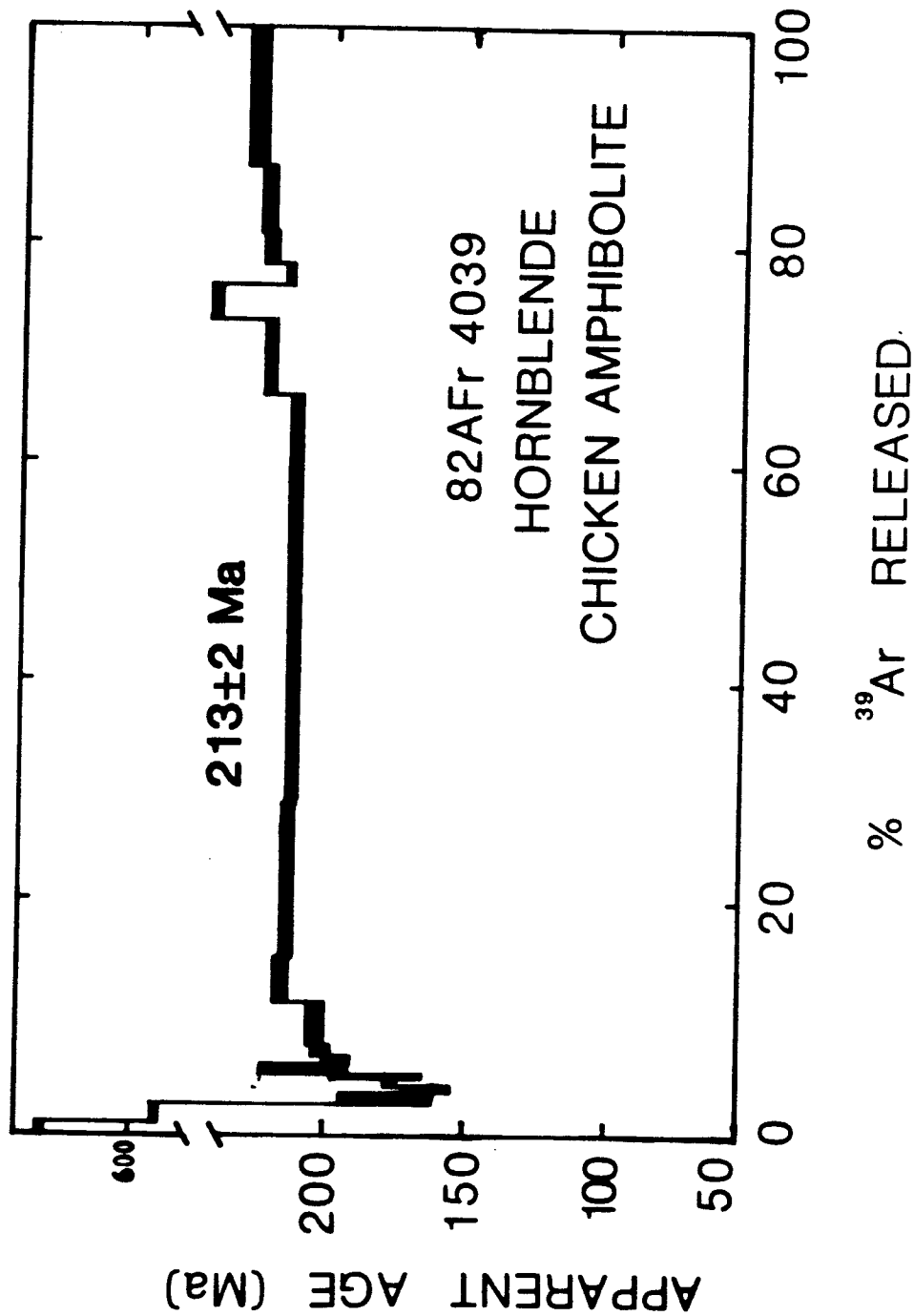
APPARENT AGE (Ma)
600
200
150
100
50
0
20
40
60
80
100
% ^{39}Ar RELEASED
213±2 Ma
82AFr 4039
HORNBLENDE
CHICKEN AMPHIBOLITE

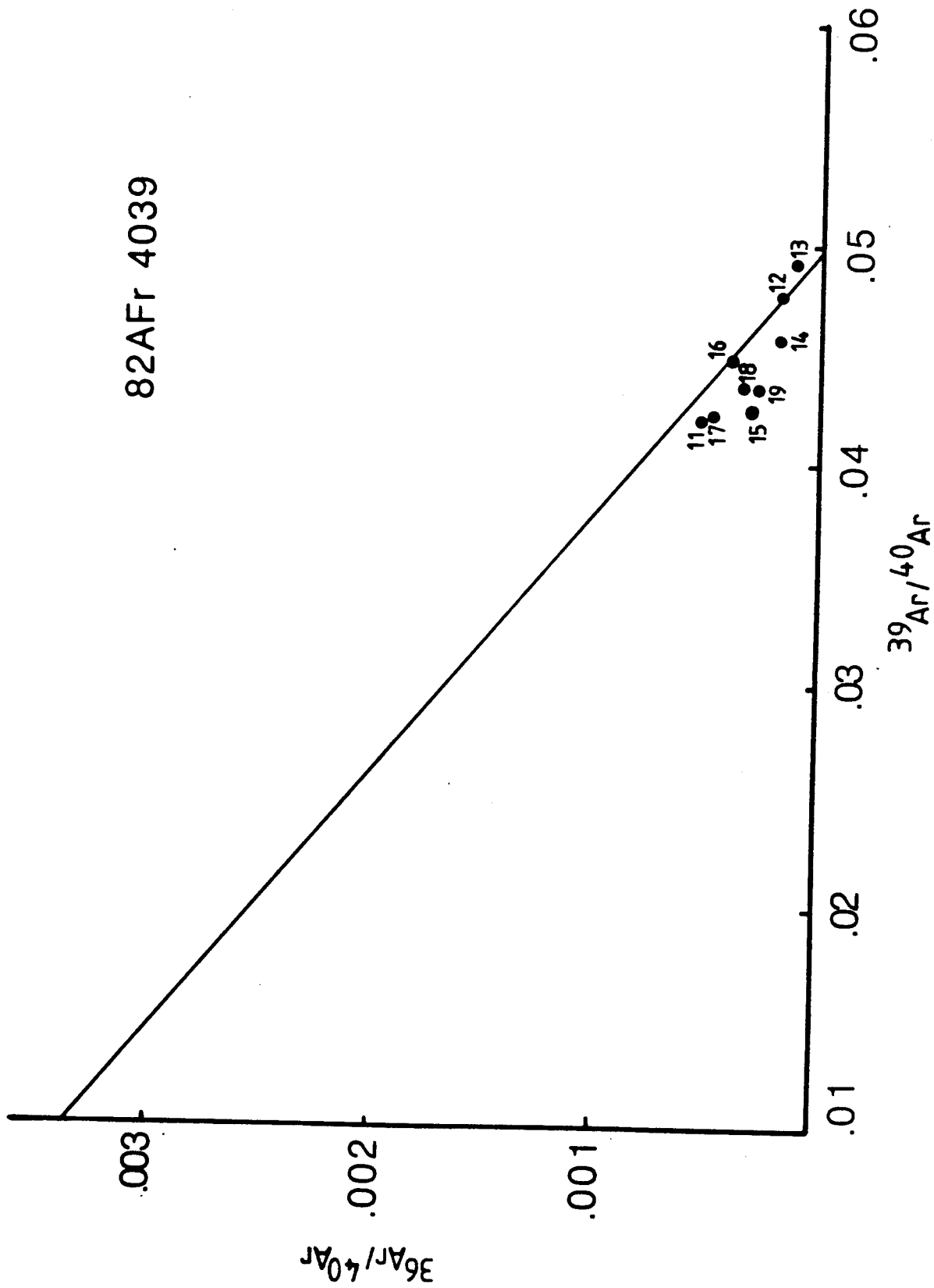
82AFr 4039
.003
.002
.001
$^{36}Ar/^{40}Ar$
.01
.02
.03
.04
.05
.06
$^{39}Ar/^{40}Ar$
11
17
15
18
19
16
14
12
13

SAMPLE #: 82AFr4039
MINERAL: Hornblende
J= .00629

TEMPERATURE (Degrees Centigrade)	(1) 40Ar/39Ar	(1) 37Ar/39Ar	(1) 36Ar/39Ar	39ArK x 10e-14 Moles	Cumulative 39Ar (%)	(2) 40Ar*/40Ar(t) (%)	40Ar*/39ArK	Apparent Age (Ma)	(3) Standard Dev. (Ma)
530	301.62	1.820	0.796600	9.23	2.8	21.9	66.448	630.0	7.5
570	385.80	2.493	1.080000	0.98	3.1	17.2	66.880	591.5	30.2
600	57.13	2.165	0.141200	1.34	3.5	26.9	15.605	168.9	13.2
650	43.05	1.621	0.095630	2.25	4.2	34.3	14.927	161.9	7.9
670	39.23	2.349	0.078430	1.10	4.6	40.4	16.260	175.7	3.1
690	35.65	2.073	0.064520	1.81	5.1	46.2	16.761	180.8	15.9
730	27.80	2.545	0.029440	2.65	5.9	68.5	19.325	207.0	16.5
780	22.72	2.564	0.016250	3.13	6.9	78.6	18.143	195.0	4.4
830	27.17	3.153	0.029330	6.05	8.8	68.6	18.785	201.5	1.3
880	25.52	5.935	0.023970	10.30	12.0	73.8	18.966	203.3	3.1
920	23.84	9.107	0.014970	12.90	16.0	84.1	20.249	216.3	1.6
950	21.03	6.591	0.005521	43.90	29.6	94.6	19.995	213.7	0.5
980	20.52	6.390	0.003923	120.00	66.7	69.7	19.938	213.2	0.4
1010	22.03	6.483	0.005801	25.30	74.6	94.3	20.912	222.9	0.3
1020	23.91	7.121	0.009307	8.76	77.3	90.4	21.810	231.9	1.2
1040	22.63	8.205	0.011180	7.70	79.7	85.6	20.069	214.5	4.0
1060	24.02	8.960	0.013580	8.19	82.2	85.7	20.821	222.0	1.7
1070	23.10	9.826	0.010360	18.90	88.0	89.8	20.941	223.2	0.1
1120	23.11	8.068	0.008576	38.70	100.0	91.6	21.317	227.0	1.0

1) Corrected for mass discrimination, machine background, orifice discrimination, and blank.
2) Total Ar includes blank.
3) Error values are for analytical error only (quoted at 1 sigma level).

primarily of massive fine grained greenstone. Outcrops are massive, unfoliated, but commonly display widely spaced (1 to several meters) joints. Calcite and epidote-filled vesicles (amygdules) are common in the greenstone. The mafic rocks in this unit show only slight variation in grain size and appear in the field to be quite homogenous in composition. Associated with the greenstone in this unit, although not in the immediate vicinity of the sample, are sedimentary rocks including sandstone, limestone, and possible chert and felsic volcanics.

The sample collected is located approximately 1 kilometer from the mapped contact of a portion of the Taylor Mountain batholith. Granitic rubble has been found closer to the greenstone locality, suggesting the presence of dikes and/or sills in the area.

The sample is a coarse grained variety of the greenstone and contains visible amphibole crystals. In thin-section, this sample appears unfoliated and contains some relict igneous textures (plate 12). The primary assemblage is amphibole + chlorite + quartz + plagioclase + epidote + relict pyroxene + minor carbonate and opaques. The amphibole is light greenish-brown to blue-green pleochroic and contains minor chlorite intergrowths and rims. Some epidote is euhedral and twinned and may be primary. Relect pyroxene grains have ragged edges suggesting possible reaction rims. The amphibole mineral separate contains minor quartz and epidote composites and minor epidote and pyroxene grains. The amphiboles are medium green and were

PLATE 12: Photomicrograph of sample 82AFr4041 (Greenstone).

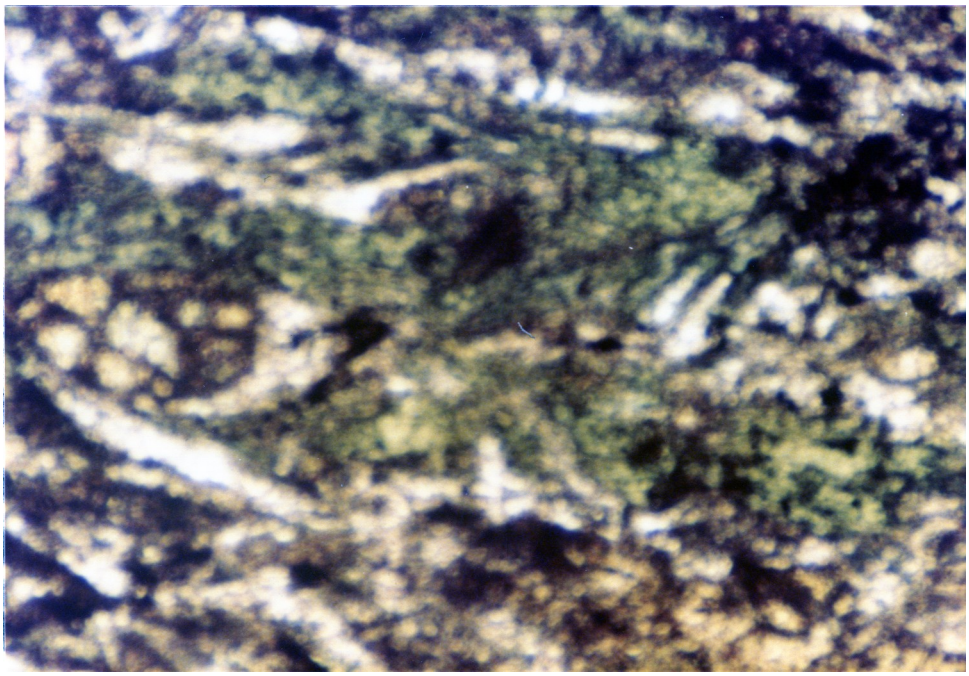

PLATE 12: Photomicrograph of sample 82AFr 4041 (greenstone).

sized to -60 to +100 mesh for analysis.

The age spectrum for this analysis is shown in figure 30. There was no detected inherited radiogenic ^{40}Ar in this sample. The first three steps show a progressive increase in age from 121 ± 2 Ma to 157 ± 2 Ma and then to 196 ± 2 Ma. This type of age spectrum is typical of a sample that has experienced episodic loss. The age spectrum has a lower intercept at about 100 Ma; a gas loss of about 4.75% is indicated. A plateau age is defined by 56.2% of the gas released, and yields an integrated age of 201 ± 5 Ma. This plateau is defined by steps 5-12 and 14-15, which fall close to the isochron in figure 31. Although a plateau is defined, a slow cooling gradient is suggested by a gradual increase in age across the spectrum. With either interpretation, it is clear that the sample was at elevated temperatures during the indicated apparent ages. The higher temperature steps 13 and 16-18 yield ages averaging about 214 Ma, which is approximately 7% higher than the plateau age. Steps 13, 17, and 18 plot distinctly off the isochron plot while step 16 plots in an intermediate position. The K_2O content of this sample is estimated to be about 0.22%.

The following two samples of interest were collected along the Forty Mile River near the intersection of the Taylor Highway and the river (figure 25). These samples are located well within the biotite gneiss and amphibolite unit (PzpЄb) of Foster (1976). The first sample described is 82AFr4034, and was collected less than 100 meters downstream

FIGURES 30 & 31: Age spectrum and isochron plot: Sample 82AFr 4041 (Amphibole).

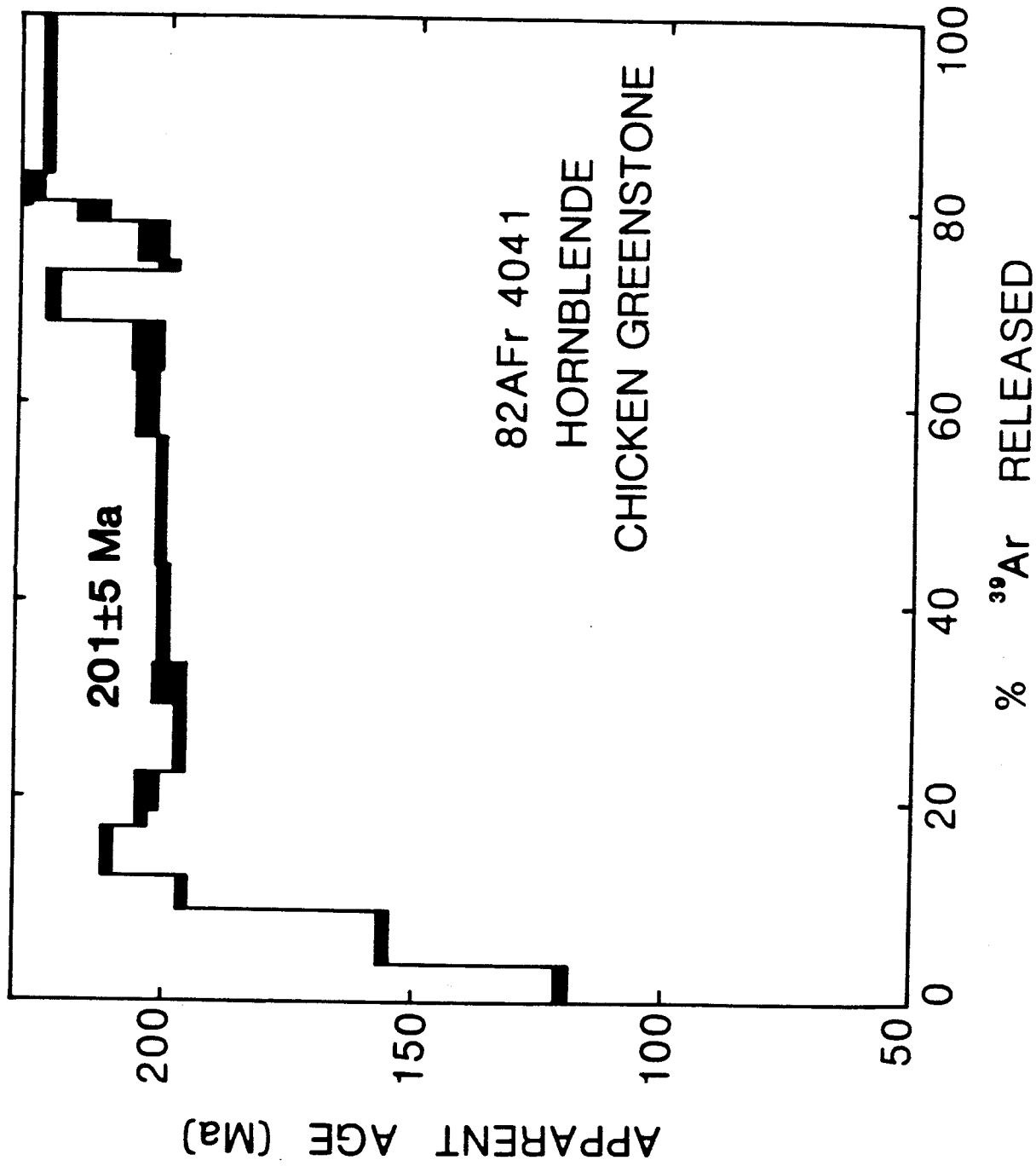
APPARENT AGE (Ma)
200
150
100
50
0
20
40
60
80
100
% ^{39}Ar RELEASED
201±5 Ma
82AFr 4041
HORNBLENDE
CHICKEN GREENSTONE

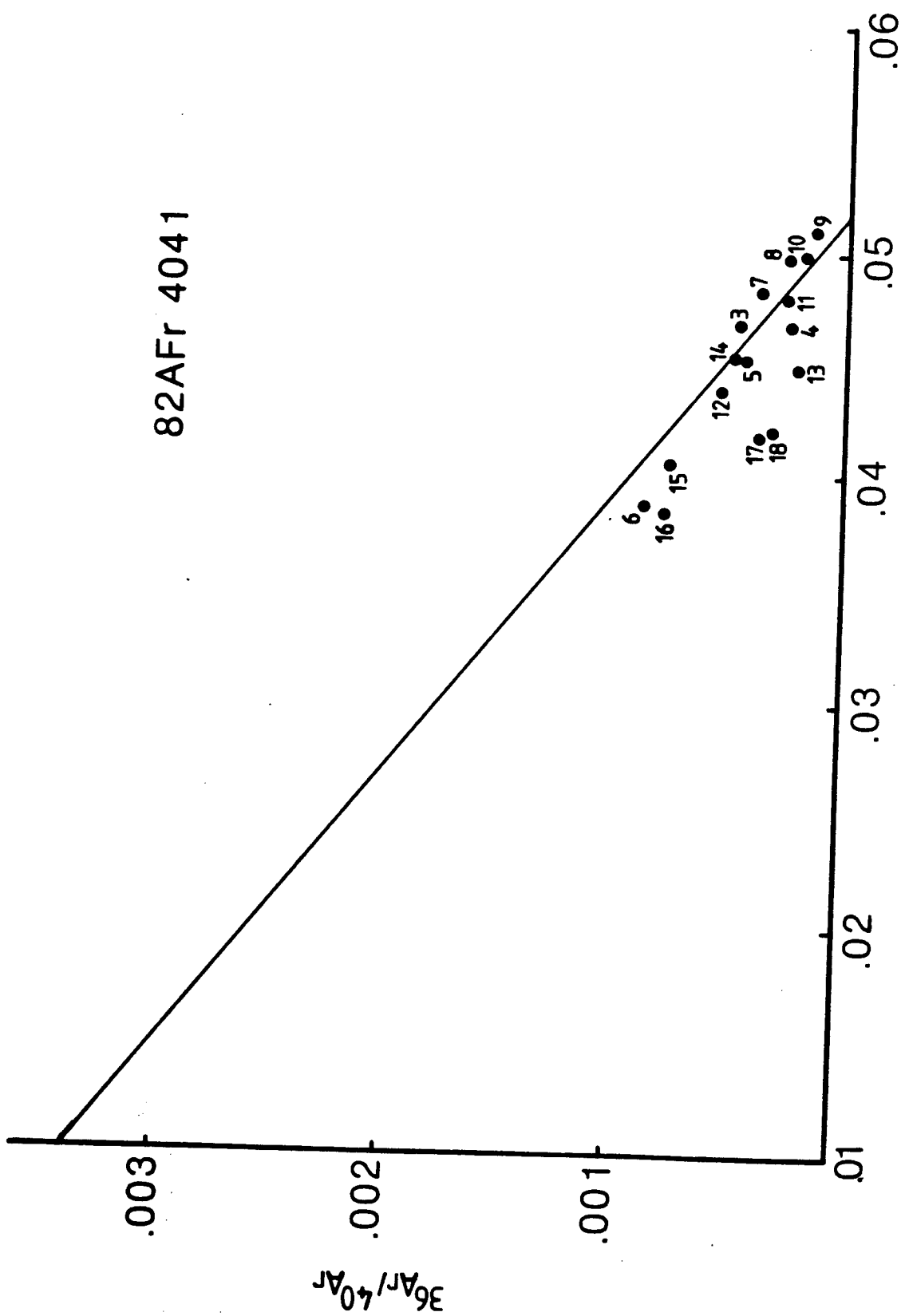
82AFr 4041
$^{36}Ar/^{40}Ar$
$^{39}Ar/^{40}Ar$
.003
.002
.001
.01
.02
.03
.04
.05
.06
1
2
3
4
5
6
7
8
9
10
11
12
13
14
15
16
17
18

SAMPLE #: 82AFr4041
MINERAL: Amphibole
J= .006268

TEMPERATURE (Degrees Centigrade)	(1) 40Ar/39Ar	(1) 37Ar/39Ar	(1) 36Ar/39Ar	39ArK x 10e-14 Moles	Cumulative 39Ar (%)	(2) 40Ar*/40Ar(t) (%)	40Ar*/39ArK	Apparent Age (Ma)	(3) Standard Dev. (Ma)
500	22.62	1.844	0.039660	8.85	3.0	48.6	11.052	120.8	2.0
540	17.56	1.698	0.010940	14.70	8.7	82.0	14.473	156.7	0.7
580	21.32	1.785	0.010580	10.30	12.5	85.6	18.352	196.4	1.3
620	21.34	2.020	0.005537	13.30	17.4	92.7	19.885	211.9	1.2
650	22.15	2.927	0.011210	4.17	18.9	85.1	19.103	204.0	1.6
680	25.72	3.397	0.023680	10.30	22.7	73.5	19.027	203.3	3.1
740	20.70	4.203	0.009028	20.50	30.3	88.5	18.410	197.0	0.8
780	20.04	4.019	0.006014	10.50	34.2	92.2	18.625	199.2	5.6
820	19.60	2.900	0.003797	26.50	44.0	95.2	18.736	200.3	0.9
860	19.98	5.091	0.005385	35.70	57.2	93.9	18.844	201.4	1.2
890	20.67	12.480	0.009021	18.60	64.1	91.6	19.133	204.3	3.5
920	22.54	15.520	0.015520	13.20	69.0	83.5	19.083	203.8	6.4
950	22.04	21.930	0.010570	15.60	74.8	93.3	20.928	222.4	4.3
980	21.76	19.510	0.016140	8.31	77.9	84.6	18.753	200.5	4.2
1000	24.31	22.970	0.024990	4.00	7.4	76.2	19.004	203.0	5.5
1020	25.56	26.880	0.026220	3.94	80.9	77.1	20.268	215.8	5.5
1050	23.44	28.770	0.015410	8.38	84.0	89.7	21.539	228.5	6.6
1250	23.34	26.390	0.015480	44.10	100.0	89.1	21.191	225.0	0.8

1) Corrected for mass discrimination, machine background, orifice discrimination, and blank.
2) Total Ar includes blank.
3) Error values are for analytical error only (quoted at 1 sigma level).

from the bridge. In outcrop, this amphibolite appears well foliated and contains fine grained hornblende and plagioclase parallel to this foliation. This gneissic foliation is deformed around tight, generally inclinal folds, ranging in amplitude and wavelength from a few centimeters to several hundred meters. Later open folds are also evident with a related fold axis lineation. These structures are typical of this unit and have been previously described.

In thin-section, this sample exhibits very fine grained light blueish-green to green-brown pleochroic, optically homogenous hornblende, that range in length from 0.1 to 0.25 millimeters (plate 13). The primary assemblage observed in this sample is hornblende + quartz + plagioclase + white mica + epidote + sphene + opaques + very minor chlorite. The slightly more bluish-green hornblende and the abundance of epidote and chlorite suggests this sample has been metamorphosed to the epidote-amphibolite or amphibolite facies.

The mineral separate of this sample contained only minor epidote grains in addition to the hornblende. The separate used for analysis was sized to -100 to +200 mesh.

The first step in this analysis yielded an anomalously high age and is probably the result of inherited radiogenic ^{40}Ar. The remaining steps of this analysis yield spurious ages ranging from 187 ± 25 Ma to 312 ± 23 Ma with no defined plateau or lower intercept ages. This age spectrum cannot be used to interpret a thermal history. Due to the fine

PLATE 13: Photomicrograph of sample 82AFr 4034 (amphibolite).

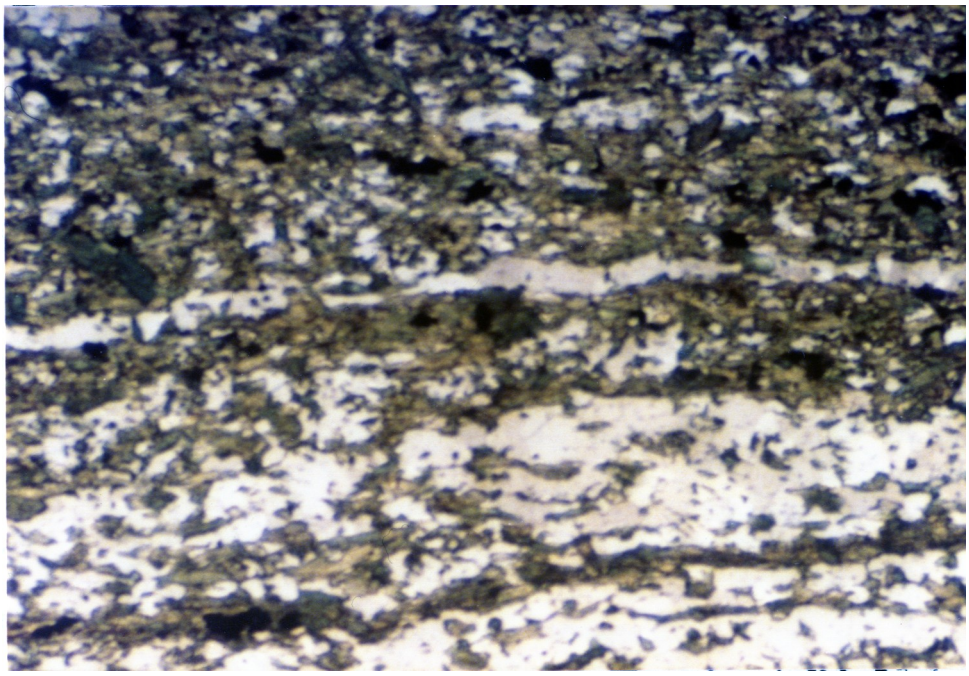

PLATE 13: Photomicrograph of sample 82AFr 4034 (amphibolite).

grained nature of this sample, it is likely that the distribution of ^{39}Ar is heterogenous due to recoil redistribution caused by the high energy of the ^{39}K (N,P) ^{39}Ar reaction. It has been hypothesized (Harrison, 1983) that the redistribution of ^{39}Ar near grain edges could be compensated by the flux of incident ^{39}Ar from adjacent grains, although is is possible that the buried atoms are differently bound in the crystal structure as a result of lattice damage. This suggests the possiblity that the bulk age of such a sample could be geologically more significant. Such an age would be similar to a K-Ar age. The bulk age calculated for this sample is 231 Ma.

The other sample collected near this locality yielded more significant results. Sample 83AFr4072 was collected approximately 300 meters downstream from the Forty Mile bridge. In this area, the river has cut through the bedrock exposing a continuous section for about one half mile. The section primarily consists of pelitic gneiss, amphibolite, and minor crystalline marble. Pelitic rocks are generally composed of quartz + plagioclase + white mica + biotite + garnet ± carbonate. Amphibolites range in mineralogy from hornblende + plagioclase + quartz + epidote + white mica + chlorite + opaques to the above assemblage plus various proportions of biotite + garnet (some chloritized) + carbonate.

A cream white crystalline marble outcrop occurs, in this section, as a discontinuous, isoclinally folded pod within

PLATE 14: Photomicrograph of sample 83AFr 4072 (amphibolite).

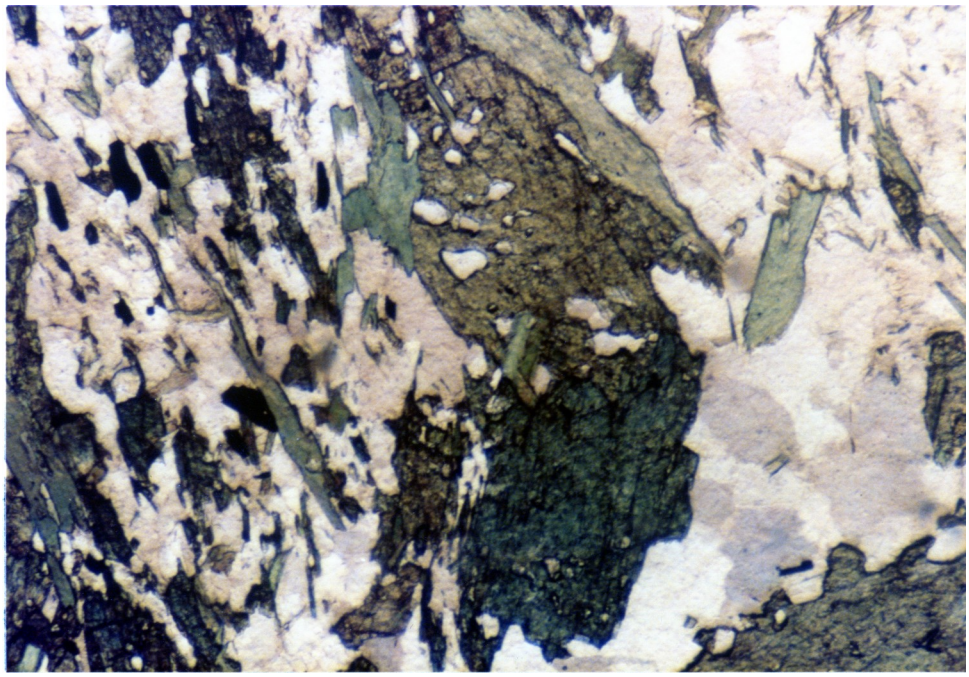

PLATE 14: Photomicrograph of sample 83AFr 4072 (amphibolite).

SAMPLE #: 82AFr4034
MINERAL: Hornblende
J= .006453

TEMPERATURE (Degrees Centigrade)	(1) 40Ar/39Ar	(1) 37Ar/39Ar	(1) 36Ar/39Ar	39ArK x 10e-14 Moles	Cumulative 39Ar (%)	(2) 40Ar*/40Ar(t) (%)	40Ar*/39ArK	Apparent Age (Ma)	(3) Standard Dev. (Ma)
450	143.60	3.338	0.31280	0.40	0.4	35.2	51.576	518.3	121.4
500	77.01	4.419	0.16910	0.92	1.3	35.1	27.475	294.5	32.3
540	57.28	2.773	0.11860	0.92	2.2	38.4	22.474	244.3	51.2
580	34.82	2.206	0.02472	1.43	3.6	77.9	27.727	297.0	42.8
620	34.82	4.340	0.05366	1.60	5.1	54.5	19.395	212.7	31.8
650	38.16	2.344	0.03070	1.32	6.4	75.2	29.300	312.4	23.1
690	44.25	5.543	0.08198	1.06	7.5	45.3	20.532	224.5	20.3
720	37.71	7.063	0.06803	0.89	8.3	46.8	18.244	200.8	24.5
770	34.14	9.728	0.06105	1.14	9.3	48.1	16.971	187.5	25.2
850	33.15	20.680	0.03124	2.92	12.0	76.2	25.888	278.7	4.9
900	26.72	33.360	0.02445	5.40	17.1	82.1	22.596	245.6	12.5
950	20.84	20.740	0.01248	47.10	61.9	89.9	19.027	208.9	1.2
970	23.24	22.190	0.01308	3.78	65.5	89.8	21.415	233.5	3.4
1000	30.33	35.330	0.02132	1.26	66.7	86.1	27.436	294.1	12.7
1020	24.50	32.590	0.01937	3.19	69.7	85.9	21.792	237.4	8.7
1050	21.94	29.110	0.01663	13.90	82.9	87.6	19.675	215.6	4.6
1080	24.82	26.370	0.01780	9.98	92.4	86.7	22.001	239.5	5.5
1120	30.36	22.510	0.02070	3.80	96.0	84.8	26.383	283.6	9.2
1250	33.18	25.480	0.05843	2.33	98.2	53.2	18.208	200.4	8.6
1300	39.57	28.200	0.06999	1.59	100.0	52.4	21.494	234.3	11.5

1) Corrected for mass discrimination, machine background, orifice discrimination, and blank.
2) Total Ar includes blank.
3) Error values are for analytical error only (quoted at 1 sigma level).

the amphibolite and pelitic gneiss. The major structures in this area are typical of the biotite gneiss and amphibolite unit and are described with the previous sample (82AFr4034). In thin-section, the sample collected for analysis consists of hornblende + plagioclase + chlorite + epidote + white mica + opaques (plate 14). The hornblende is blue-green to green-brown pleochroic, slightly poikilitic containing inclusions of quartz + plagioclase + opaques and with minor chlorite intergrowths. No folds were observed in thin-section and the foliation is well defined primarily by the hornblende and plagioclase. Due to the blue-green color of the hornblende and the abundance of epidote and chlorite, this sample has probably been metamorphosed to the epidote-amphibolite or amphibolite facies.

This hornblende separate had very minor quartz and epidote composites and the size fraction used for analysis was -60 to +80 mesh.

The age spectrum for this analysis is shown in figure 32. The first two steps of this analysis have components of inherited radiogenic ^{40}Ar as indicated by the anomalously high ages. The third step yielded the lowest age of the analysis (128 ± 5) with the following six, steps (4-9) showing a general increase in age up to 180 Ma. The slow cooling curve fit to the data has a lower intercept at about 110 Ma. An integrated plateau age for this sample has not been determined due to the general progressive increase in age across the spectrum. As illustrated in figure 33, no single isochron is defined by the data points. This type of

FIGURES 32 & 33: Age spectrum and isochron plot: Sample 83AFr 4072 (hornblende).

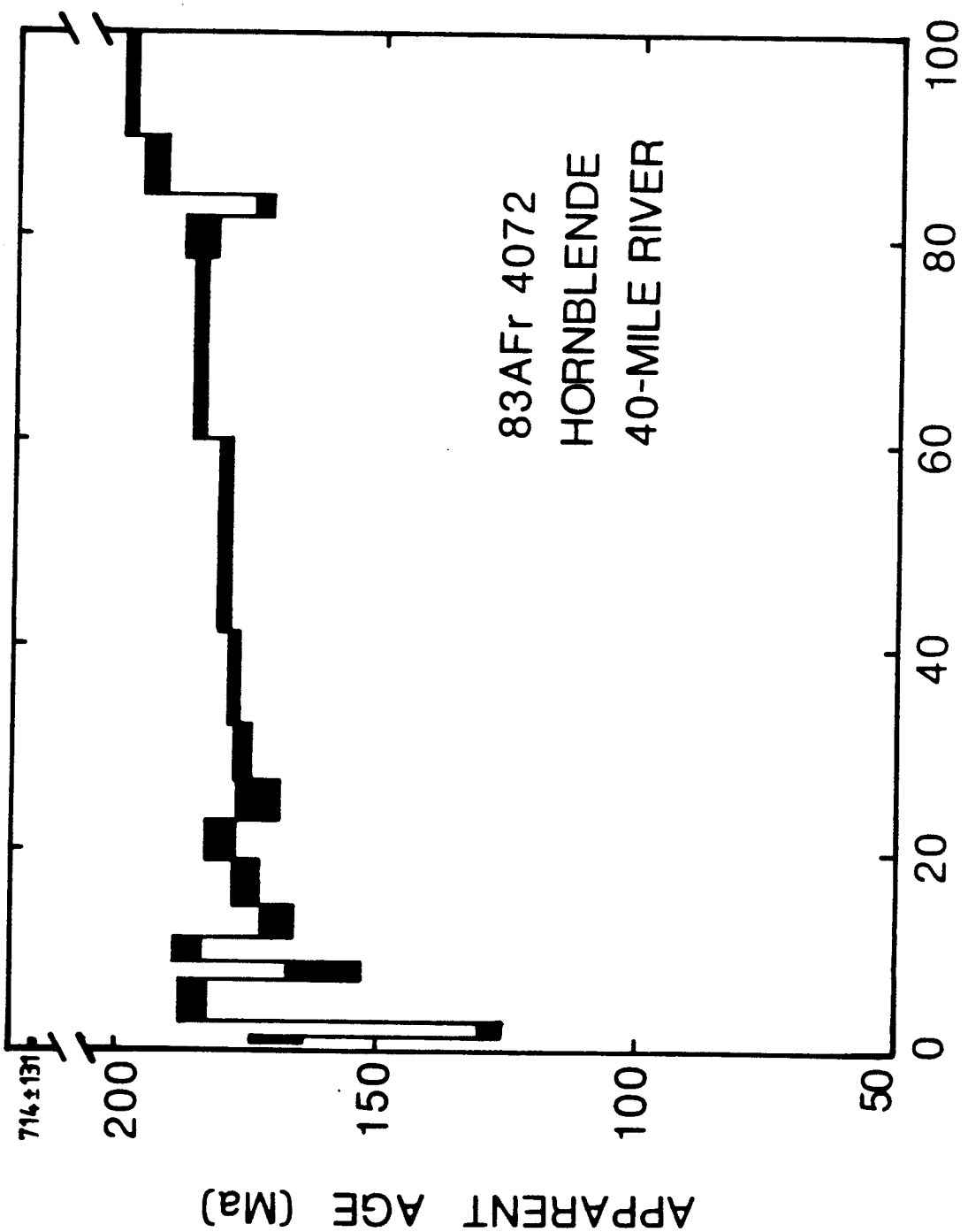
714±131
200
150
100
50
0
20
40
60
80
100
% ^{39}Ar RELEASED
APPARENT AGE (Ma)
83AFr 4072
HORNBLENDE
40-MILE RIVER

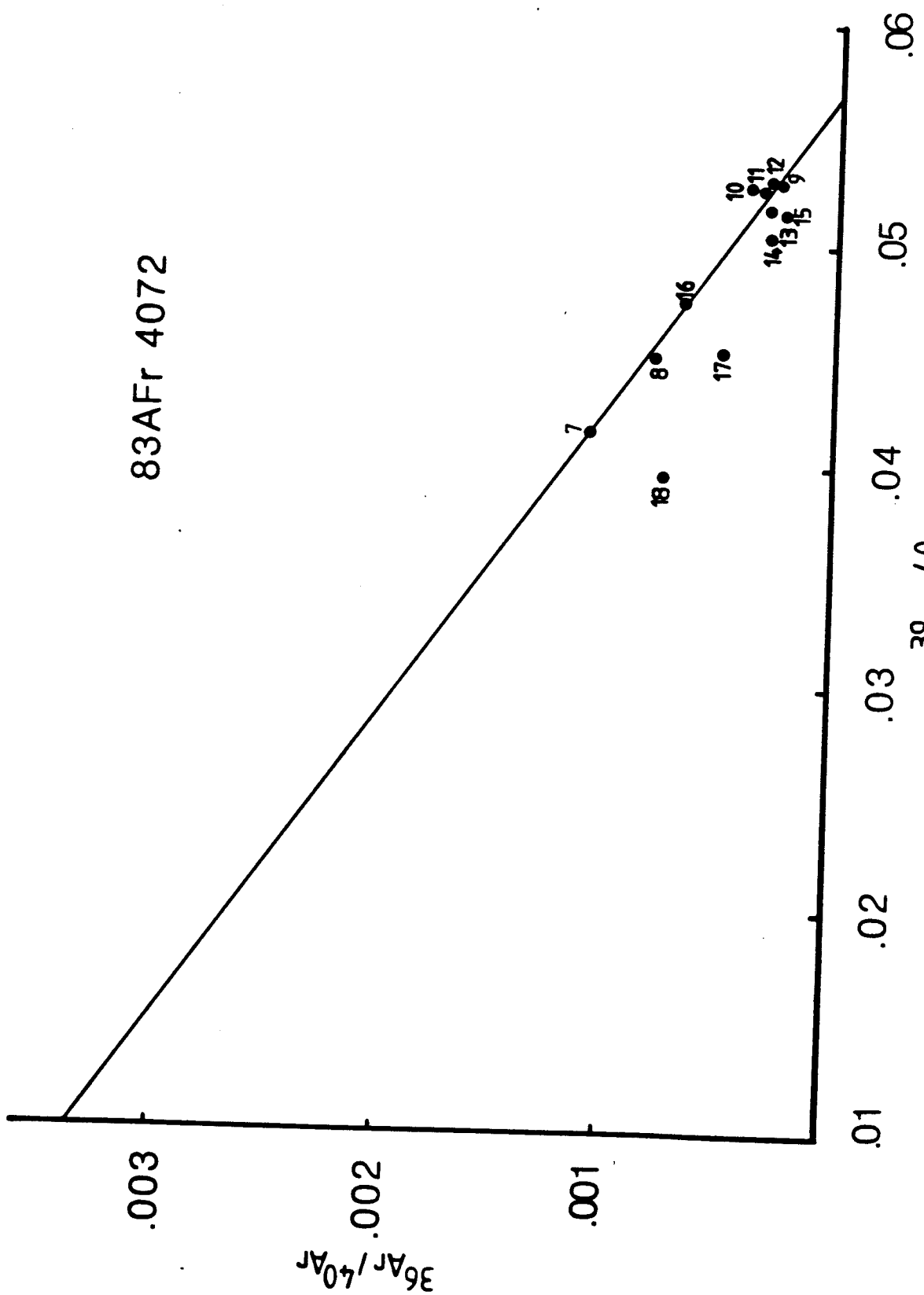
83AFr 4072
$^{36}Ar/^{40}Ar$
$^{39}Ar/^{40}Ar$
.003
.002
.001
.01
.02
.03
.04
.05
.06
7
8
9
10
11
12
13
14
15
16
17
18

SAMPLE #: 83AFr4072
MINERAL: Hornblende
J= .005956

TEMPERATURE (Degrees Centigrade)	(1) 40Ar/39Ar	(1) 37Ar/39Ar	(1) 36Ar/39Ar	39ArK x 10e-14 Moles	Cumulative 39Ar (%)	(2) 40Ar*/40Ar(t) (%)	40Ar*/39ArK	Apparent Age (Ma)	(3) Standard Dev. (Ma)
450	165.30	3.9550	0.285300	0.20	0.01	47.7	81.545	714.2	131.5
490	51.66	1.9330	0.119400	2.90	1.50	31.7	16.509	169.2	10.2
530	24.21	1.0620	0.040350	3.58	3.30	50.4	12.345	128.0	4.8
580	24.88	0.8201	0.022820	7.90	7.20	72.6	18.175	185.4	4.8
620	24.03	0.8177	0.028500	3.02	8.70	64.2	15.647	160.8	14.2
660	23.13	0.9746	0.016530	5.09	11.20	78.4	18.303	186.7	4.5
710	24.28	1.4600	0.026380	6.20	14.30	67.8	16.585	170.0	6.2
800	22.44	3.3810	0.018840	8.76	18.60	75.9	17.163	175.6	4.8
830	19.04	5.2680	0.006368	8.16	22.60	91.8	17.648	180.3	4.9
860	18.99	11.1200	0.010310	7.93	26.50	88.1	16.991	173.9	8.1
890	18.98	14.3500	0.010450	11.10	32.00	89.5	17.259	176.5	1.9
920	18.89	14.6000	0.009428	18.80	41.30	91.4	17.495	178.8	1.0
950	19.27	16.5500	0.010740	38.60	60.30	90.5	17.692	180.7	1.0
980	19.78	17.3700	0.010970	37.40	78.70	90.7	18.211	185.8	1.1
1010	19.39	14.4900	0.008852	6.67	82.00	91.9	18.162	185.3	6.4
1050	20.90	21.8900	0.020360	5.28	84.60	79.2	16.987	173.9	2.2
1100	22.00	21.4700	0.016800	11.00	90.00	85.2	19.112	194.5	3.5
1250	25.08	20.6700	0.025170	20.50	100.00	77.0	19.671	199.9	0.7

1) Corrected for mass discrimination, machine background, orifice discrimination, and blank.
2) Total Ar includes blank.
3) Error values are for analytical error only (quoted at 1 sigma level).

age spectrum is typical of a sample that cooled slowly through a temperature range where radiogenic ^{40}Ar is partially retained.

The next two samples to be discussed were collected 9 kilometers downstream from the the bridge along the northern bank of the Forty Mile River. These samples are located well within the mapped biotite gneiss and amphibolite unit (Foster, 1976). At this locality, a complex fault zone was found, but difficult access restricted study of much of the zone. This fault zone is generally on strike with the southern most fault zone along the Taylor Highway (figure 19) and could be an equivalent or related structure. Where observed, the fault zone involved only rocks of the biotite gneiss and amphibolite unit. The zone extends for several hundred meters, and contained numerous distinct faults. One accessible fault revealed a highly brecciated and silicified zone several meters wide, containing lenticular, discontinuous marble blocks up to one half meter in length. A sense of offset of south over north was inferred along an east-west striking fault plane as indicated by the apparent offset of a single tracable layer. In the rubble at the base of the outcrop, a serpentinized ultramafic block was observed, but not found in place. The general rock types observed here included amphibolite with plagioclase ± garnet ± cross biotite and quartzite with muscovite and biotite. Several places within the massive amphibolite, fault zones were observed from several

centimeters to a meter wide containing actinolite + biotite schist. Commonly, this lower grade schist was strongly foliated parallel to the fault plane and contained numerous asymmetric, discontinuous folds.

The two samples collected for analysis were obtained from the massive amphibolite and the actinolite + biotite schist. At the eastern end of the exposure, the amphibolite sample was collected within several meters of a fault zone containing actinolite + biotite schist. This fault was approximately one meter wide, and contained the previously described strongly foliated schist. A sample of the schist was collected to obtain the biotite for analysis.

In outcrop, the amphibolite is well foliated, primarily defined by the alignment of hornblende and plagioclase. No obvious folds were observed in this gneiss. Biotite formed across the foliation in much of the amphibolite. In thin-section, the amphibolite contains the assemblage bluish-green to greenish-brown hornblende + plagioclase + quartz + carbonate + opaques + minor biotite and chlorite (plate 15). This assemblage is stable in the epidote-amphibolite to amphibolite facies. The mineral separate used for analysis contained very minor quartz composites and biotite. The sample was hand picked, then counted, to ensure the biotite content was less than one half percent. The size fraction used for analysis was -60 to +100 mesh.

The age spectrum for this analysis (83AFr4087A) is shown in figure 34. The first step recorded an age of 119 ± 2 Ma and represents approximately 0.5% gas loss. The following

PLATE 15: Photomicrograph of sample 83AFr 4087A (amphibolite).

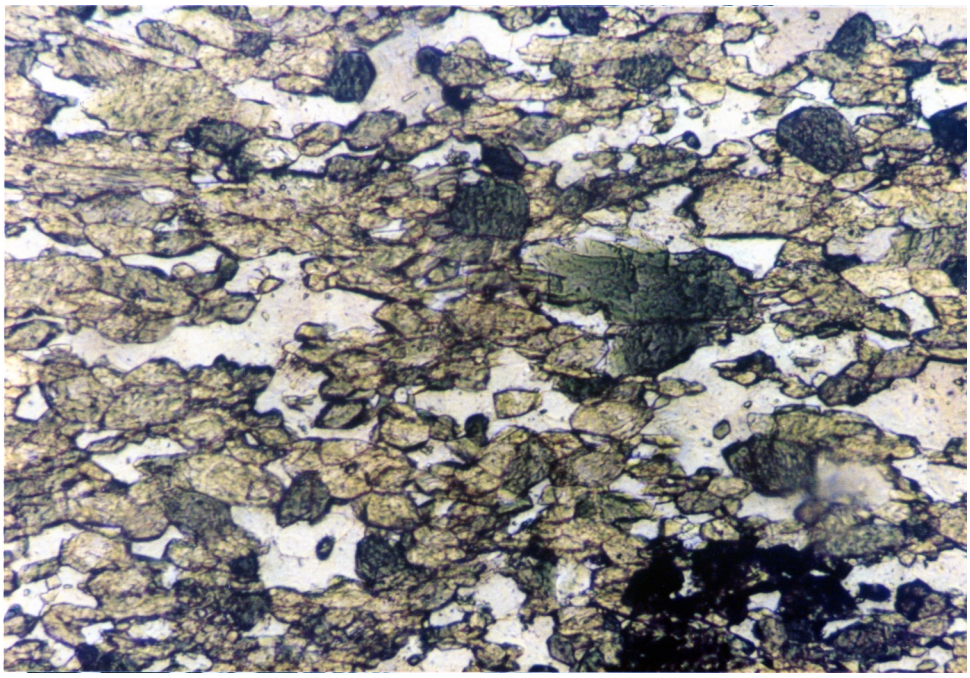

PLATE 15: Photomicrograph of sample 83AFr 4087A (amphibolite).

FIGURES 34 & 35: Age spectrum and isochron plot: Sample 83AFr 4087A (hornblende).

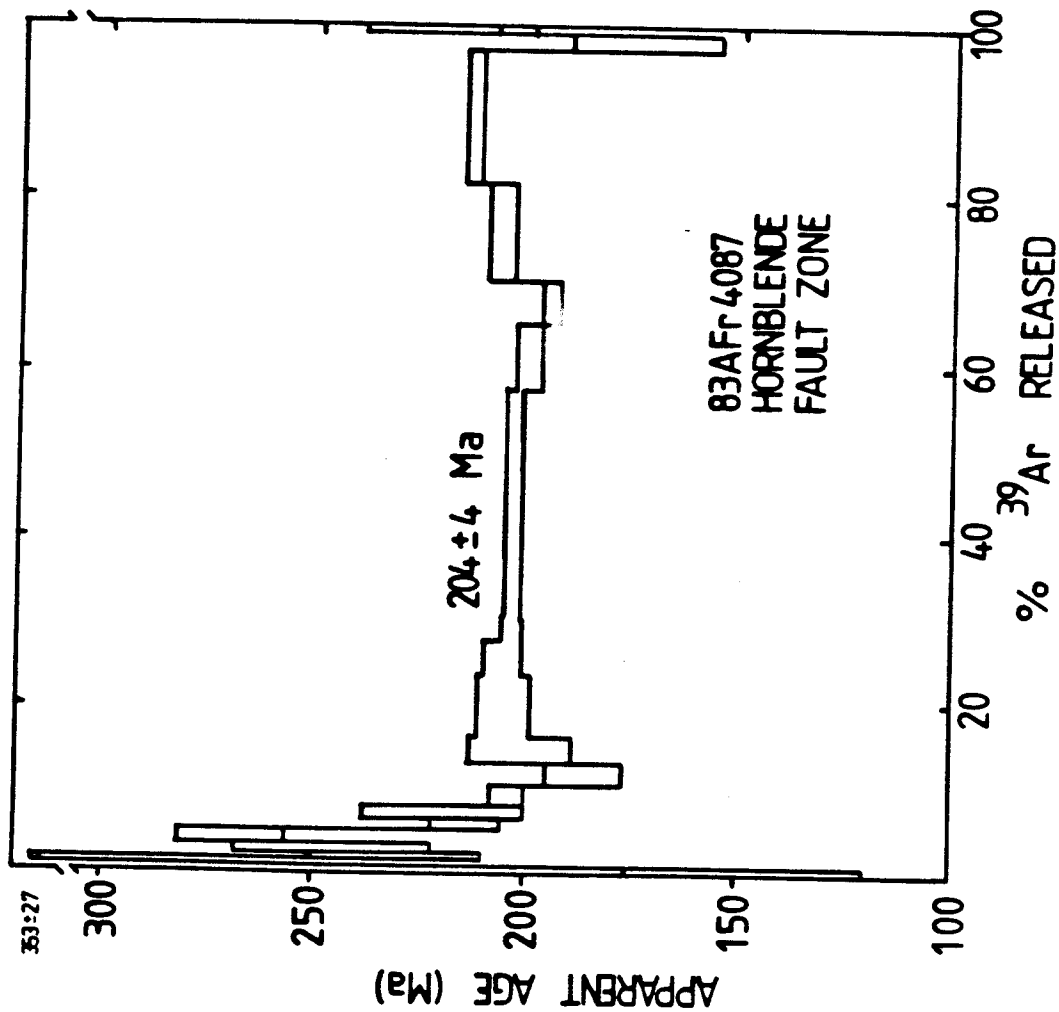
353:27
300
250
200
150
100
APPARENT AGE (Ma)
20
40
60
80
100
% ^{39}Ar RELEASED
204±4 Ma
83AFr4087
HORNBLENDE
FAULT ZONE

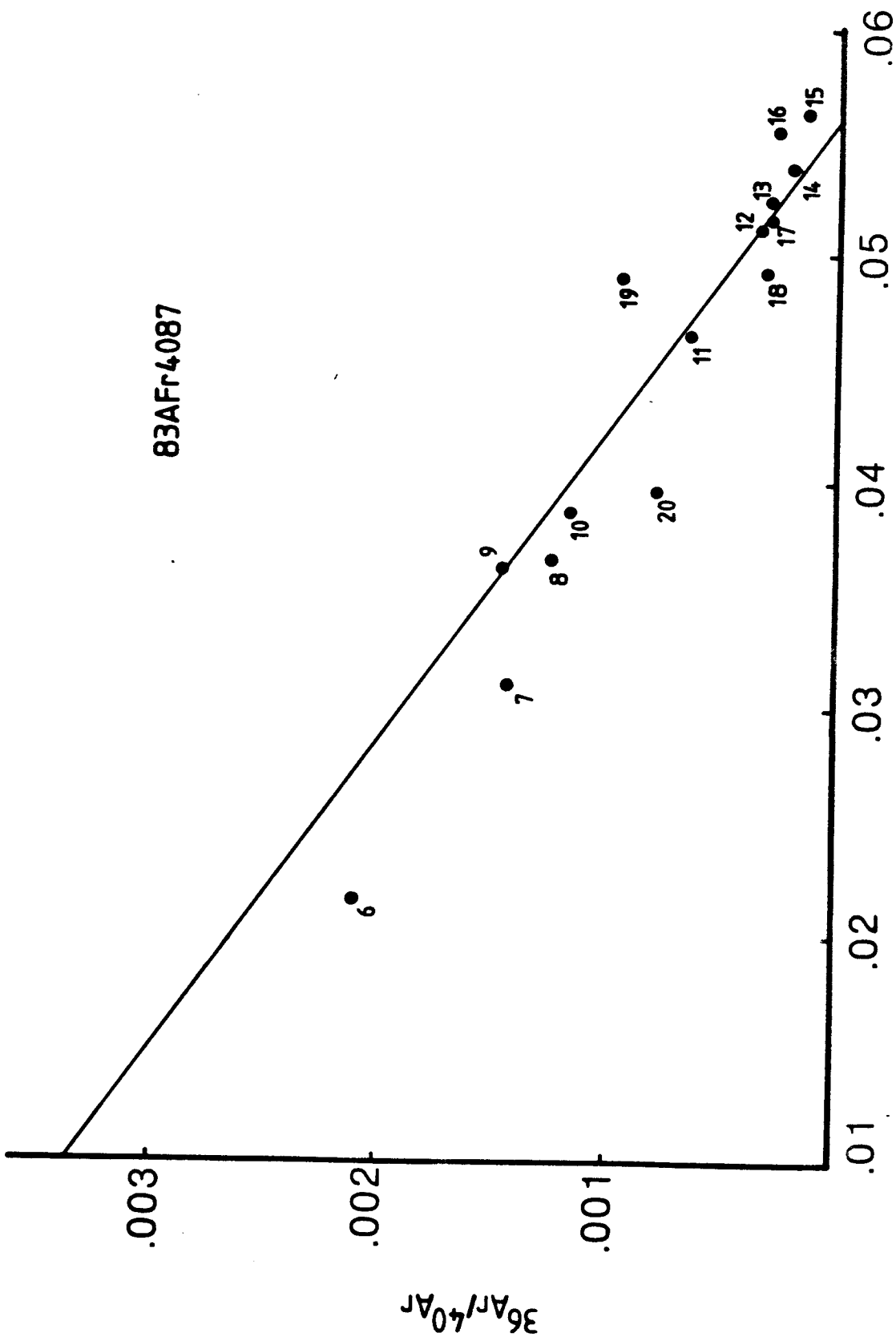
83AFr4087
$^{36}Ar/^{40}Ar$
$^{39}Ar/^{40}Ar$
.003
.002
.001
.01
.02
.03
.04
.05
.06
6
7
8
9
10
11
12
13
14
15
16
17
18
19
20

SAMPLE #: 83AFr4087
MINERAL: Hornblende
J= .006852

TEMPERATURE (Degrees Centigrade)	(1) 40Ar/39Ar	(1) 37Ar/39Ar	(1) 36Ar/39Ar	39ArK x 10e-14 Moles	Cumulative 39Ar (%)	(2) 40Ar*/40Ar(t) (%)	40Ar*/39ArK	Apparent Age (Ma)	(3) Standard Dev. (Ma)
450	27.62	0.2084	0.051110	1.40	0.8	44.1	12.497	148.3	27.7
500	225.80	3.8880	0.658500	1.10	1.4	13.9	31.580	353.4	49.0
540	99.57	2.4090	0.270300	1.64	2.3	19.8	19.887	230.5	20.4
580	74.14	2.7410	0.171900	2.19	3.5	28.4	21.245	245.1	22.6
620	68.05	4.1130	0.152100	2.55	4.9	34.2	23.490	269.2	13.4
650	46.82	3.0840	0.097250	2.97	6.5	38.8	18.346	213.7	7.5
690	32.40	2.5470	0.046650	3.13	8.2	57.4	18.829	218.9	19.1
740	27.56	2.2310	0.035010	4.10	10.4	62.8	17.496	204.3	3.7
790	27.78	7.0190	0.042480	4.54	12.9	56.4	15.868	186.2	9.3
840	258.91	9.0620	0.032280	5.24	15.8	65.5	17.220	201.2	11.5
890	21.48	13.2500	0.017700	14.00	23.5	80.5	17.528	204.6	5.5
920	19.56	10.2200	0.009648	6.95	27.3	89.0	17.676	206.3	4.0
940	19.08	10.3500	0.008705	5.72	30.4	90.1	17.492	204.2	1.8
960	18.60	10.2900	0.007001	48.50	57.0	93.3	17.502	204.3	0.7
990	17.84	7.2840	0.004783	14.40	64.9	95.0	17.099	199.9	2.4
1020	18.10	7.8090	0.007302	9.40	70.1	91.0	16.664	195.0	1.3
1060	19.39	12.8800	0.009560	21.30	81.8	90.6	17.793	207.5	2.6
1100	20.24	12.9100	0.010330	27.10	96.7	90.0	18.427	214.5	1.6
1150	20.43	12.2900	0.022970	3.80	98.8	70.8	14.786	174.1	17.8
1250	25.20	12.3800	0.023590	2.30	100.0	75.1	19.428	225.5	15.5

1) Corrected for mass discrimination, machine background, orifice discrimination, and blank.

2) Total Ar includes blank.

3) Error values are for analytical error only (quoted at 1 sigma level).

six steps (2-7) yielded older than plateau ages and probably represent inherited radiogenic ^{40}Ar. The plateau is defined by steps 8 through 15, which consist of 48% of the ^{39}Ar released. These steps fall on the isochron between atmospheric composition and the corresponding $^{39}Ar/^{40}Ar$ ratio (figure 35). The integrated plateau age for this sample is 204 ± 4 Ma. Steps 18 and 20 yield ages approximately 4% higher than the plateau age and define a line on the isochron plot between the plateau age and a $^{39}Ar/^{40}Ar$ composition well below atmospheric composition. These high temperature steps probably represent gas extracted from sites within the crystal that contain inherited radiogenic ^{40}Ar. Step 19 yielded an anomalously low age for unknown reasons.

Sample 83AFr4087B is the actinolite + biotite schist collected in the fault zone. In thin-section, this sample contains clear to light green pleochroic actinolite + biotite + quartz + plagioclase + opaques (plate 16). This assemblage is stable in the greenschist facies. Actinolite and biotite define the foliation in this schist, and in thin-section microfolds of both minerals are present. Biotite was separated from this sample and used for analysis.

The age spectrum for this analysis (figure 36) shows a very old age (2244 ± 1289 Ma) for the first step, which indicates significant inherited radiogenic ^{40}Ar. The following step (2) gave a zero age due to a high atmospheric

PLATE 16: Photomicrograph of sample 83AFr 4087B (actinolite + biotite schist).

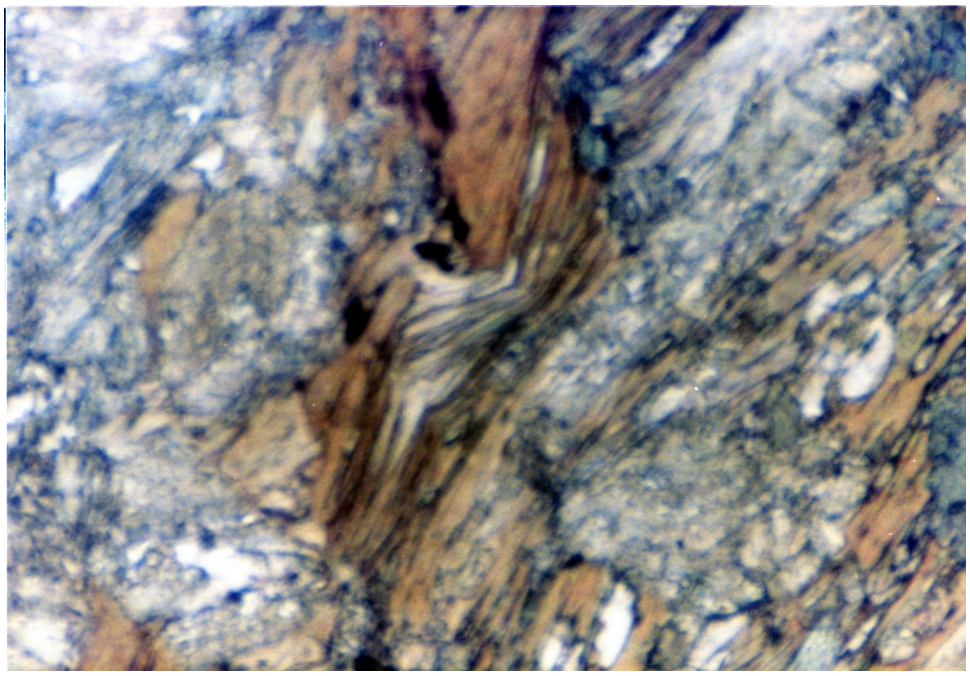

PLATE 16: Photomicrograph of sample 83AFr 4087B (actinolite + biotite schist).

FIGURES 36 & 37: Age spectrum and isochron plot: Sample 83AFr 4087B (Biotite).

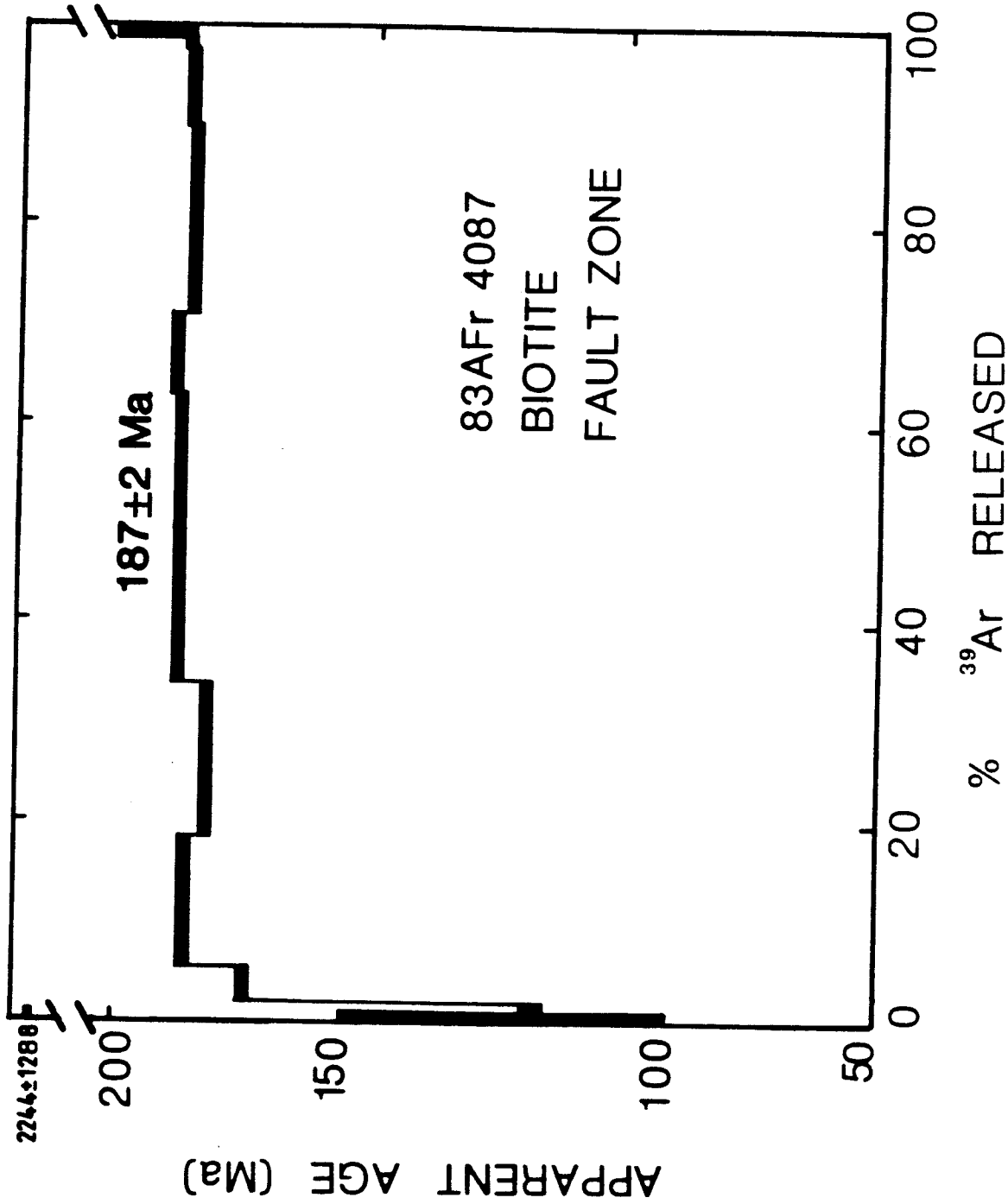
APPARENT AGE (Ma)
200
150
100
50
2244±1288
187±2 Ma
83AFr 4087
BIOTITE
FAULT ZONE
0
20
40
60
80
100
% ^{39}Ar RELEASED

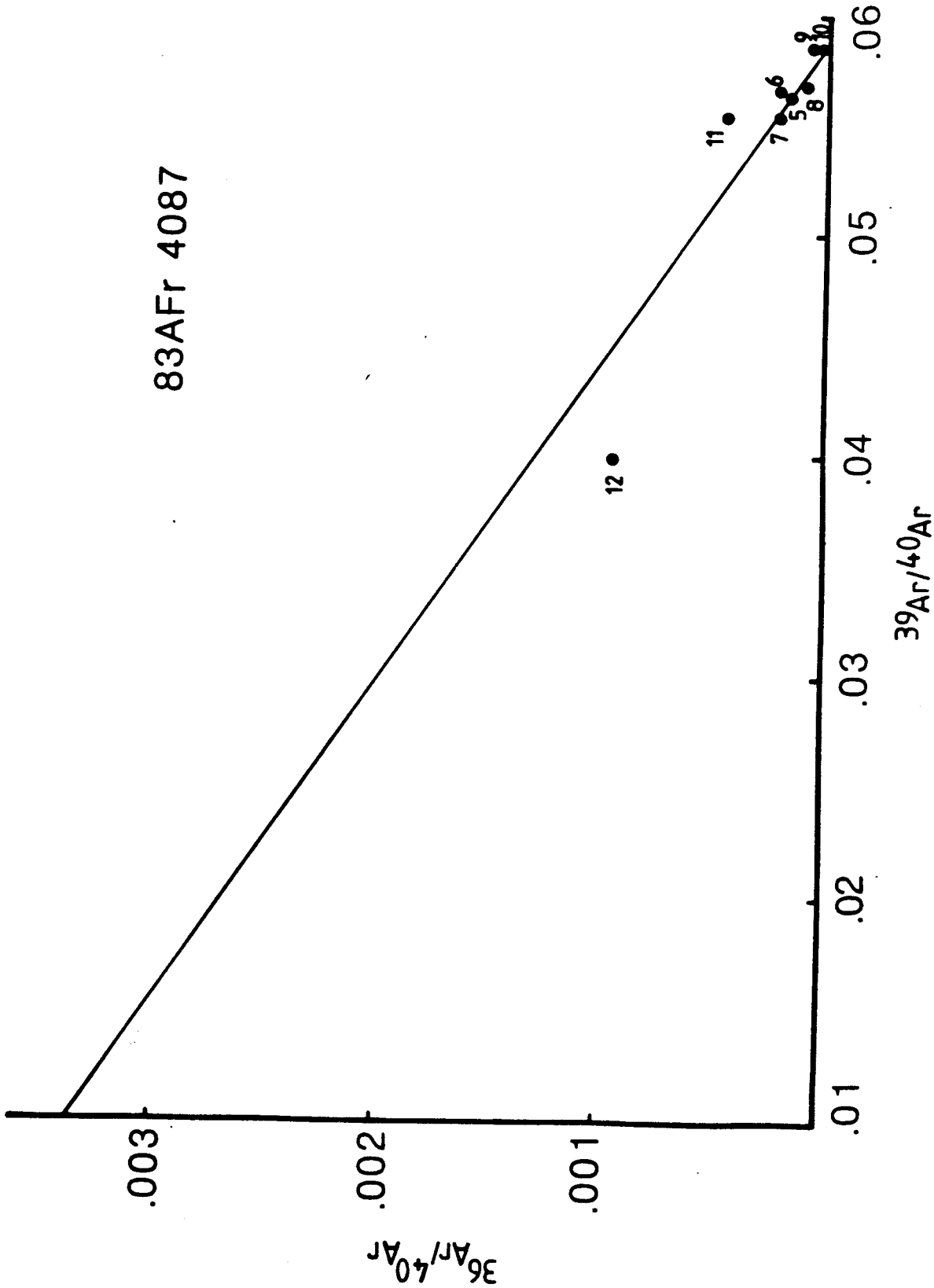
83AFr 4087
$^{36}Ar/^{40}Ar$
.003
.002
.001
.01
.02
.03
.04
.05
.06
$^{39}Ar/^{40}Ar$
11
12
7
5
8
6
2
10

SAMPLE #: 83AFr4087
MINERAL: Biotite
J= .006398

TEMPERATURE (Degrees Centigrade)	(1) 40Ar/39Ar	(1) 37Ar/39Ar	(1) 36Ar/39Ar	39ArK x 10e-14 Moles	Cumulative 39Ar (%)	(2) 40Ar*/40Ar(t) (%)	40Ar*/39ArK	Apparent Age (Ma)	(3) Standard Dev. (Ma)
400	527.60	0.000000	0.473100	0.01	0.001	64.5	386.080	2244.0	1288.00
520	27.31	0.051570	0.055050	0.77	0.090	38.5	11.014	122.9	31.80
600	16.42	0.056000	0.019900	13.20	1.700	63.7	10.507	117.4	2.20
650	18.08	0.021210	0.007504	33.86	5.700	87.4	15.829	174.0	0.86
710	17.95	0.007535	0.002997	109.45	18.700	94.8	17.023	186.6	0.43
780	17.88	0.006238	0.003975	126.06	33.700	93.2	16.672	182.9	0.89
850	18.33	0.031700	0.003703	193.44	56.700	93.8	17.199	188.3	0.23
980	17.76	0.080210	0.001626	122.86	71.300	97.1	17.253	188.9	0.32
1050	17.24	0.058260	0.000766	156.00	89.900	98.5	16.985	186.1	0.28
1100	17.23	0.021370	0.000397	65.82	97.700	99.0	17.078	187.1	0.74
1250	19.71	0.179200	0.008833	16.46	99.700	86.4	17.082	187.1	0.74
1300	25.33	0.117400	0.024400	2.16	100.000	70.1	18.095	197.7	21.20

1) Correced for mass discrimination, machine background, orifice discrimination, and blank.
2) Total Ar includes blank.
3) Error values are for analytical error only (quoted at 1 sigma level).

content, but is considered irrelevant because of the small fraction of gas extracted. Steps 3 and 4 yielded ages of 123 ± 32 and 117 ± 2 Ma respectively and indicate gas loss at about that time. The gas loss caused by this late heating event is approximately 0.1%. A cooling curve drawn to these data intersects the y-axis at about 110 Ma.

The integrated plateau age for this sample is 187 ± 2 Ma and is defined by 94% of the gas released. The isochron plot (figure 39) shows that all but points 13 and 14 fall close to the line between atmospheric composition and the plateau age. Most of the points plot relatively close to the x-axis, which reflects their radiogenic nature. Steps 13 and 14 are the high temperature gas fractions and plot above and below the isochron, respectively, and represent anomalous $^{39}Ar/^{40}Ar$ compositions.

3. Igneous Rocks

Igneous rocks were analyzed by the $^{40}Ar/^{39}Ar$ method for several specific reasons. One important issue in understanding the tectonic development of this region is determining the timing of significant structural events. Relatively undeformed igneous rocks in the area were analyzed to determine the minimum age of specific structures. Also of importance is the timing, extent, and influence of thermal events that post date the principal metamorphism in the area. To analyze this, some of the oldest (based on K-Ar dates) relatively unmetamorphosed igneous rocks were studied.

Sample 83AFr4045 was collected from a felsic dike which crosscuts certain structures in the northern portion of the biotite gneiss amphibolite unit (figure 25). This sample was collected just south of the southernmost fault zone along the Taylor Highway. This fault zone was previously described. The dike is approximately 0.5 to 1 meter in width and strikes northeasterly across the main foliation in the country rock. Several fold hinges and fold axis lineations are cut by the dike. These folds and related structures are typical in style and orientation to the major folds (F_2) in the biotite gneiss and amphibolite unit. The dike is unfoliated, relatively unmetamorphosed and composed of quartz + feldspar + white mica + biotite.

In thin-section, there is no preferred orientation of

PLATE 17: Photomicrograph of sample 83AFr 4045 (aplite dike).

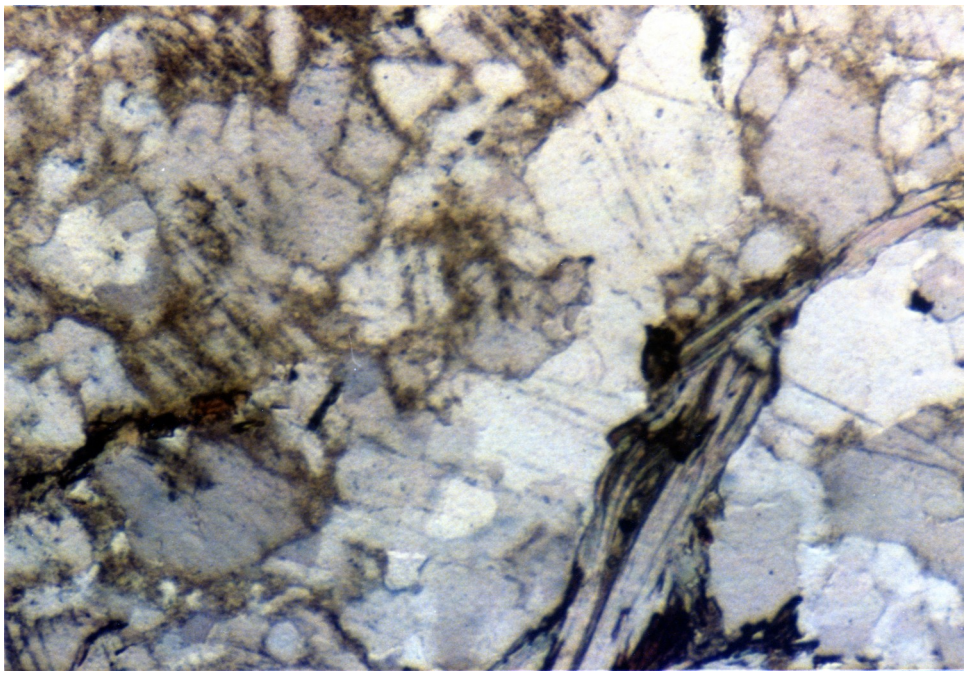

PLATE 17: Photomicrograph of sample 83AFr 4045 (aplite dike).

FIGURES 38 & 39: Age spectrum and isochron plot: Sample 83AFr 4045 (muscovite).

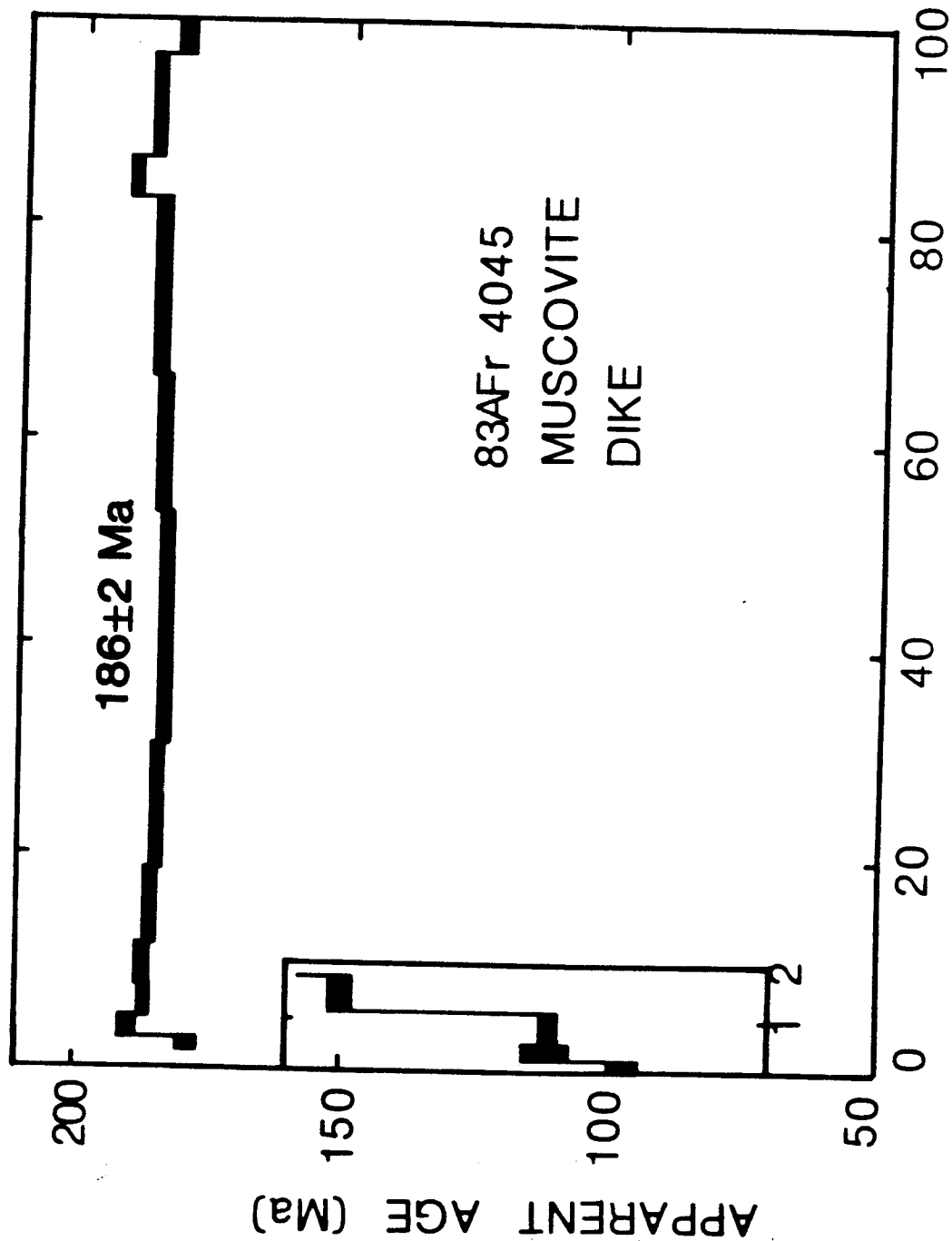
186±2 Ma
83AFr 4045
MUSCOVITE
DIKE
APPARENT AGE (Ma)
200
150
100
50
0
20
40
60
80
100
% ^{39}Ar RELEASED
1
2

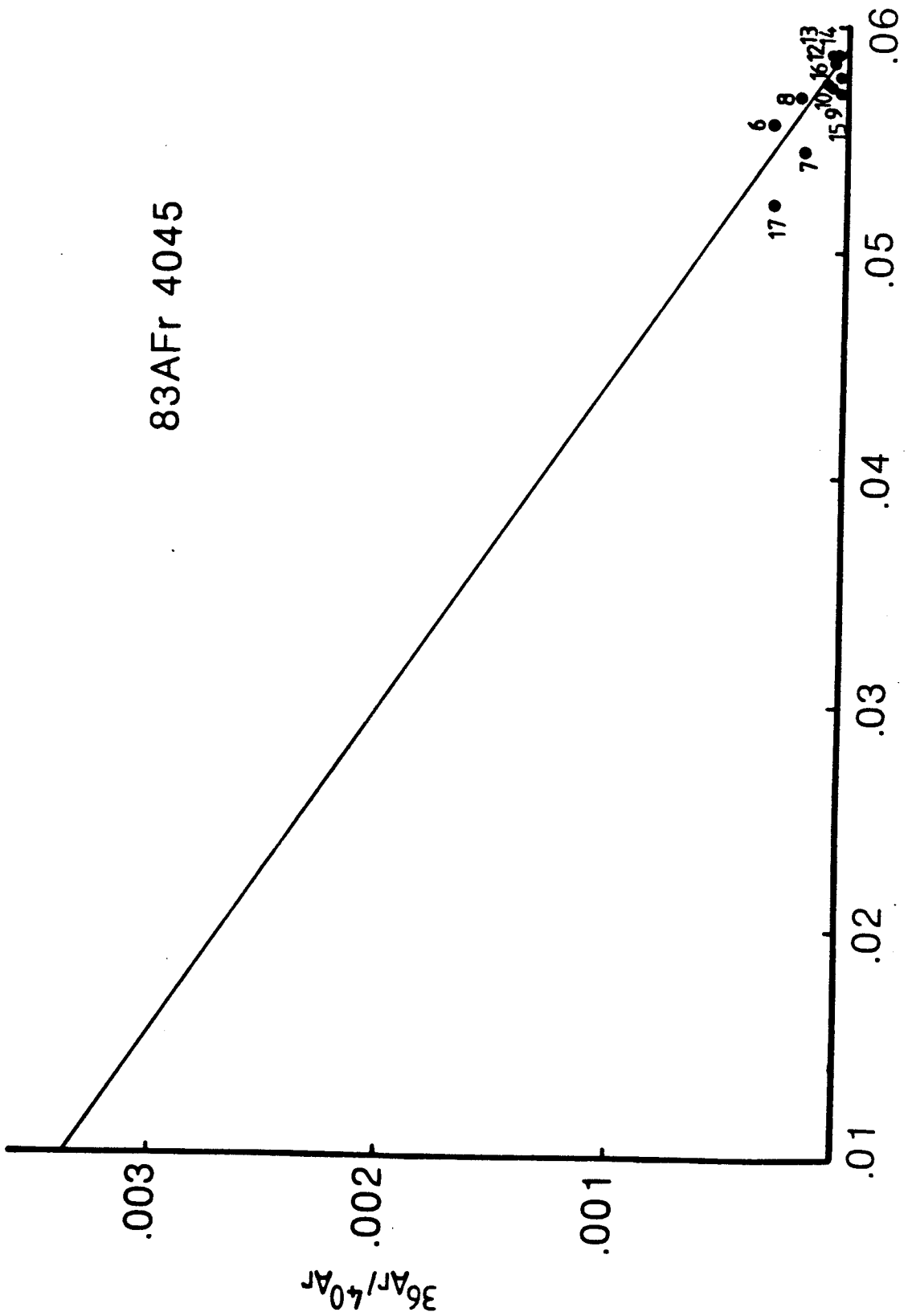
83AFr 4045
$^{36}Ar/^{40}Ar$
$^{39}Ar/^{40}Ar$
.003
.002
.001
.01
.02
.03
.04
.05
.06
6
7
8
9
10
12
13
14
15
16
17

SAMPLE #: 83AFr4045
MINERAL: Muscovite
J= .006366

TEMPERATURE (Degrees Centigrade)	(1) 40Ar/39Ar	(1) 37Ar/39Ar	(1) 36Ar/39Ar	39ArK x 10e-14 Moles	Cumulative 39Ar (%)	(2) 40Ar*/40Ar(t) (%)	40Ar*/39ArK	Apparent Age (Ma)	(3) Standard Dev. (Ma)
350	42.33	0.79940	0.0521500	0.30	0.01	59.1	26.9610	285.8	238.10
390	23.53	0.43120	0.0501200	2.75	0.20	36.5	8.7216	97.5	4.50
440	17.29	0.34960	0.0243800	5.19	0.50	57.7	10.0870	112.3	8.70
490	14.18	0.15680	0.0140700	9.88	1.10	70.0	9.9996	111.3	3.10
540	15.95	0.09559	0.0075890	14.50	1.80	85.4	13.6800	150.7	3.60
580	18.18	0.09778	0.0057740	18.40	2.80	90.2	16.4430	179.6	2.40
620	18.56	0.07136	0.0034500	36.54	4.80	94.2	17.5140	190.7	0.87
660	17.77	0.05764	0.0018810	50.89	7.80	96.6	17.1820	187.3	0.76
700	17.64	0.04652	0.0012990	62.18	11.80	97.5	17.2190	187.7	1.20
740	17.62	0.04475	0.0016810	122.30	18.80	96.9	17.0850	186.3	0.38
780	17.52	0.07209	0.0015100	216.87	31.80	97.2	17.0440	185.8	0.24
820	17.31	0.06313	0.0010970	356.64	52.80	97.9	16.9500	184.9	0.21
860	17.36	0.63640	0.0011870	234.07	66.80	98.0	17.0370	185.8	0.31
900	17.35	0.84940	0.0009426	278.92	83.80	98.6	17.1140	186.6	0.40
950	17.69	0.10800	0.0003871	44.74	86.80	99.1	17.5520	191.1	1.40
1050	17.43	0.33120	0.0007464	176.97	97.80	98.6	17.2010	187.5	0.22
1150	18.39	1.07100	0.0057670	40.17	100.00	90.9	16.7520	182.8	2.20

1) Corrected for mass discrimination, machine background, orifice discrimination, and blank.
2) Total Ar includes blank.
3) Error values are for analytical error only (quoted at 1 sigma level).

any of the minerals, and the igneous texture (hypidiomorphic granular) is preserved (plate 17). White mica was separated from this sample for analysis. The separate was pure with minor oxidized or weathered grain edges and the size fraction used was -60 to +70 mesh. The age spectrum for this analysis (figure 38) shows no inherited radiogenic ^{40}Ar. The first 5 steps show a progressive increase in age from 97 ± 5 to 180 ± 3 Ma. This represents episodic loss associeted with a thermal event at approximately 100 Ma. The amount of gas loss during this event is approximately 0.5%. The integrated plateau age for this analysis is 186 ± 2 Ma and is defined by 90% of the gas released. As illustrated on the isochron plot in figure 39, steps 8-14 and 16 define the plateau and plot close to the line between atmospheric composition and the corresponding $^{39}Ar/^{40}Ar$ ratio. Most points plot near the x-axis and define the intercept very well. Steps 15 and 17 yielded slightly anomalous ages and plot the greatest distance from the isochron.

Sample 63AFr2C was collected from a pluton in the southwest portion of the Eagle quadrangle (Eagle A-5) (figure 25). This intrusive is called the Mt. Veta pluton, and is mapped as a syenite, although it is quite variable in composition. Phases of the pluton include hornblende syenite, hornblende quartz monzonite, hornblende tonalite, quartz monzonite, and granite. This pluton is bounded on the north and south by granitic rocks mapped as Mesozoic to

FIGURES 40 & 41: Age spectrum and isochron plot: Sample 68AFr 2C (hornblende).

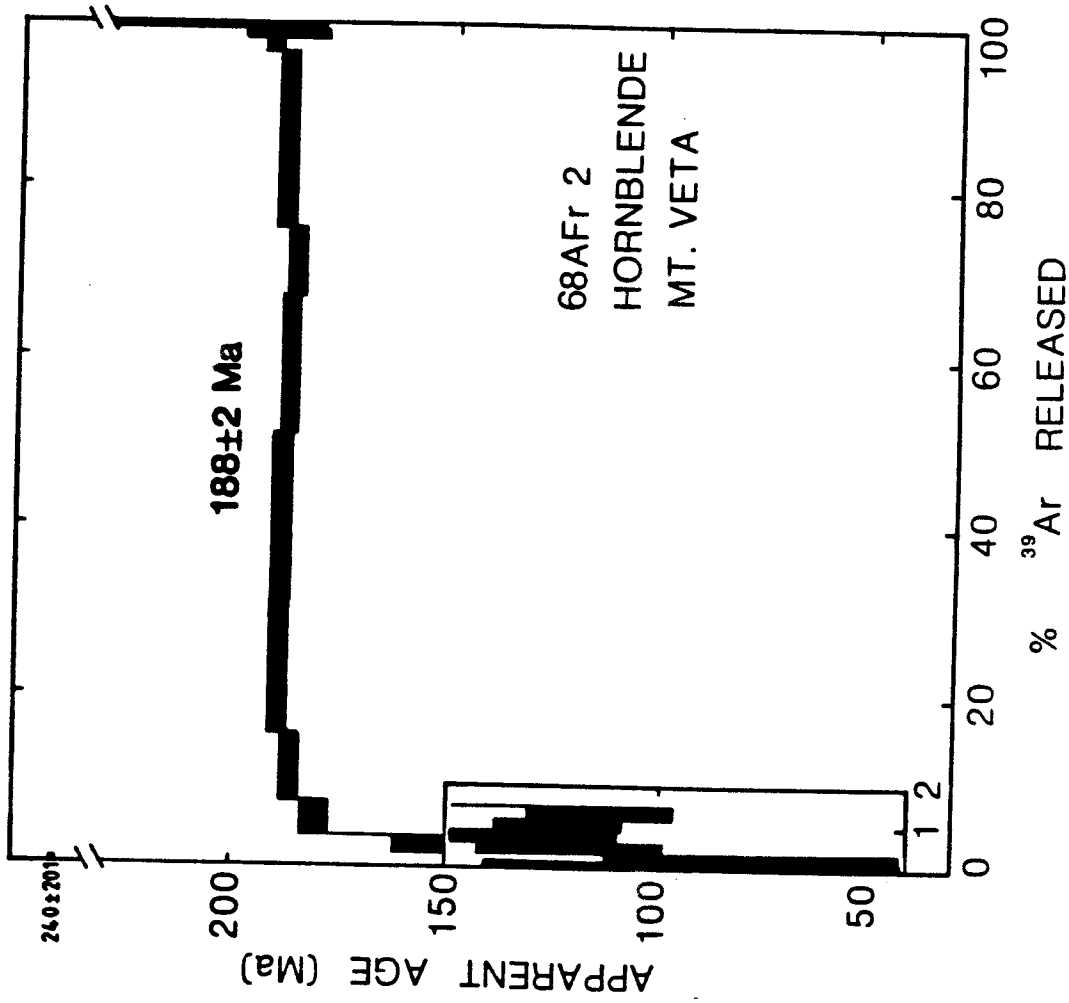
240±20
200
150
100
50
APPARENT AGE (Ma)
188±2 Ma
68AFr 2
HORNBLENDE
MT. VETA
1
2
0
20
40
60
80
100
% ^{39}Ar RELEASED

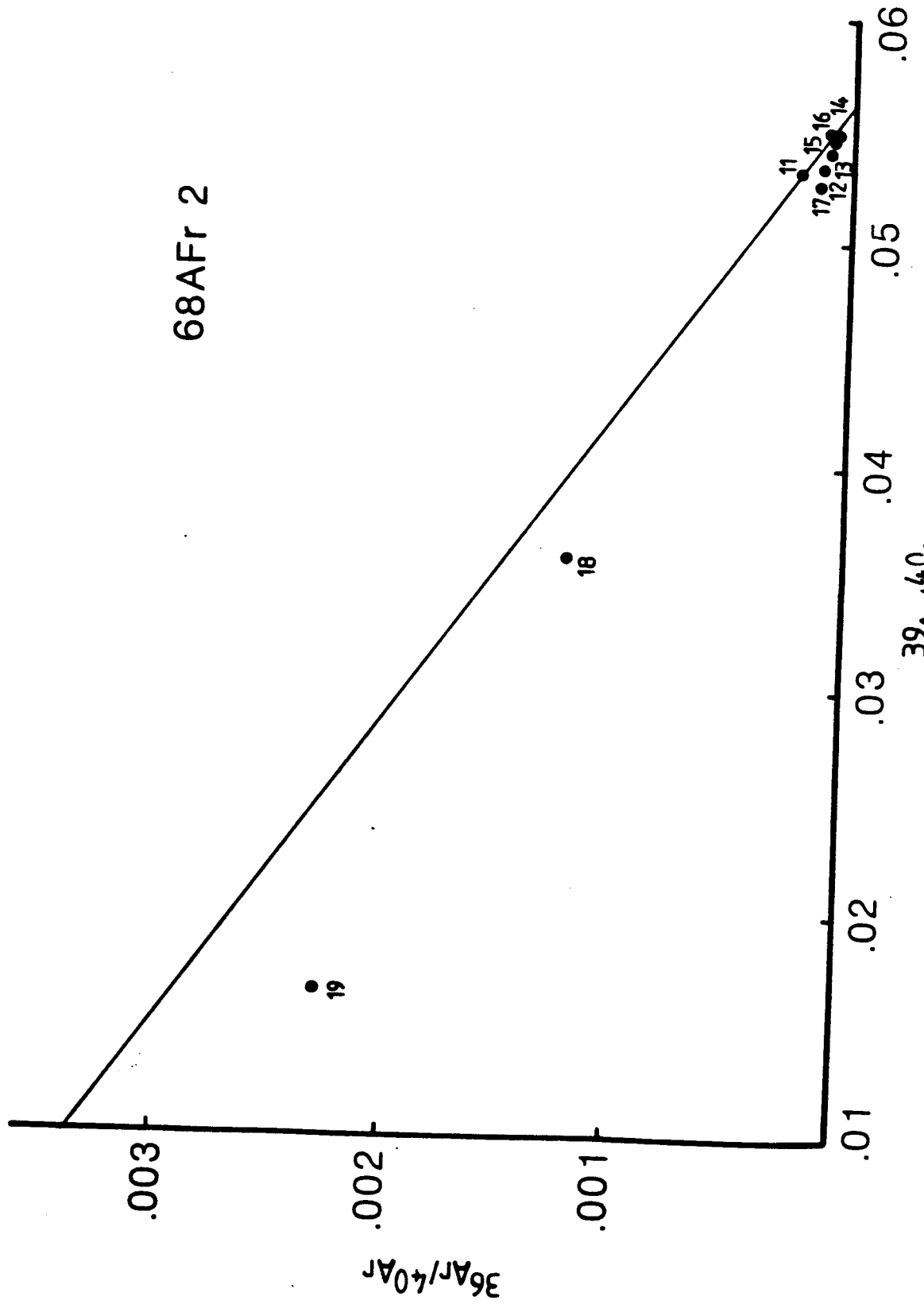
68AFr 2
$^{36}Ar/^{40}Ar$
.003
.002
.001
.01
.02
.03
.04
.05
.06
$^{39}Ar/^{40}Ar$
11
12
13
14
15
16
17
18
19

SAMPLE #: 68AFr2C
MINERAL: Hornblende
J= .006134

TEMPERATURE (Degrees Centigrade)	(1) 40Ar/39Ar	(1) 37Ar/39Ar	(1) 36Ar/39Ar	39ArK x 10e-14 Moles	Cumulative 39Ar (%)	(2) 40Ar*/40Ar(t) (%)	40Ar*/39ArK	Apparent Age (Ma)	(3) Standard Dev. (Ma)
520	57.47	0.0000	0.114600	0.21	0.03	37.4	23.2320	240.4	201.40
570	23.20	3.0070	0.049170	1.48	0.20	37.3	8.9203	96.1	45.70
600	22.74	5.0130	0.054100	0.96	0.30	30.0	7.1607	77.6	35.80
650	28.45	0.4265	0.058210	1.69	0.60	38.9	11.2820	120.7	22.70
700	27.36	0.0000	0.051780	2.27	0.90	43.3	12.0510	128.7	21.80
750	32.70	1.6180	0.072010	2.18	1.20	34.8	11.5510	123.5	15.70
800	24.32	2.5100	0.047080	2.03	1.50	42.7	10.6200	113.9	17.40
850	21.93	5.0430	0.026000	5.97	2.40	66.2	14.6850	155.6	7.40
890	20.05	6.2360	0.011550	16.80	5.40	85.1	17.1900	180.9	2.00
930	18.88	4.4770	0.005271	51.40	13.30	93.5	17.7200	186.1	0.64
960	18.73	3.6220	0.003293	100.00	28.30	96.2	18.0830	189.8	0.69
990	18.51	3.4350	0.002558	133.00	48.30	97.3	18.0560	189.5	0.30
1020	18.24	3.4990	0.002284	104.00	64.30	97.7	17.8770	187.8	0.32
1050	18.23	3.6930	0.002611	57.00	72.40	97.2	17.7900	186.9	1.00
1100	18.33	3.7410	0.002484	166.00	97.40	97.5	17.9330	188.3	0.29
1150	19.03	3.4770	0.003362	19.60	99.40	95.9	18.3480	192.4	1.60
1250	28.04	3.9710	0.035040	5.65	99.60	63.8	18.0340	189.3	9.90
1300	61.17	4.0810	0.140600	1.17	100.00	32.1	19.9920	208.7	28.10

1) Corrected for mass discrimination, machine background, orifice discrimination, and blank.
2) Total Ar includes blank.
3) Error values are for analytical error only (quoted at 1 sigma level).

Tertiary in age (Foster, 1976). On the east, this unit is in contact with the Paleozoic greenstone unit (Foster, 1976). To the west, the pluton is in contact with and has presumably intruded metamorphic rocks of Paleozoic age. In general, igneous textures are preserved throughout the pluton, although some samples show alignment of mineral grains defining a foliation. These foliated samples may be restricted to border facies. The sample chosen for analysis is a quartz monzodiorite and shows some alignment of hornblende in thin-section. The mineralogy of this sample is hornblende (35%), K-feldspar (10%), plagioclase (45%) and quartz (10%). Accessory minerals include apatite and sphene, and the rock shows minor alteration to chlorite and epidote (Foster, 1978). The amphibole separate used for this analysis contained only minor quartz or feldspar composites. The size fraction used for analysis was -100 to +120 mesh.

The first two fractions of gas released from this sample gave anomalously high ages (773 and 240 Ma respectively) with errors of over 80%. This may be the result of inherited radiogenic ^{40}Ar and no significance is placed on these ages because of the large error and small fraction of gas analyzed. The age spectrum for this analysis (figure 40) shows the first two steps plotted yielded ages of 96 ± 46 and 78 ± 36 Ma, which suggest some gas loss about that time. The following four steps (5-8) gave very similar ages and suggest a small plateau at that time. An integrated age of 122 Ma was calculated for those four steps. These steps

were plotted on an isochron diagram (figure 41) and they plot very close to a line between atmospheric composition and the $^{39}Ar/^{40}Ar$ ratio corresponding to the plateau age. This is strong evidence for gas loss at that time. As a whole, these early gas fractions represent 0.15% of the total gas in the sample. The following steps (9 and 10) show a progressive increase in age towards the plateau. The integrated plateau age calculated for this sample is 188 ± 2 Ma and is based on 84% of the ^{39}Ar released. The steps representing the plateau (11-16) are plotted on the isochron diagram in figure 41 and due to their radiogenic nature, they cluster close to the x-intercept. The last three steps of the analysis yield slightly anomalous ages and plot off the plateau isochron in figure 43. The three steps form a distinct line with the x-intercept close to the $^{39}Ar/^{40}Ar$ ratio corresponding to the plateau age and a y-intercept considerably lower than atmospheric composition. This probably is the result of high temperature gas releases from sites with excess radiogenic ^{40}Ar.

Conventional K-Ar analysis of hornblende from this sample yielded an age of 177 ± 5 Ma (Report No.54, Menlo Park, 1969, by J.C. VonEssen).

Taylor Mountain Batholith

The Taylor Mountain batholith has been subject to considerable isotopic studies due to its accessibility and potential importance in the geologic history of the region.

As previously discussed, the batholith is the oldest relatively undeformed, unmetamorphosed intrusive in the region.

The first age date on this pluton was done by the Rb/Sr method on biotite and gave an age of 190 Ma (Wasserburg and others, 1963). The thermal history of the batholith is critical in interpreting the thermal history of the entire region, constraining the timing of major metamorphic events, and in understanding the tectonic development of the area.

The batholith is primarily composed of unfoliated granodiorite, but also contains minor quartz monzonite, quartz diorite, diorite and lamprophyre dikes (Foster and others, 1976). Locally, usually near the margins of the pluton, there is a weak to moderate foliation defined by the alignment of hornblende and biotite.

Hornblende, biotite, and potassium feldspar from the batholith were analyzed in this study. The samples were collected along the Taylor Highway in the Tanacross quadrangle by Dr. Helen Foster and the separates were obtained from her.

The hornblende separate was very pure with very minor epidote grains and -45 to +70 size fraction was used for analysis.

The first gas fraction from this sample yielded an anomalously high age of 331 ± 34 Ma, which is attributed to inherited radiogenic ^{40}Ar (figure 42). The following 10 steps (2 to 11) show a general progressive increase in age

FIGURES 42 & 43: Age spectrum and isochron plot: Sample 74ASj 113 (hornblende).

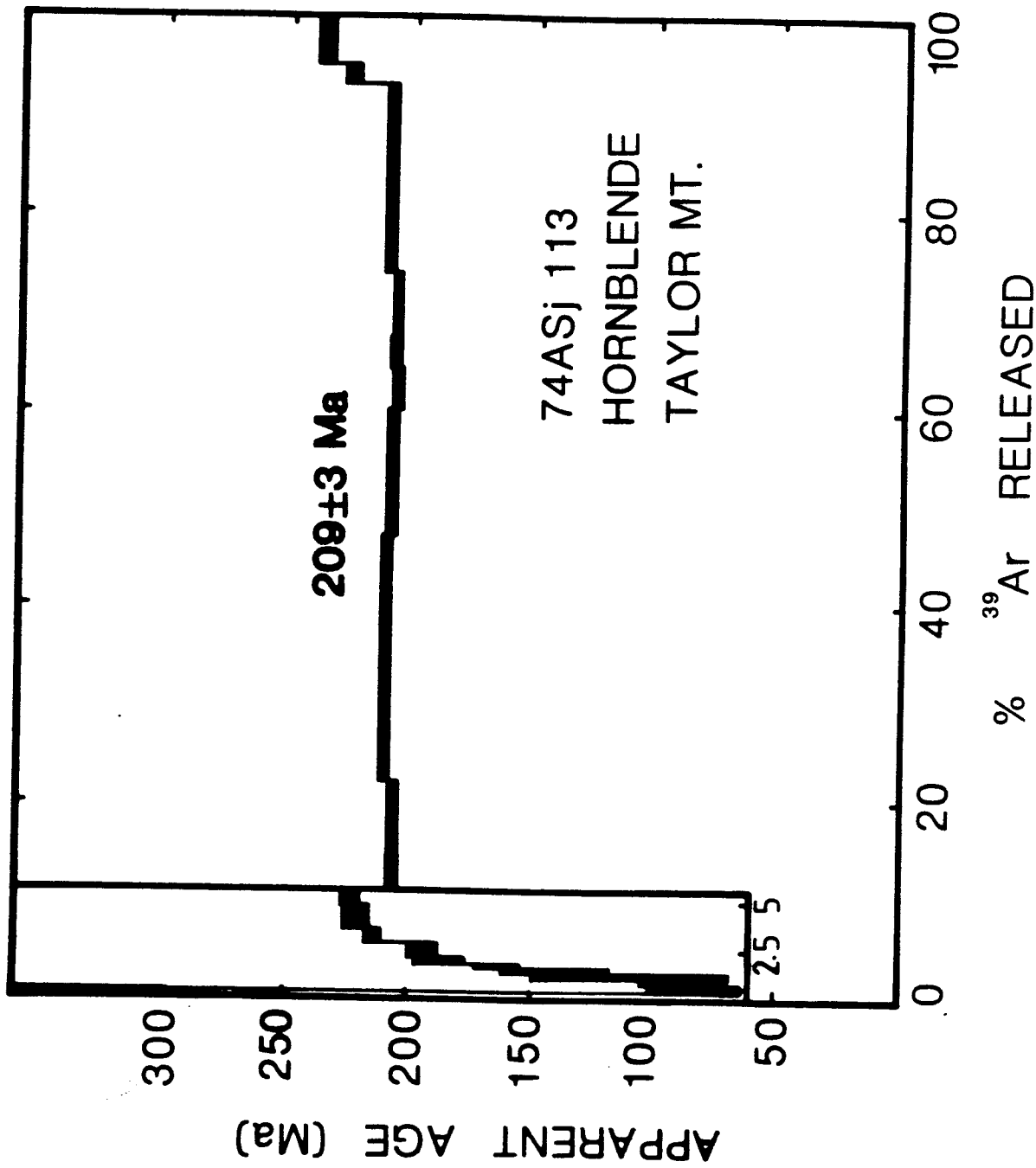
APPARENT AGE (Ma)
300
250
200
150
100
50
0
20
40
60
80
100
% ^{39}Ar RELEASED
209±3 Ma
74ASj 113
HORNBLENDE
TAYLOR MT.
2.5 5

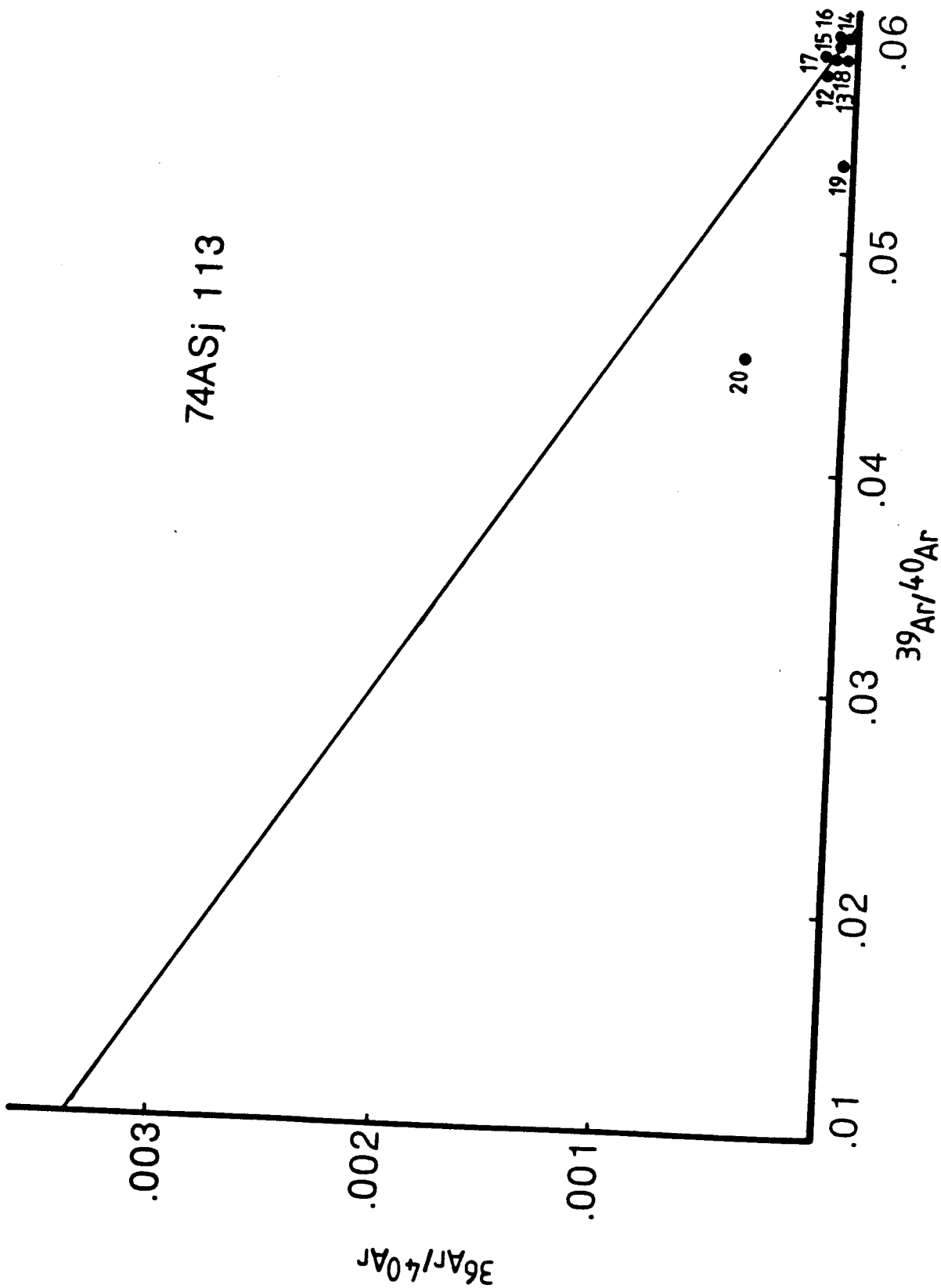
74ASj 113
.003
.002
.001
$^{36}Ar/^{40}Ar$
.01
.02
.03
.04
.05
.06
$^{39}Ar/^{40}Ar$
20
19
17
12
13
18
15
16
14

SAMPLE #: 74ASj113
MINERAL: Hornblende
J= .007295

TEMPERATURE (Degrees Centigrade)	(1) 40Ar/39Ar	(1) 37Ar/39Ar	(1) 36Ar/39Ar	39ArK x 10e-14 Moles	Cumulative 39Ar (%)	(2) 40Ar*/40Ar(t) (%)	40Ar*/39ArK	Apparent Age (Ma)	(3) Standard Dev. (Ma)
520	67.870	1.8350	0.1366000	1.390	0.3	39.0	27.6520	331.5	34.30
560	11.640	0.7198	0.0178100	1.570	0.7	45.1	6.4002	82.3	19.40
590	8.624	0.4594	0.0000000	0.892	0.9	67.1	8.7982	112.2	1.20
630	15.090	0.7524	0.0223000	1.130	1.2	45.8	8.5322	108.9	41.50
670	22.090	0.7150	0.0376300	1.270	1.4	43.5	10.9980	139.2	22.30
710	15.540	0.6972	0.0088570	1.180	1.7	68.4	12.9460	162.8	8.50
760	18.170	0.9703	0.0112300	1.820	2.1	73.1	14.9030	186.2	9.80
810	18.400	1.6060	0.0103900	2.730	2.8	77.7	15.4420	192.6	5.40
860	17.320	2.6030	0.0010460	2.730	3.4	91.5	17.2230	213.5	2.10
910	19.410	6.1820	0.0072210	6.120	4.8	88.5	17.8440	220.8	4.30
960	17.530	6.3060	0.0002107	2.980	5.5	95.2	18.0450	223.1	1.60
980	17.390	5.1220	0.0036400	71.000	21.9	95.8	16.7730	208.2	0.44
1000	17.100	5.1080	0.0021300	109.000	47.1	98.4	16.9310	210.1	0.27
1020	16.950	5.0640	0.0020870	56.900	60.2	98.3	16.7900	208.4	0.43
1040	16.920	5.3400	0.0027270	18.600	64.5	96.5	16.5920	206.1	1.00
1050	17.030	5.3180	0.0026400	12.500	67.4	96.0	16.7260	207.7	1.70
1070	17.220	5.4050	0.0036280	27.900	73.8	95.4	16.6340	206.6	1.40
1100	17.310	5.3990	0.0028820	82.000	92.7	97.2	16.9470	210.3	0.49
1150	18.360	5.0980	0.0017570	10.400	95.1	97.3	18.3040	226.1	1.90
1250	22.180	3.6830	0.0110500	21.000	100.0	85.8	19.2450	237.0	1.90

1) Corrected for mass discrimination, machine background, orifice discrimination, and blank.
2) Total Ar includes blank.
3) Error values are for analytical error only (quoted at 1 sigma level).

from 82 ± 19 Ma to 223 ± 3 Ma.

The third and fourth steps gave ages of 112 ± 2 Ma and 109 ± 42 Ma suggesting possible loss at about that time. These early gas fractions may be reflecting two thermal events separated in time, but this cannot be determined from the above data. As a whole, these early steps represent approximately 0.75% gas loss and do indicate some early thermal event.

The integrated plateau age for this sample is 209 ± 3 Ma and is based on 87% of the ^{39}Ar released. The steps representing the plateau (12 to 18) are plotted on the isochron diagram in figure 43, and due to their radiogenic nature, plot very close to the x-intercept. The last two steps gave high ages and plot off the plateau isochron, which is probably the result of high temperature gas releases from sites with inherited radiogenic ^{40}Ar.

The age spectrum for the biotite analyzed in this study is shown in figure 44. The first six steps in this spectrum show a progressive increase from 47 ± 3 Ma to 202 ± 2 Ma and represents approximately 2.6% gas loss. The lower intercept age of about 40 Ma is possibly an indication of an episodic thermal event at that time. The plateau age of 204 ± 9 Ma is based on steps 6 to 16, which correspond to 94% of the ^{39}Ar released. The steps on the plateau are plotted on an isochron diagram in figure 45, and they cluster near the x-axis due to their radiogenic nature. The plateau age for the biotite is about 4 Ma younger than the hornblende which is the result of different closure temperatures.

FIGURES 44 & 45: Age spectrum and isochron plot: Sample 74ASj 113 (biotite).

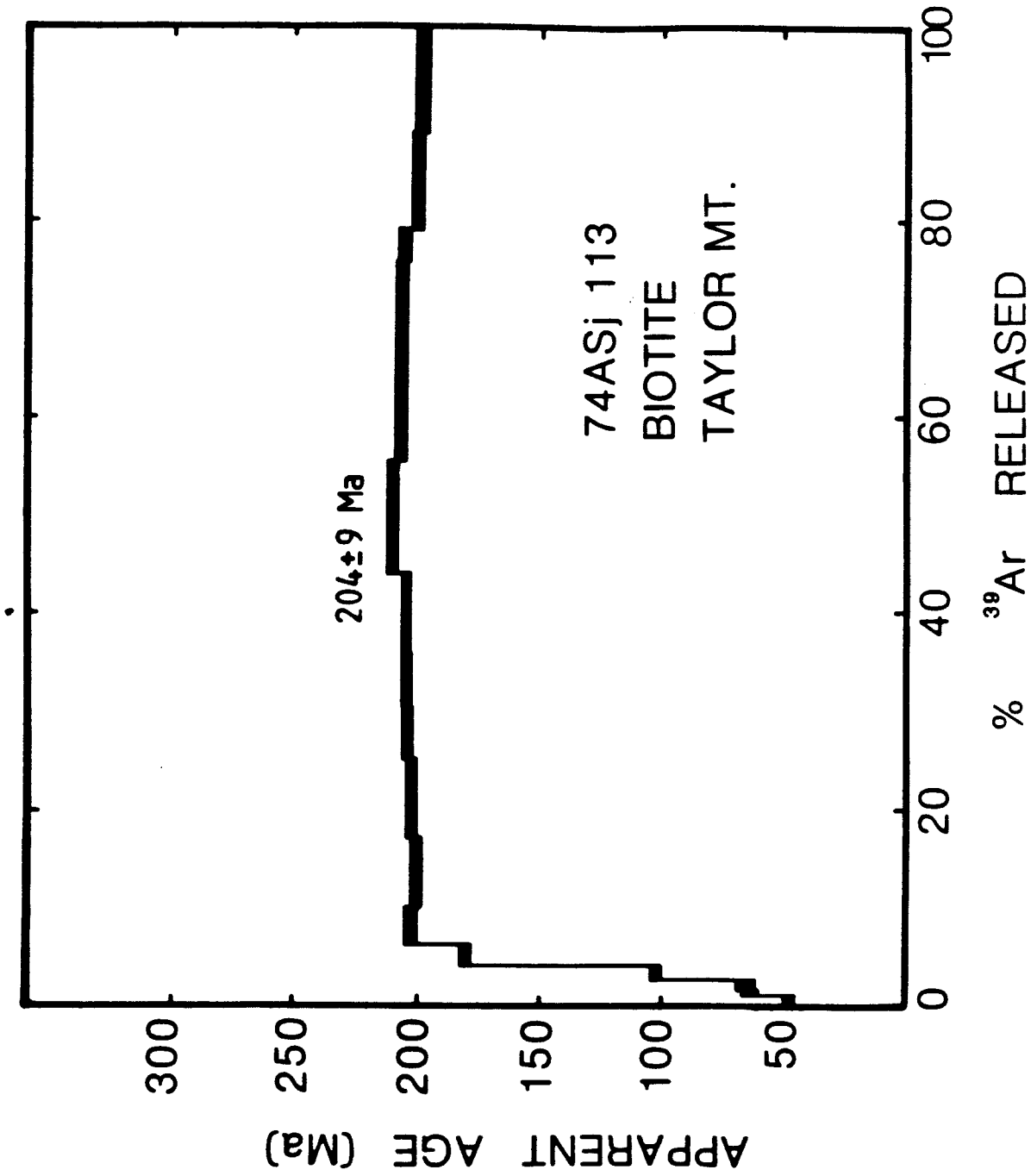
APPARENT AGE (Ma)
300
250
200
150
100
50
0
20
40
60
80
100
% ^{39}Ar RELEASED
74ASj 113
BIOTITE
TAYLOR MT.
204±9 Ma

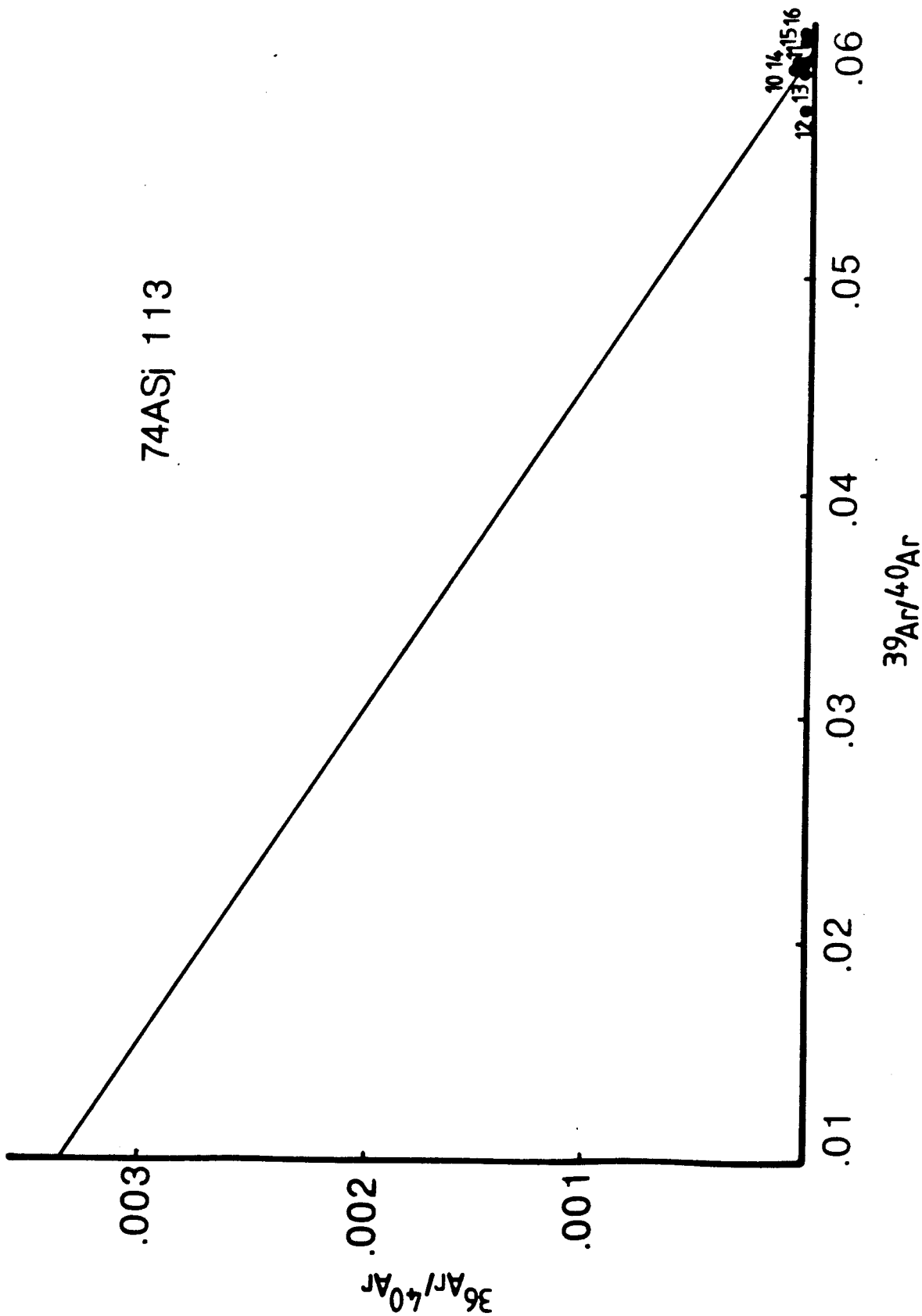
74ASj 113
.003
.002
.001
$^{36}Ar/^{40}Ar$
.01
.02
.03
.04
.05
.06
$^{39}Ar/^{40}Ar$
10
14
15
16
12
13

SAMPLE #: 74ASj113
MINERAL: Biotite
J= 007256

TEMPERATURE (Degrees Centigrade)	(1) 40Ar/39Ar	(1) 37Ar/39Ar	(1) 36Ar/39Ar	39ArK x 10e-14 Moles	Cumulative 39Ar (%)	(2) 40Ar*/40Ar(t) (%)	40Ar*/39ArK	Apparent Age (Ma)	(3) Standard Dev. (Ma)
480	20.780	0.120400	0.0577600	14.50	0.8	17.5	3.685	47.6	2.50
520	10.610	0.102100	0.0192900	7.73	1.2	43.9	4.882	62.8	3.40
550	8.193	0.081890	0.0102600	17.90	2.2	60.9	5.129	65.9	3.90
580	10.260	0.043730	0.0074250	28.80	3.8	77.2	8.035	102.2	1.80
620	16.750	0.024590	0.0076880	38.30	5.9	85.7	14.444	179.8	1.10
660	17.610	0.015970	0.0041660	74.50	10.0	92.5	16.340	202.1	0.46
700	16.960	0.011420	0.0024660	127.00	17.1	95.3	16.197	200.5	0.47
730	16.770	0.009687	0.0014400	139.00	24.8	97.1	16.311	201.8	0.27
760	16.890	0.010940	0.0013700	105.00	30.6	97.2	16.452	203.5	0.56
790	17.010	0.014220	0.0014830	96.30	35.9	97.0	16.537	204.4	0.38
840	16.920	0.013280	0.0010910	150.00	44.2	97.7	16.556	204.7	0.47
890	17.490	0.018370	0.0012500	206.00	55.6	97.5	17.085	210.8	0.64
940	17.110	0.014520	0.0008945	380.00	76.6	98.1	16.814	207.7	0.56
990	16.920	0.013390	0.0006246	43.60	79.1	98.2	16.700	206.3	0.80
1040	16.390	0.009994	0.0003319	184.00	89.3	99.0	16.257	201.2	1.20
1250	16.320	0.032540	0.0007759	194.00	100.0	98.3	16.053	198.8	0.37

1) Corrected for mass discrimination, machine background, orifice discrimination, and blank.
2) Total Ar includes blank.
3) Error values are for analytical error only (quoted at 1 sigma level).

The age spectrum of the potassium feldspar is illustrated in figure 46. The first two gas fractions yield high ages of 366 ± 64 Ma and 587 ± 10 Ma and are the result of inherited radiogenic ^{40}Ar. Steps one through seven show a progressive decrease in age and probably all contain some inherited radiogenic component. Steps seven through nineteen show a general increase in age from 172 ± 2 Ma to 189 ± 2 Ma and is interpreted to represent a slow cooling gradient through the temperature range of partial retention of radiogenic ^{40}Ar. The last two steps of the analysis yield an integrated plateau age of 189 ± 2 Ma, which represents 38% of the ^{39}Ar released. Although this is not a very well defined plateau, it is based on the largest gas fractions within analytical error. This plateau age is 16 Ma younger than the biotite age and is again attributed to the different closure temperatures for the two minerals.

FIGURES 46 & 47: Age spectrum and isochron plot: Sample 79AFr 2005 (potassium feldspar).

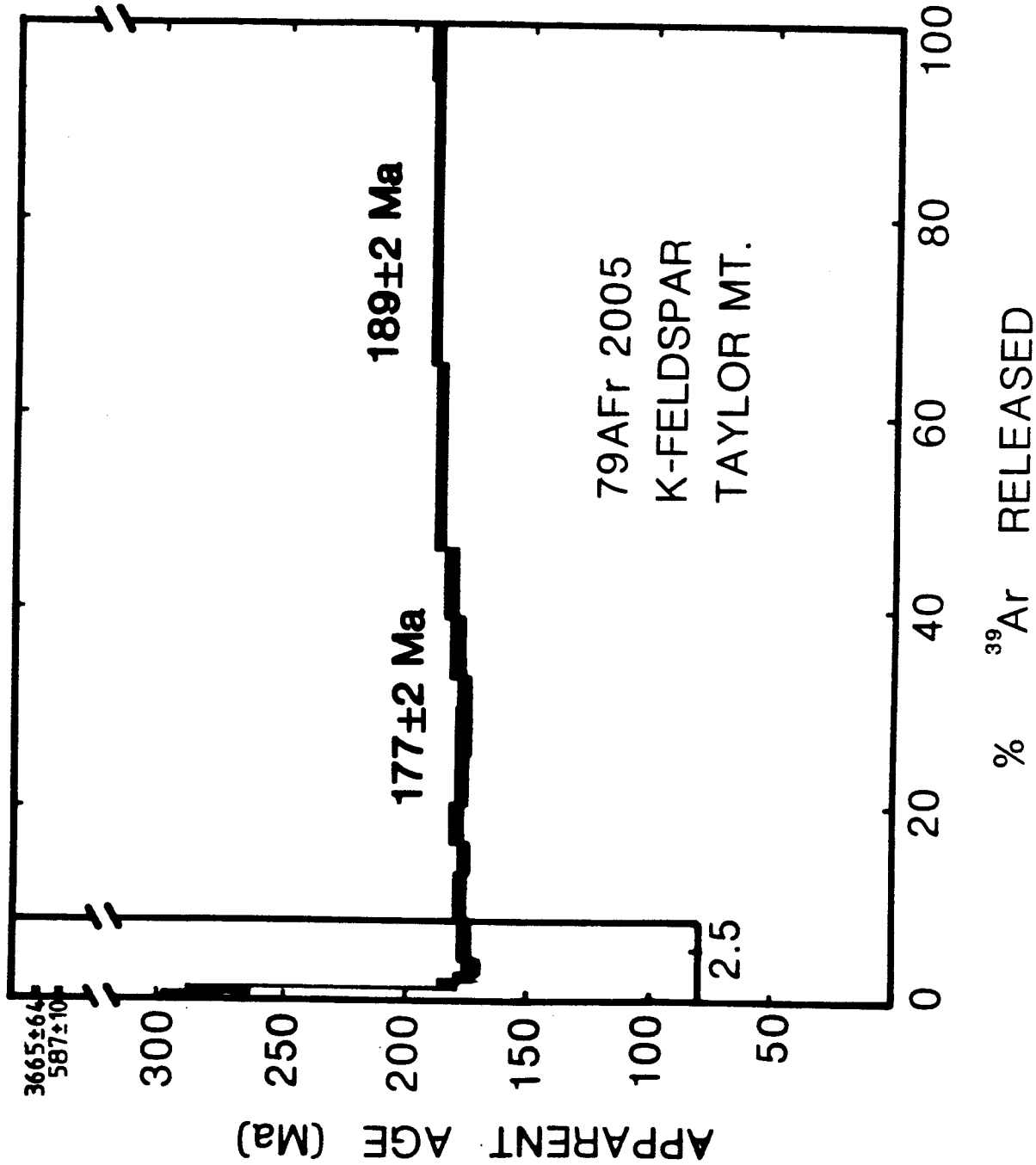
3665±64
587±10
300
250
200
150
100
50
APPARENT AGE (Ma)
189±2 Ma
177±2 Ma
2.5
79AFr 2005
K-FELDSPAR
TAYLOR MT.
0
20
40
60
80
100
% ^{39}Ar RELEASED

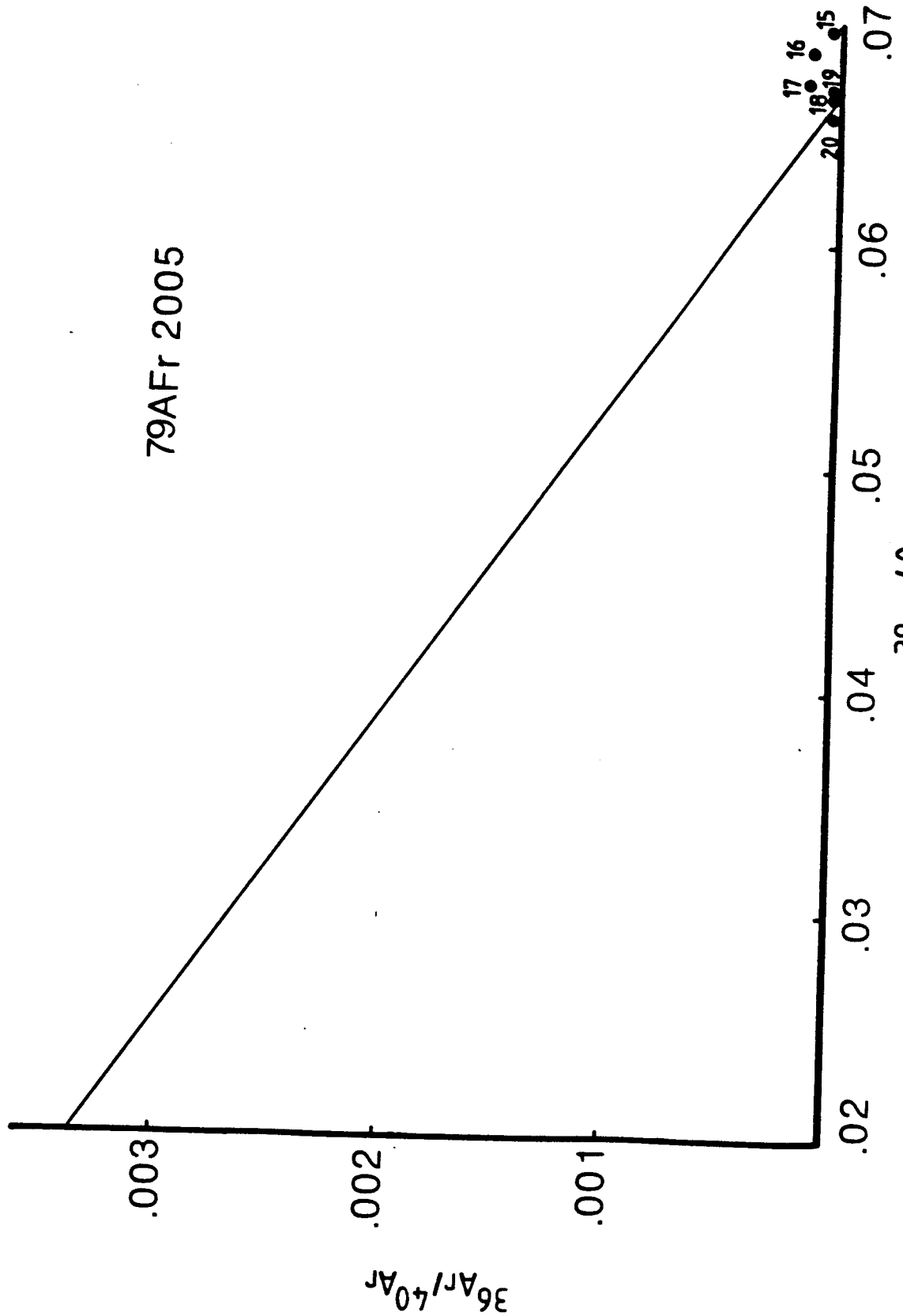
79AFr 2005
.003
.002
.001
$^{36}Ar/^{40}Ar$
.02
.03
.04
.05
.06
.07
$^{39}Ar/^{40}Ar$
15
16
17
18
19
20

SAMPLE #: 79AFr2005
MINERAL: K-Feldspar
J= .007344

TEMPERATURE (Degrees Centigrade)	(1) 40Ar/39Ar	(1) 37Ar/39Ar	(1) 36Ar/39Ar	39ArK x 10e-14 Moles	Cumulative 39Ar (%)	(2) 40Ar*/40Ar(t) (%)	40Ar*/39ArK	Apparent Age (Ma)	(3) Standard Dev. (Ma)
430	174.80	0.34620	0.4879000	0.606	0.03	16.9	30.673	366.5	63.70
470	80.27	0.13880	0.0944000	1.440	0.10	63.0	52.357	587.0	8.90
500	33.48	0.08912	0.0328000	1.510	0.20	65.8	23.762	290.2	8.20
540	28.06	0.07254	0.0184700	4.020	0.30	77.7	22.573	276.7	12.40
570	15.86	0.05236	0.0046650	7.070	0.70	88.0	14.449	181.9	2.60
600	14.81	0.04312	0.0028460	8.400	1.00	91.2	13.938	175.8	1.90
640	14.72	0.04879	0.0034270	23.300	2.10	91.8	13.672	172.6	1.60
680	14.45	0.04240	0.0016590	47.900	4.30	95.8	13.929	175.7	0.79
720	14.18	0.04365	0.0006399	76.600	7.70	98.1	13.961	176.1	0.45
760	14.25	0.05052	0.0004621	114.000	12.80	98.6	14.084	177.6	0.46
800	14.29	0.06240	0.0006378	66.700	15.80	98.0	14.065	177.3	0.62
840	14.28	0.06814	0.0002977	97.900	20.20	98.9	14.161	178.5	0.59
890	14.29	0.06096	0.0006093	102.000	24.80	98.2	14.074	177.4	0.34
940	14.26	0.03803	0.0007474	99.700	29.30	97.9	14.006	176.6	0.39
980	14.37	0.02935	0.0009264	91.100	33.40	97.5	14.059	177.3	0.37
1020	14.74	0.03480	0.0018380	121.000	38.90	95.9	14.160	178.5	0.47
1080	15.07	0.05407	0.0020740	168.000	46.40	95.6	14.426	181.7	0.30
1150	15.28	0.03828	0.0013140	407.000	64.70	97.1	14.859	186.9	0.96
1250	15.29	0.01136	0.0007270	657.000	94.30	98.2	15.043	189.0	0.32
1300	15.38	0.02297	0.0009620	127.000	100.00	97.7	15.056	189.2	0.50

1) Corrected for mass discrimination, machine background, orifice discrimination, and blank.
2) Total Ar includes blank.
3) Error values are for analytical error only (quoted at 1 sigma level).

CONCLUSIONS AND DISCUSSION

Structure

The structural elements of the three units studied suggest that there are significant similarities and differences in their structural histories. In this section, the structural elements of the biotite gneiss and amphibolite unit, the quartz-mica schist unit and the greenstone unit are briefly summarized and discussed.

1. Biotite Gneiss and Amphibolite Unit

It is evident that the biotite gneiss and amphibolite unit has been folded at least twice and, in places, a third fold generation is present. The least obvious fold generation is considered the oldest because it is defined by rarely observed fold closures axial planar to the prominent foliation. All later folds deform this foliation, and must therefore be relatively younger.

The most prominent folds observed in this unit have northeast-southwest trending axes, and are tight and asymmetric. These folds range considerably in amplitude and wavelength, and are the most obvious in outcrop and on a regional scale. These folds verge slightly to the southeast, and are probably formed by major northwest-southeast compressional stresses.

The youngest generation of folds are gentle to open folds, and they deform all other structures. Fold axis

lineations trend north-south, and an axial planar cleavage is rarely associated. This cleavage commonly fans the fold, and is therefore only rarely axial planar.

The occurrence of isolated, lensoid shaped marble blocks within portions of the biotite gneiss and amphibolite unit suggests at least some shearing was involved in their deformation. The origin of these blocks is not known, but possibilities include olistrostromal blocks, melange, or attenuated marble layers.

Due to the relatively homogenous and coherent nature of the surrounding rocks, the melange interpretation is least likely. To interpret between the remaining possibilities is difficult, and will not be attempted. The occurrence of these blocks does suggest the possibility of olistrostromal deposits, and their present shape suggests that shearing, at some time in their history, was an active deformation mechanism.

2. Quartz-Mica Schist Unit

The structural elements of the quartz-mica schist unit are, in part, different from those of the biotite gneiss and amphibolite unit.

The prominent foliation in this unit ranges from a schistosity to a phyllitic foliation. It is defined by chlorite and white mica in the schist, and primarily by graphitic concentrations in the phyllites.

There is no evident fold generation associated with the

development of this foliation. The first fold generation is defined by tight to isoclinal folds that deform the prominent foliation and range in wavelength and amplitude from a few millimeters to several meters. Associated fold axes and fold axis lineations trend approximately east-west. The second generation folds are open to gentle and deform all other structures. There is a rarely observed cleavage associated with this generation which generally fans the fold. The orientation of fold axes and associated cleavage is indistinguishable from the open fold generation observed in the biotite gneiss and amphibolite unit.

In the graphitic member of this unit, there are distinctive asymmetric, rootless folds (1-10 cm in wavelength and amplitude) defined by cream to white colored polycrystalline quartz. These folds are of the first generation described above, and are characteristic of the dark gray graphitic quartzite. These folded quartz bands commonly show, in a single outcrop, variable degrees of folding, from lens shaped structures to asymmetric sigmoids, to complex refold structures. In most cases, these structures are confined between distinct foliation planes (generally defined as a fracture cleavage or phyllitic foliation), although rarely, folded quartz bands are truncated at the foliation plane.

A possible origin and developmental history of these structures can be inferred from the regional analysis of these features. A progressive change in the character of these structures was observed along several traverses north

of the fault contact between this unit, and the biotite gneiss and amphibolite unit. Within portions of the graphitic quartzite member north of the fault contact with the gneiss unit, only rare cream-white quartz bands were observed. These generally appear as small sigmoids, slightly inclined to the subhorizontal foliation. These structures occur as quartz filled sigmoidal extension fractures, and are associated with asymmetric open folds. These sigmoids are only a few to 10 centimeters in length.

Such structures have been described by Ramsay (1967) and are interpreted to develop as a result of flexural slip along bedding or foliation planes. If a body of rock is flexed, individual planes can slip by each other and give rise to extensional domains within a particular layer. These structures, which in this study are quartz filled, could progressively deform with continued shearing along the foliation plane.

Several outcrops of this graphitic member were studied on a southerly traverse approaching the interpreted fault contact with the gneissic unit. The progressive change in the white quartz bands included more tightly folded sigmoids and an associated closely spaced cleavage in outcrop. This cleavage is parallel to the prominent foliation, except at fold hinges. More folds of the first generation (F_1 - tight, asymmetric), and an increase in cream to white polycrystalline quartz bands were observed. A variation in the degree that the quartz bands were folded could be

observed in a single outcrop.

Closer to the contact, the variation in folded quartz bands is particularly evident. Most all bands were tightly folded; many were defined as rootless isoclines, and in the most extreme case, "refolded" isoclines were observed (figure 48). The cleavage in outcrop was very closely spaced (0.5-3 cm) and small faults were observed with fault planes parallel to the above cleavage (figure 49). The folded quartz bands are commonly truncated by the cleavage.

Sense of shear indicators were also observed in the outcrops close to the fault. Asymmetric augen structures consisting of the tightly "refolded" quartz bands within the cleavage planes were evident, with tails of fine grained polycrystalline quartz material. A few examples were observed where the tightly folded quartz bands failed, yielding broken and displaced hard grains in a more ductile matrix (figure 50). In one outcrop of greenschist near the proposed fault, several rounded, asymmetric augen shaped blocks of greenstone, 20 to 40 centimeters across, were observed with tails of highly cleaved greenstone (plate 18).

Although such structures have not previously been suggested as sense of shear indicators, they are very similar in nature to some described by Simpson (1983). The indicators used by Simpson (1983), including the asymmetric augen structures and the broken, displaced grains, were primarily observed in granitic gneisses and mylonites. In this study, the augen structures and the broken grains consisted of tightly "refolded" polycrystalline quartz

FIGURE 48: Refolded isoclines defined by white quartz bands.

FIGURE 49: Small fault with fault plane parallel to cleavage.

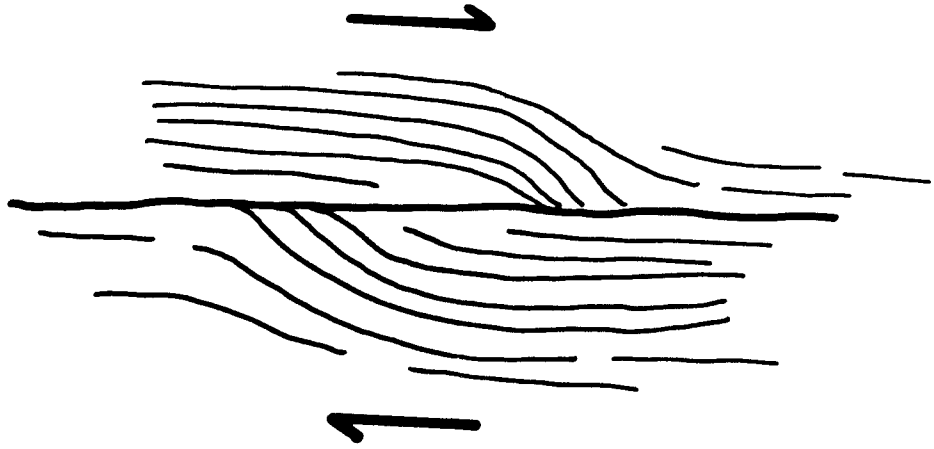

FIGURE 50: Broken and displaced hard grains in a ductile matrix.

FIGURE 51: Asymmetric augen shaped block in greenstone/greenschist.

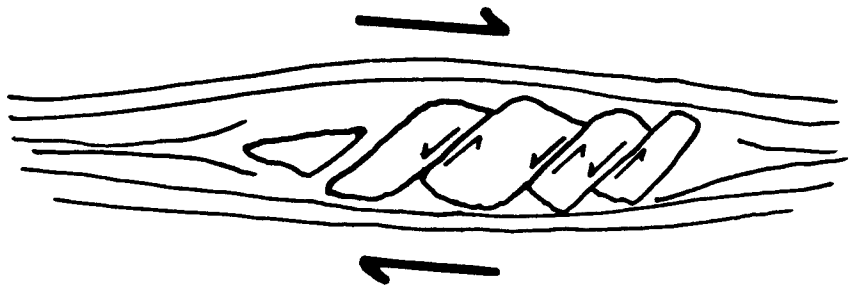

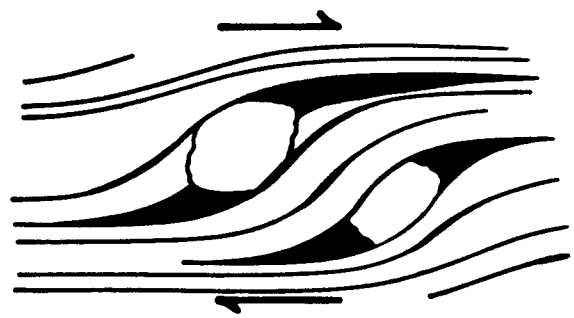

material and greenstone blocks of unknown origin in a highly cleaved matrix. The features therefore, are not identical to those described by Simpson (1983), but in general character, they are very similar.

In the cases where these structures were identifiable, the sense of shear indicated south side over north. This sense was also indicated by small faults within the same outcrop. One measured fault plane was N56°W 29°SW, and was subparallel to the fracture cleavage and the prominent foliation in this outcrop. Other evidence for this sense of movement was obtained from related faults along the Taylor Highway. These faults were previously described, and are discussed in the following section.

The accumulated evidence for the sense of displacement along major faults in this region and along minor faults in specific outcrops are consistent with the sense of shear indicators described above. The parallel to subparallel nature of the fracture cleavage, minor fault planes, and prominent foliation, in conjunction with the consistent sense of movement on these features, suggests a possible genetic relationship.

The folded quartz bands, the asymmetric augen structures, and the larger folds, were developed in a ductile environment. The broken and displaced grains in a ductile matrix suggest intermediate conditions within the brittle-ductile transition zone. The major and minor faults, and the parallel cleavage suggest development under

PLATE 18: Two photographs of asymmetric augen shaped block of greenstone in cleaved greenstone matrix.

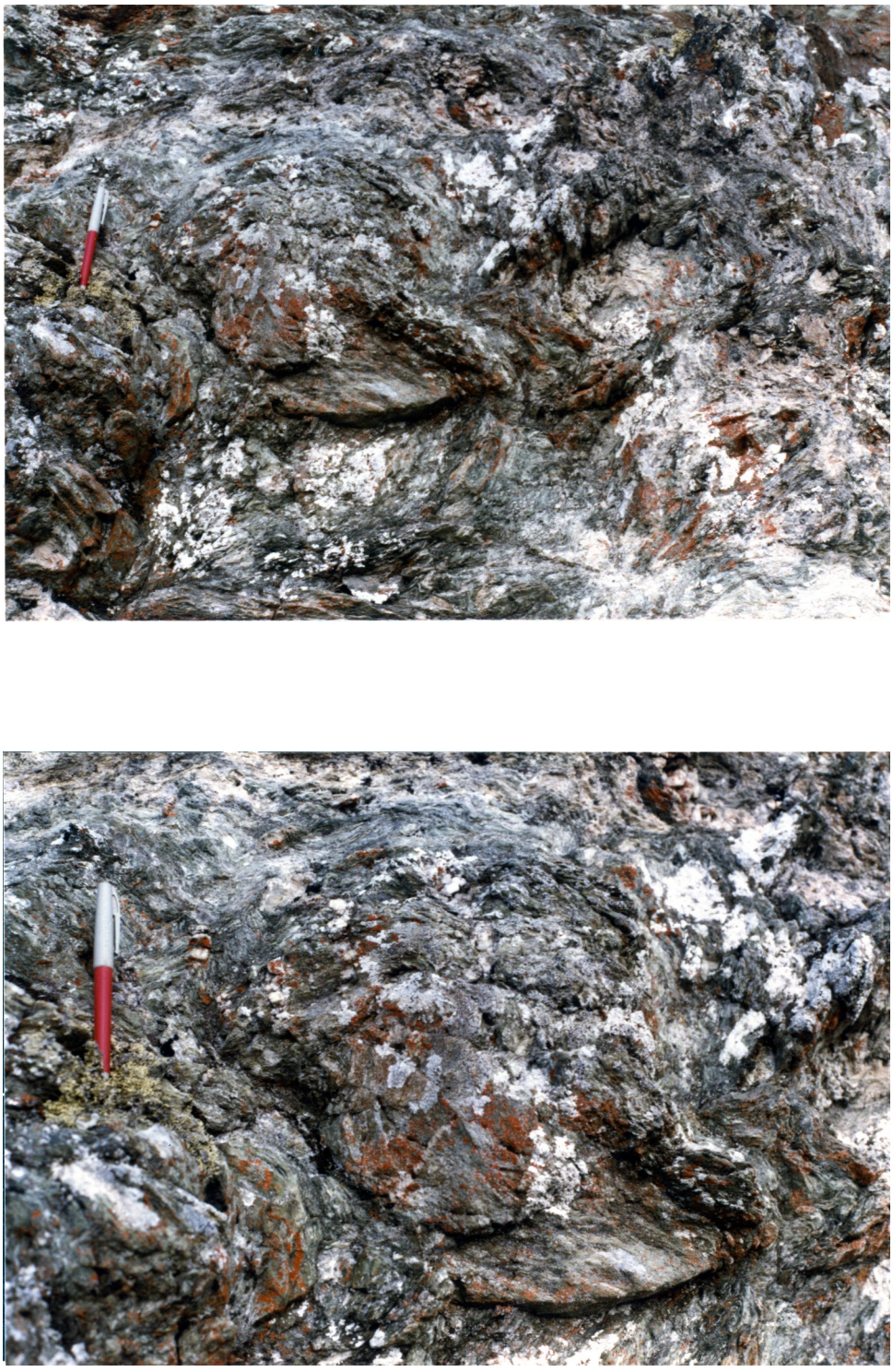

PLATE 18: Two photographs of asymmetric augen shaped block of greenstone in cleaved greenstone matrix.

brittle conditions. The coaxial nature (coaxial in the sense of coincident fold axes) of major folds (F_1), folded quartz bands, and "refolded" quartz bands again may suggest a possible genetic relationship between these structures.

The possible scenario may have involved north-south compression with associated north over south sense of shear. In ductile environments, folds of the first generation formed. In less ductile environments, flexural slip may have occurred, producing extensional quartz filled sigmoids. As thrusting and shearing continued, thrust loading would depress the lower plate into more ductile regimes, resulting in the ductile folding and "refolding" of sigmoidal quartz bands.

At high crustal levels and/or with increased strain rate, brittle failure could produce the observed faults. One such ductile to brittle field transition is recorded in a thin-section of graphitic quartzite obtained from the northern fault-melange zone. This sample was from a lensoid shaped block that was in a matrix of unconsolidated gauge. The thin-section showed a center to rim transition from elongated quartz grains with abundant fluxion structure, to angular, broken quartz grains.

Therefore, the deformational features discussed above could have developed in a single deformational event.

It is necessary to note that this model does not suggest an origin for the prominent foliation in this unit. Although such genetic relationships between specific structural elements are difficult to establish, the above

model is presented as a possible interpretation.

It is common in structural geology to relate specific structural elements to specific structural events. This is obviously due to the inherent inability of structural elements to contain absolute temporal information. This limitation has bred an episodic approach to the interpretation of structural elements.

The dynamic interpretation presented in this thesis is not only due to the fortuitous occurrence of a progressive development of strain markers, but is also suggested by isotopic evidence obtained from the gneiss unit.

Several samples obtained from the biotite gneiss and amphibolite unit and analyzed by the $^{40}Ar/^{39}Ar$ method indicate that major metamorphism, ductile folding, and faulting, occurred within this unit during a minimum and maximum time span of 2 and 12 Ma respectively. The faulting is present in the northern portion of the gneiss unit near the contact with the schist unit, and is most likely related to the tectonic juxtaposition of these groups of rocks. Therefore, by inference, the faulting and related structures in the graphitic member of the schist unit probably developed over the same period of time. This model can therefore explain, with a single structural event, the progressive development of specific structures in the schist unit, and the transition from ductile to brittle behavior.

To summarize the above interpretation, it is thought that a progression in the intensity of folded quartz

stringers in the schist unit approaching the fault zone between the gneiss and schist unit is evidence for increased shearing related to tectonic juxtaposition across the fault. Very close to the fault, within the schist unit, these quartz stringers can appear as refold structures within the same outcrop as less intensely folded quartz stringers. This is also interpreted as evidence for a progressive development of such structures.

These quartz structures, in the most extreme cases, form asymmetric augen structures and broken grains, interpreted to indicate sense of shear. Within the same outcrop, small faults are present, indicating the same sense of movement as the shear indicators. A fracture cleavage is also present, with the same orientation as identifiable fault planes.

This transition from ductile to brittle structures is interpreted to have developed under a single principle stress axis orientation and is related to the tectonic juxtaposition of these two units.

Isotopic data from the biotite gneiss and amphibolite unit suggest that a similar ductile to brittle transition occurred in this unit within the absolute time span of 204 Ma to 187 Ma, and was also related to the tectonic juxtaposition of these two units.

3. Greenstone Unit

The structural elements of the greenstone unit were not studied in significant detail, but several traverses were made across two portions of the unit, and some of the observations are worth summarizing and discussing. The two occurrences of greenstone that were studied include the body just north of Chicken and the body just north of the contact between the gneiss and schist unit (figure 10).

The northern body primarily consists of massive greenstone, with widely spaced joints (1 to several meters). Pillow structures are present in several outcrops and show some strain, although selvages and pillow boundaries are easily recognizable.

At two localities in this unit, a closely spaced fracture cleavage was observed, and seemed to progressively intensify near the contact with the country rock. A general gradation was observed from relatively massive greenstone to fissile, well cleaved greenstone near the contact with the country rock. Also observed near this greenstone-country rock contact is a lens shaped serpentinized ultramafic body over 100 meters across. This relationship can also be observed on the map to the west, where a significantly larger ultramafic body is present between the greenstone unit, and the country rock.

The occurrence of these ultramafic slices and the highly cleaved greenstone, suggests that the greenstone may be in fault contact with the underlying schist unit. It was

also observed that the contact between the schist and greenstone units is quite curved, suggesting a relatively flat lying contact.

The southern greenstone unit is also quite massive in general, with widely spaced joint surface. No pillow structures were observed in this unit, although associated sediments include chert, siltstone, a fine grained limestone. No highly cleaved greenstone was observed near the contact with the country rock. In the case of this southern greenstone body, the metamorphic country rock is amphibolite, and there is a clear metamorphic break observed at the contact. This suggests that this contact is a post-peak-metamorphic thrust fault.

4. Comparison of Biotite Gneiss and Amphibolite Unit To Quartz-Mica Schist Unit

It is clear from the previous discussion that there are both similarities and differences in the structural elements observed within the gneiss and schist units.

The gneiss unit has a well developed gneissic foliation, which is, in places, axial planar to isoclinally folded plagioclase bands. The most obvious fold generation varies considerably in wavelength and amplitude and is well defined by style and orientation. Fold axis orientations are well constrained, and plot in the northeast and southwest quadrants. This generation is generally upright to slightly inclined, and verges slightly to the southeast.

In contrast, the first generation folds of the quartz-mica schist unit are tight, inclinal to recumbent near the contact with the gneiss unit, and verge to the north. These folds tend to be more upright to the north farther from the contact with the gneiss unit. Fold axes trend west-northwest - east-southeast, and folds vary in wavelength and amplitude from less than a meter to a few meters.

These differences in orientation and style strongly indicate that these structures are not of the same generation.

The open fold generation that is observed to overprint all older structures in both units is interpreted as the same generation. Fold axes of this generation trend north-south and associated cleavage strikes approximately north-south and dips steeply. Plots of these structures from the two units are indistinguishable, and are therefore interpreted as postdating the juxtaposition of these two units.

5. Fault Zone

The three major fault zones previously described indicate that there are significant structural breaks between and within the biotite gneiss and amphibolite unit, and the quartz-mica schist unit. The character of these fault zones will be discussed in this section and their significance interpreted.

(a) Northern Fault Zone

The northern fault zone is characterized by a melange with coherent blocks of both the biotite gneiss and amphibolite unit, and the quartz-mica schist unit. Minor blocks of serpentinite and silica-carbonate rocks are present. The analysis of major zones of dislocation between blocks indicate that the fault planes strike east-southeast - west-northwest, and dip from about 40°-85°. Most fault planes dip to the south, although, in the southern portion of the zone, many fault planes dip to the north. The relatively steep dipping fault planes, at this exposure, indicate that this fault is high angle.

The along strike nature of the fault has been studied by Foster (personal communication), both to the east and west of this exposure. The fault zone itself is generally covered, but the contact between the two units displays a curved or irregular map pattern, suggesting a relatively shallow dipping fault plane.

Fold axis orientations measured on folds in most of the

blocks in the fault zone show similar orientations as the fold axes in the quartz-mica schist unit to the north. The fold axes measured within the fault zone were obtained from both gneiss and schist unit rocks. These folds commonly fold both the massive and the highly cleaved and fractured rocks, suggesting a genetic relationship between this generation of folding and faulting.

This same relationship was interpreted from the minor folds and faults within the schist unit just north of the fault. The genetic relationship between the regional scale fold generation and faulting in this area suggests that the faults developed in response to major compressional stresses.

The presence of minor serpentinite and silica-carbonate rocks within the fault zone suggests the involvement of ophiolitic material in the imbricated section.

Along other fault zones in this area, it was recognized that individual faults commonly steepen significantly (approaching vertical) near the top of the particular exposure. Integrating this with the other characteristics of the fault zone, it is interpreted that this exposure represents the upper portion of a thrust fault. No diagnostic thrust direction indicators were observed here, so no specific direction is interpreted.

(b) Central Fault Zone

The central fault zone is considerably more coherent than the other two fault zones. Specific fault planes are identified, and apparent offset can be determined.

The largest single fault within this zone has an apparent bend fold associated with it, and indicates south over north displacement. The fault plane in this situation varies form N30-85E strike, and has a south dip of 85° to 15°. This fault plane can be traced from near vertical where it has cut up section through the main foliation in the gneissic rocks to a gentle south dip parallel or subparallel to the same foliation.

It is understood that associated bend folds do not indicate a unique thrusting direction, but with the gently south dipping fault plane, the general south over north apparent offset direction is the best interpretation.

Other attempts to better define the thrusting direction were made by studying the orientation of minor folds near and within the fault zone. These data are plotted in figure 23, and include both fold axes in massive rock and fold axes in cleaved, unconsolidated fault related material. Also plotted on the same stereogram, are the set of 115 fold axes typical of the gneissic unit.

It is clear from this figure that fold axes in this zone have been reoriented out of the well defined maxima. It is interpreted that this is the result of the rotation of fold axes towards the thrusting direction.

Although very meager, fold axes in the cleaved, unconsolidated material show a similar scattered orientation. a sequence of fold axes in this unconsolidated material was observed starting from the hanging wall, and measured successively towards the center of the gauge or cleaved zone. These data are also plotted in figure 23, and numbered successively.

The interpretation of these folds is that the axis closest to the hanging wall is the youngest, and formed by compression perpendicular to the fold axis. The successive change in orientation away from the hanging wall represents the ductile reorientation of axes towards the thrusting direction.

Again, these data are extremely meager, but show a progressive reorientation towards the set of scattered points representing fold axis orientations in this fault zone. These scattered points plot in the southwest, west, and northwest quadrants. If fold axis number one (figure 23), which is in contact with the hanging wall, represents the normal to the thrusting direction, then the scatter of fold axes show a successive rotation towards that final direction. Based on this analysis, the thrusting direction for this particular fault is N64W.

The field relations at this fault zone are also used to suggest a general thrusting direction. Near the base of the exposed outcrop, there are several subhorizontal faults which juxtapose highly graphitic schist below gneissic rocks of the higher grade unit. These graphitic schists commonly

contain garnets, and they are therefore interpreted to be higher grade fault slices of the graphitic schist member. Garnetiferous graphitic schist was also found as imbricated slices in the northern fault zone.

In this central zone, these various rock types are juxtaposed across generally east-west striking fault planes with gentle south dips. With the occurrence of the graphitic rocks structurally below the gneissic rocks, and the regional occurrence of the graphitic member to the north and the gneissic rocks to the south, these relationships support the interpretation of northward thrusting.

(c) Southern Fault Zone

The southern fault zone is characterized by a complex melange zone. Large, (3-5 meters across), crystalline marble blocks are present and are set in a matrix of highly cleaved and fractured fault related material. Where the rock types are identifiable in the matrix, they generally consist of well foliated schists and gneisses, most probably derived from the higher grade unit. Also present are zones containing significant graphitic material, probably representing highly cleaved blocks of the graphitic member.

A relatively continuous outcrop exposure is present to the north and south of this fault zone. Therefore, a study of fold axis orientations within and away from the fault zone was undertaken for comparative purposes. The results of this study are plotted on a stereogram in figure 24.

Also plotted on this stereogram are the two maxima corresponding to the 115 fold axes typical of the gneissic unit. Fold axes within the cleaved matrix are differentiated from the fold axes measured on massive rock on either side of the fault zone.

It is evident that all the fold axes show a scattered pattern from the typical maxima (NE-SW quadrants) to the north-northwest and south-southeast quadrants. The pattern of points suggests a progressive counterclockwise reorientation towards the northwest-southeast quadrants. These reoriented folds axes were recognized most significantly within a few hundred meters of the fault zone, and did not show a simple progressive change. Typically, fold axes within a single exposure showed a variety of orientations.

These fold axes are interpreted to have been ductilely rotated towards the thrusting direction. Although no specific direction can be determined, the scatter of points suggests a maximum rotation to N50W. Such an interpretation does not yield information to differentiate between a northwest or southeast thrusting direction, but to be consistent with previous interpretation, a northwestern direction is preferred.

(d) Summary of Fault Zones

The three fault zones are interpreted to represent a related complex thrust zone that juxtaposes the higher grade biotite gneiss and amphibolite unit over the quartz-mica

schist unit. Field relations with gneissic rocks structurally above schistose and graphitic rocks along gently south dipping fault planes is used as evidence for a general northward to northwestward thrusting direction. Although fold axis data are meager for particular faults, the general agreement of the various analyses is significant and suggests a north to northwestward thrusting direction.

It should be noted that this study involves only a small portion of this fault zone. The larger scale view of the two juxtaposed units shows a very irregular map pattern involving local variations in the orientation of the thrust front. Local studies will possibly yield significantly different interpretations for the thrusting direction.

Thermal History - Geochronology

As previously outlined, the purpose for analyzing the thermal history of this region was to constrain accurately the timing of specific metamorphic, intrusive, and structural events. The age of major metamorphism has never been accurately constrained, due to a complex overprinting thermal history. In this study, the age of major metamorphism has been assessed by dating both the oldest unmetamorphosed pluton in the region and hornblendes from amphibolite facies metamorphic rocks. Overprinting thermal events are identified by early gas fractions and corresponding lower intercept ages. The timing of specific structural events is estimated from the age of a cross-cutting igneous dike and a fault related schist.

1. Major Metamorphism

The age of major metamorphism is best estimated from the plateau ages obtained from metamorphic hornblendes.

Sample 82AFr4039 was collected from an amphibolite approximately 300 meters from the contact with the Taylor Mountain batholith. Dikes or sills from the batholith have intruded the country rock, and are present within tens of meters of this sample. Heat flow calculations using minimum melt temperatures for the intrusive body (680° - 700°) suggest that this sample experienced temperatures well above 500°C following the intrusion of Taylor Mountain. The

plateau age therefore represents the cooling of the amphibolite and Taylor Mountain batholith following intrusion. The plateau age is 213 ± 2 Ma, and is interpreted to represent the cooling of the regional geotherm through approximately 500°C.

Due to the relatively undeformed nature of the batholith, the foliation in the amphibolite must predate the intrusion. Therefore, the peak of metamorphism, and the development of the prominent foliation predates the plateau age of 213 ± 2 Ma recorded in this sample.

Higher temperature steps above the plateau yield ages ranging from 215 Ma to 232 Ma, and generally plot off the isochron. This suggests that the Ar released in these steps represents a trapped component with non-atmospheric composition. The $^{37}Ar/^{39}Ar$ ratio does not change significantly for these steps, suggesting no correlation with Ca sites in the hornblende.

These higher temperature steps are not clearly understood, and therefore little geologic significance is assigned to these older ages. The possibility that these ages are significant cannot be ruled out, but more work is needed to understand them.

Sample 82AFr4033 was collected from an amphibolite along the Boundary road. This sample is several kilometers from any mapped intrusive body, although numerous small intrusives are within a ten kilometer radius. The intrusives that are present are interpreted to be Cretaceous

or Tertiary in age (Foster, personal communication). The early gas fractions in this analysis indicate no systematic gas loss due to a Cretaceous or Tertiary event, so that the plateau age of 194 ± 2 Ma most probably records the age of the cessation of major metamorphism in this area.

The last two steps of this analysis yield older ages of 204 Ma and 201 Ma respectively, and do not plot on the isochron. These higher temperature steps again suggest released gas with non-atmospheric compositions, but show no correlation with Ca sites due to the relatively consistent $^{37}Ar/^{39}Ar$ ratios. These older ages are therefore enigmatic, and are not used for significant geologic interpretation.

The two most reasonable interpretations are: (1) the high ages are the result of excess radiogenic ^{40}Ar released from high temperature sites, or, (2) the ages actually do represent the age of metamorphism preserved within the interior of the crystal.

The age and cooling history of the Taylor Mountain batholith has been determined from analyses of hornblende, biotite and K-feldspar. From these data, a time-temperature curve can be generated (figure 52) and indicates an average cooling rate of $10^{o}C\ Ma^{-1}$.

In the northern portion of the biotite gneiss and amphibolite unit, four samples were analyzed, and are used to constrain the age of major metamorphism in that area.

Sample 83AFr4072 is a hornblende collected from an amphibolite along the Forty-Mile River. As illustrated by the age spectrum, no well defined plateau is established.

FIGURE 52: Cooling history of Taylor Mountain Batholith.

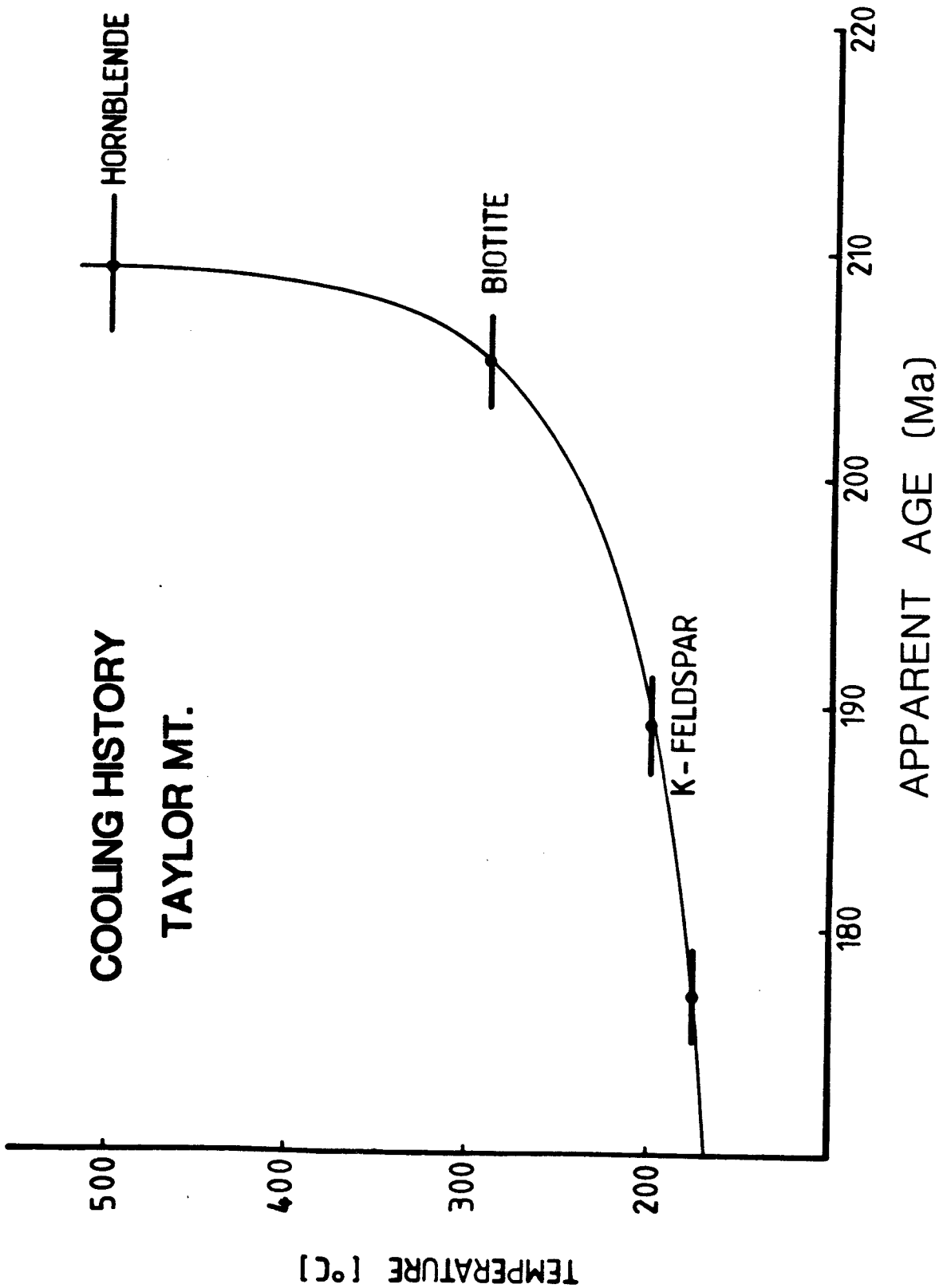
COOLING HISTORY
TAYLOR MT.
HORNBLENDE
BIOTITE
K-FELDSPAR
500
400
300
200
TEMPERATURE [°C]
180
190
200
210
220
APPARENT AGE (Ma)

The two largest steps within the same 95% confidence level represent only 28% of the ^{39}Ar released. The spectrum shows a general progressive rise in age from 169 Ma to 200 Ma, and most probably represents slow cooling following the younger thermal event. Since no plateau is established in this analysis, no specific age of metamorphism can be interpreted.

The older ages in the last several steps (194-200 Ma) may represent the closest estimates of the age of metamorphism. These high temperature gas releases do not plot on the isochron, and cannot be correlated with Ca sites due to the consistent $^{37}Ar/^{39}Ar$ ratio. Therefore, these steps may have released gas with non-atmospheric compositions, but cannot be unequivocally explained.

Despite the ambiguities of these high temperature releases, they are interpreted to most closely represent the age of major metamorphism, although they may only represent a minimum age.

Another hornblende sample, (83AFr4087) from an amphibolite along the Forty-Mile River was analyzed, and yielded a plateau age of 204 ± 4 Ma.

A biotite sample (83AFr4087) from the same outcrop yielded a plateau age of 187 ± 2 Ma. This sample was obtained from an actinolite schist within a fault zone. The mineral assemblage in the schist suggests stability in the greenschist facies. The plateau age therefore, is interpreted to represent regional cooling following the

amphibolite facies metamorphic event.

A lower limit on the age of metamorphism was obtained from a relatively undeformed, unmetamorphosed igneous dike. This dike (83AFr4045) was collected along the Taylor Highway north of the Forty-Mile River. Muscovite was analyzed, and yielded a very well-defined plateau age of 186 ± 2 Ma.

2. Overprinting Thermal Events

Overprinting thermal events are indicated by most of the samples by the apparent ages of the early gas releases. Lower intercept ages can be used as an approximation of the age of a particular event if a slow cooling gradient is observed in the age spectrum.

In this study, every sample except 82AFr4033 (Boundary Road) shows relatively young early gas fractions and a general progression to older apparent ages with higher temperature releases.

The lower intercept ages are shown on the individual age spectra in figure 54. As illustrated, these ages range from approximately 70 Ma to 125 Ma, but concentrate near 110 Ma. The sample from the intrusive at Mt. Veta shows a lower intercept at approximately 70 Ma and then five steps averaging 122 Ma before reaching a plateau age at 188 Ma. This sample is the westernmost sample analyzed and is close to numerous undated plutonic rocks. The lower intercept and the small plateau at 122 Ma may be significant reheating ages, but more dating is necessary to establish this.

The remaining samples all show lower intercepts in the range of 95 to 110 Ma. This range of ages is supported by K-Ar dates on igneous rocks in the Upland.

Wilson and others (in press) point out that igneous rocks yielding ages between 50 and 70 Ma are distributed throughout the Upland. They also point out that an igneous event is evident in the western portion of the upland between 85 Ma and 105 Ma.

It is therefore clear that the dated igneous events in the area correspond closely to the lower intercepts obtained in this study. It should be noted that the only K-Ar date on post-Jurassic igneous rocks in the Eagle quadrangle was obtained from a granodiorite in the northern portion of the quadrangle, and yielded ages of 89 Ma and 92.8 Ma on hornblende and biotite respectively (Foster, 1976).

An additional complication is suggested by Wilson and others (in press), who interpret a distinct metamorphic event between 100 Ma and 125 Ma, as evidenced by K-Ar dates on metamorphic rocks in the eastern portion of the study area. This interpretation cannot be critically evaluated in this study, but if such a metamorphic event did occur, it would have caused additional argon loss in the samples dated in this project.

The problem of multiple episodic loss has been studied in some detail by Harrison (1983), and he indicates that $^{40}Ar/^{39}Ar$ age spectra will not necessarily illustrate the complex thermal history of a sample that has undergone more

than one reheating event. Therefore, with the suggestion of possible episodic loss in this region, the lower intercept ages should be interpreted with care. The strong correlation between the K-Ar igneous ages (85 Ma to 105 Ma) and the lower intercept ages for many of the samples suggests a possible genetic relationship.

Other observations concerning reheating events suggest that the western portion of the study area has experienced the most significant gas loss, and the eastern portion has experienced the least gas loss. This is simply based on the estimates of gas loss in the individual samples. This conclusion is consistent with the observation that most of the post-Jurassic igneous rocks in the quadrangle are located in the western portion.

3. Timing of Structural Events

The timing of specific structural events was studied by analyzing samples with specific structural relationships.

As previously described sample 83AFr4045 was obtained from an aplitic dike along the Taylor Highway in the northern portion of the biotite gneiss and amphibolite unit. The dike is relatively unmetamorphosed and undeformed, and clearly cross cuts the prominent foliation it the country rock. The dike also crosscuts the major folds in this unit as evidenced by truncated fold axes and fold axis lineations. These folds are of the typical northeast-southwest trending generation that are the prominent folds

in this unit.

Muscovite from this dike yielded a plateau age of 186 ± 2 Ma and a lower intercept at approximately 95 Ma. This suggests that the dike was intruded just after the peak of metamorphism and may have resulted from partial melting of the country rock. The plateau age therefore helps constrain the age of this prominent fold generation to post-major metamorphism (204 Ma to 187 Ma) and pre - 186 ± 2 Ma. The age of the dike also confirms other data that indicate that the major metamorphic event had subsided by that time.

Sample 83AFr4087B is an actinolite + biotite schist that was collected from within a fault zone in the northern portion of the study area. The schist is present in a one to several meter wide zone of dislocation within massive amphibolite.

The boundaries of the fault zone are well defined by the truncation of the prominent foliation in the amphibolite, and the differently oriented schistosity in the schist. The schist has a well developed schistosity defined by the alignment of biotite and actinolite, which is parallel to subparallel to the fault boundary. Numerous rootless, asymmetric folds were observed in the schist, both in outcrop and in thin section, and are interpreted to have developed in response to movement along the fault.

Therefore, the age of faulting in this area is constrained between the age of major metamorphism (204 Ma to 187 Ma) and the age of this schist (187 ± 2 Ma).

Tectonics

It has been demonstrated in this study, that two distinct groups of rock, with differing structural and thermal histories have been juxtaposed along a major fault zone. These two terranes are interpreted to have been accreted to one another in Early Jurassic time. The field, structural, and thermal characteristics of this region associate several tectonic mechanisms with the accretionary process.

Mesoscopic structural analyses of the two terranes indiate that major fold generations can be closely associated with accretion. In the higher grade metamorphic terrane to the south, major northeast-southwest trending folds developed synchronously or just prior to accretion of the two terranes. These folds most likely resulted from southeast-northwest compression and/or associated shearing related to the collision of this terrane to the northern one.

In the northern terrane, it has been suggested that a major east-west trending fold generation is associated with thrust faults and related structures. These folds are similar in style and orientation to fault related folds in the northern fault zone. These folds become less tight and decrease in abundance away from major faults.

The two generations of folds, each unique to the individual terrane, are not similar in orientation or style. This may reflect a change in principal stress orientations

during the accretionary episode.

Major metamorphism of the southern block is clearly associated with convergence and final accretion of the two terranes. $^{40}Ar/^{39}Ar$ data from metamorphic rocks indicate that the closure of hornblendes (approximately 500°C) in the amphibolite facies rocks occurred between approximately 213 ± 2 Ma and 204 ± 2 Ma. This was closely followed by northward thrusting of the southern terrane as indicated by the age (187 ± 2 Ma) of the actinolite-biotite schist within the fault zone. Cooling of the amphibolite facies rocks occurred at an average rate of approximately $10^{o}C\ Ma^{-1}$ as estimated from $^{40}Ar/^{39}Ar$ data.

Thrust faults and related structures indicate a ductile to brittle transition during accretion. Minor structures within the northern unit, including refold structures and sense of shear indicators, signify that ductile deformation precluded faulting. A similar transition is indicated in the higher grade unit to the south. $^{40}Ar/^{39}Ar$ results indicates that faulting closely followed amphibolite facies metamorphism and ductile folding.

Thrust faulting involved ophiolitic material usually as blocks of ultramafic rocks and/or silica carbonate rocks in fault melanges or as blocks in metamorphic country rock. These ultramafic rocks occur within both the terranes, but are most common near the contact between the two. Ultramafic blocks are mapped (Foster, 1976) along the strike of fault zones identified in this study, suggesting a genetic relationship.

The next most common field association of ultramafic rocks is with the numerous greenstone units in the study area. They generally appear as small bodies in contact with larger greenstone bodies. Some of the greenstones are known to contain pillow structures and have associated sedimentary rocks. It has been suggested, based on structural and metamorphic data, that the greenstone bodies are in thrust contact with underlying metamorphic rocks.

$^{40}Ar/^{39}Ar$ data on igneous and metamorphic rocks in the Chicken area suggest a possible Jurassic age of metamorphism and thrusting of the greenstone unit in that area. The cooling history for the Taylor Mountain batholith suggests rapid cooling of the pluton through about 500°C at 209 ± 2 Ma. This is supported by the amphibolite analyzed near the pluton, (82AFr4039), which yielded a plateau age of 213 ± 2 Ma. The Chicken greenstone body is a similar distance from the Taylor Mountain batholith, as is the above mentioned amphibolite sample. Therefore, the greenstone would have experienced a similar thermal history if it were in its present position at the time the batholith was intruded. The age spectrum for the greenstone sample (82AFr4041) indicates it experienced a significant thermal pulse at 201 ± 5 Ma. The age spectrum also signifies a thermal pulse at approximately 110 Ma, which correlates with most of the other analyses in this region. The mineral assemblage of the greenstone indicates metamorphism to the greenschist facies (350-400°C).

These metamorphic, structural and isotopic data strongly suggest that the Chicken greenstone body was thrust into its present position after the regional geotherm cooled below approximately 500°C (209 ± 2 to 213 ± 2 Ma) and probably before the indicated thermal pulse at 201 ± 5 Ma. This later thermal pulse is most simply related to continued decay of the regional geotherm as indicated by the cooling history of the Taylor Mountain batholith and the range in plateau ages of metamorphic rocks in the region.

This inferred thrusting age closely correlates with the age of northward thrusting, estimated from $^{40}Ar/^{39}Ar$ data, of the southern terrane onto the northern lower grade rocks. The above field relationships and isotopic data strongly suggest that convergence and accretion in this region involved oceanic crust and associated mantle material.

The age of the ophiolitic material in this region is poorly known. $^{40}Ar/^{39}Ar$ data on the greenstone unit does not define an original igneous age. The Mt. Sorenson ophiolite complex to the north has associated Mississippian and Permian sediments and may be the best estimate of the age of oceanic crust and associated sediments in this region. The complex relationship between convergence and the emplacement of ophiolitic material precludes any specific interpretation as to the origin of individual ophiolitic blocks.

The tectonic model proposed for the evolution of this region involves the closing portion of the Wilson cycle. It is clear that major Early Jurassic accretion has taken place

in this region. Associated with this accretion is major metamorphism, the development of regional fold generations, plutonic activity, thrust faulting between and within individual tectonostratigraphic terranes, and probably the emplacement of allocthonous ophiolitic material.

The age of the ophiolitic material, although meager, suggests that an ocean basin of Mississippian to Permian age was closed in this convergent tectonic regime. Convergence culminated in the Late Triassic - Early Jurassic major metamorphism of the southern metamorphic terrane. The emplacement of the Taylor Mountain batholith was synchronous with, or closely followed major metamorphism as indicated by the cooling history of the intrusive and the metamorphic rocks. Accretion of the southern terrane onto the northern lower grade rocks occurred by Early Jurassic time.

The regional implications of this study suggest that Mesozoic convergence and terrane accretion was fundamental in the tectonic development of this portion of the Yukon-Tanana Upland. The origin of these terranes is enigmatic and the subject of considerable debate. Correlation of units across the international border suggests the northern rocks of this study are equivalent to the Nasena series in Canada. The Nasena series are interpreted as Paleozoic outer shelf sediments of the ancient continental margin of North America (Tempelman-Kluit, 1979). If this interpretation is correct, the Early Jurassic accretion of the southern terrane marks the beginning of terrane

accretion in this portion of Alaska.

REFERENCES

Albarede, F., 1978. The recovery of spacial isotope distributons from step-wise degassing data: Earth and Planetary Science Letters, V. 39, p. 387-397.

Aleinikoff, J.N., Dusel-Bacon, C., and Foster, H.L., 1981a. Geochronologic studies in the Yukon-Tanana Upland, east-central Alaska: Albert, N.R.D., and Hudson, T., editors, The United States Geological Survey in Alaska: Accomplishments during 1979: U.S. Geological Survey Circular 8234-B p. 34-37.

Aleinikoff, J.N., Dusel-Bacon, C., Foster, H.L., and Futa, K., 1981b. Proterozoic zircon from augen gneiss, Yukon-Tanana Upland, east-central Alaska: Geology, V. 9, p. 469-473.

Aleinikoff, J.N., Dusel-Bacon, C., and Foster, H.L., in press, Geochronology of orthoaugen gneiss and related rocks, Yukon-Tanana Terrane, east-central Alaska: Geological Society of America Bulletin.

Brabb, E.E., and Churkin, M., Jr., 1969. Geologic map of the Charley River quadrangle, east-central Alaska, scale 1:250,000, U.S. Geological Survey Miscellaneous Geological Investigations Map, I-573.

Chapman, R.M., Weber, F.R., and Taber, B., 1971. Preliminary geologic map of the Livengood quadrangle, Alaska: scale 1:250,000, U.S. Geological Survey Open-File Report, 71-66.

Churkin, M. Jr., Foster, H.L., Chapman, R.M., and Weber, F.R., 1982. Terranes and suture zones in east-central Alaska: Journal of Geophysical Research, V. 87,p. 3718-3729.

Churkin, M. Jr., Carter, C., and Trexler, J.H., Jr., 1980. Collision-deformed Paleozoic continental margin of Alaska-Foundation for microplate accretion: Geological Society of America Bulliten, V. 91, p. 649-654.

Coney, P.J., Jones, D.L., and Monger, J.W.H., 1980. Cordilleran suspect terranes: Nature, V. 288, p. 329-333.

Crank, J., 1975. The Mathematics of Diffusion: Oxford University Press, Oxford, p. 414.

Dadisman, S.V., 1980. Radiometric ages of rocks in south-central Alaska and western Yukon Territory: U.S. Geological Survey Open-File Report 80-183, scale 1:1,000,000, p. 82.

Dobson, M.H., 1984. Closure profiles in minerals. (Unpublished.)

Foster, H.L., 1969. Reconnaissance geology of the Eagle A-1 and A-2 quadrangles, Alaska: U.S. Geological Survey Bulletin 1271-G p. G1-G30.

Foster, H.L., 1970. Reconnaissance geologic map of the Tanacross quadrangle, Alaska: scale 1:250,000, U.S. Geological Survey Miscellaneous Geologic Investigations Map I-593.

Foster, H.L., Weber, F.R., Forbes, R.B., and Brabb, .E., 1973. Regional geology of the Yukon-Tanana Upland, Alaska, in Arctic Geology: American Association of Petroleum Geologists Memior 19, p. 388-395.

Foster, H.L., 1976, Geologic map of the Eagle quadrangle, Alaska: scale 1:250,000, U.S. Geological Survey Miscellaneous Geologic Investigations Map I-922.

Foster, H.L., Donato, M.M., and Yount, E.M., 1978. Petrografic and chemical data on Mesozoic granitic rocks of the Eagle quadrangle, Alaska: U.S. Geological Survey Open-File Report 78-253 p. 28.

Foster, H.L., Laird, J., Keith, T.E.C., Cushing, G.W., and Menzie, W.D., 1983. Preliminary geologic map of the Circle quadrangle, Alaska: scale 1:250,000, U.S. Geological Survey Open-File Report 83-170-A.

Gottfried, D., Jaffe, H.W., and Senfttle, F.E., 1959. Evaluation of the lead-alpha (Larson) method for determining ages of igneous rocks: U.S. Geological Survey Bulletin 1097-A, p. 1-63.

Hanson, G.N., Simmons, K.R., and Bence, A.E., 1975. $^{40}Ar/^{39}Ar$ age spectra for biotite, hornblende, and muscovite in a contact metamorphic zone: Geochimica Cosmochimica Acta, V. 39, p. 1269-1277.

Harrison, T.M., and McDougall, I., 1980. Investigations of an intrusive contact northwest Nelson, NZ., II Diffusion of radiogenic and excess 40Ar in hornblende from $^{40}Ar/^{39}Ar$ age spectra: Geochimica Cosmochimica Acta, V. 44, p. 2004-2020.

Harrison, T.M., and McDougall, I., 1981. Excess 40Ar in metamorphic rocks from Broken Hill, New South Wales: Implications for $^{40}Ar/^{39}Ar$ age spectra and the thermal history of the region: Earth and Planetary Science Letters, V. 55, p. 123-149.

Harrison, T.M., and McDougall, I., 1982. The thermal significance of potassium feldspar K-Ar ages inferred from $^{40}Ar/^{39}Ar$ age spectrum results: Geochimica Cosmochimica Acta, V. 46, p. 2513-2517.

Harrison, T.M., and Be, K., 1983. $^{40}Ar/^{39}Ar$ spectrum analysis of detrital microclines from the southern San Joaquin Basin, California: an approact to determining the thermal evolution of sedimentary basins: Earth and Planetary Science Letters, v. 64, p. 244-256.

Harrison, T.M., 1983. Some observations on the interpretation of $^{40}Ar/^{39}Ar$ age spectra: Isotope Geoscience, V. 1, p. 319-338.

Huneke, J,C., and Smith, S.P., 1976. The realities of recoil: 39Ar recoil out of small grains and anomalous patterns in $^{40}Ar/^{39}Ar$ dating: Proceedings-7th Lunar Science Conference, p. 1987-2008.

Jaffe, H.W., Gottfried, D., Waring,, C.L., and Worhting, H.W., 1959. Lead-alpha age determinations of accessory minerals of igneous rocks: U.S. Geological Survey Bulletin 1097-B, p. 65-148.

Jones, D.L., Silberling, N.J., Berg, H.C., and Plafker, G., 1981. Preliminary terrane map of Alaska: U.S. Geological Survey Open-File Map 81-792.

Keith, T.E.C., Foster, H.L., Foster, R.L., Post, E.V., and Lehmbeck, W.L., 1981. Geology of a alpine-type peridotite in the Mount Sorenson area, east-central Alaska: U.S. Geological Survey Professional Paper, 1170-A.

Matzko, J.J., Jaffe, H.W., and Waring, C.L., 1958. Lead-alpha age determinations of granitic rocks from Alaska: American Journal of Science, V. 256, p. 529-539.

Mertie, J.B., Jr., 1937. The Yukon-Tanana region, Alaska: U.S. Geological Survey Bulletin 872, p. 1-276.

Mitchell, J.G., 1968. The argon-^{40}/argon-^{39} method for potassium-argon age determinations: Geochimica Cosmochimica Acta, v. 32, p.781-790.

Miyashiro, A., 1973. Metamorphism and Metamorphic Belts. William Clowes and Sones, Ltd., London, pp. 492.

Payne, M.W., and Allison, C.W., 1981. Paleozoic continental-margin sedimentation in east-central Alaska: Geology, V. 9, p. 274-279.

Ramsay, J,G., 1967. Folding and Fracturing of rocks. McGraw-Hill, New York, pp. 568.

Simpson, C., and Schmid, S.M., 1983. Some criteria to deduce sense of movement in sheared rocks: Geological Society of America Bulletin, v.12, p. 95-108 .

Tempelman-Kluit, D.J., and Wanless, R.K., 1975. Potassium-argon age determinations of metamorphic and plutonic rocks in the Yukon-Crystalline Terrane: Canadian Journal of Earth Sciences, V. 12, p. 1895-1909.

Tempelman-Kluit, D.J., 1976. The Yukon Crystalline Terrane: Enigma in Canadian Cordillera: Geological society of America Bulletin, v. 87, p. 1343-1357.

Tempelman-Kluit, D.J., 1979. Transported cataclasite, ophiolite , and granodiorite in Yukon: Evidence of arc-continent collision: Geological Survey of Canada Paper, 79-14, p. 1-27.

Turner, G., Miller, J.A., and Grasty, R.L., 1966. The thermal history of the Bruderheim meteorite: Earth and Planetary Science Letters, V. 1, p. 155-157.

Turner, G., 1968. The distribution of potassium and argon in chondrites: in: L.H. Ahrens (editor), Origin and Distribution of Elements, V. 30, Pergamon, Oxford, p. 387-398.

Wasserburg, G.J., Eberlein, G.D., and Lanphere, M.A., 1963. Age of the Birch Creek Schist and some batholithic intrusions in Alaska: in Abstracts for 1962: Geological Society of America Special Paper 73, p. 258-259.

Weber, F.R., Foster, H.L., Keith, T.E.C., and Dusel-Bacon, C., 1978. Preliminary geologic map of the Big Delta quadrangle, Alaska: scale 1:250,000, U.S. Geological Survey Open-File Report, 78-529-A.

Wilson, F.H., Smith, J.G., and Shew, N., in press, Review of radiometric data from the Yukon-Crystalline Terrane, Alaska and Yukon Territory: Canadian Journal of Earth Sciences.

Wilson, J.T., 1968. Static or mobile earth: Proceedings of the American Philosophical Society, V. 112, p. 309-320.

APPENDICES

INTRODUCTION

The $^{40}Ar/^{39}Ar$ age spectrum technique is a variation of the conventional K-Ar dating method. The $^{40}Ar/^{39}Ar$ technique is based on the formation of ^{39}Ar by the irradiation of potassium bearing samples with fast neutrons in a nuclear reactor. The desired reaction, $^{39}_{19}K(n,p)^{39}_{18}Ar$ represents the transmutation of an atomic species (^{39}K) representative of the parent isotopes (^{40}K) to an isotope of the naturally occurring daughter product (^{39}Ar). This allows an age to be calculated simply from the isotopic ratios of argon.

The number of ^{39}Ar atoms formed in the sample by the neutron irradiation is represented by (Mitchell, 1968)

$$^{39}Ar = {}^{39}K \; \Delta T \int \Phi(\varepsilon)\,\sigma(\varepsilon)\,d\varepsilon \qquad (A1)$$

where ^{39}K is the number of atoms of this isotope in the irradiated sample, T is the length of irradiation, (Φ) is the neutron flux density at energy , (σ) is the capture cross section of ^{39}K for neutrons having energy (ε). The number of ^{40}Ar atoms present in a sample due to the decay of ^{40}K is represented by

$$^{40}Ar^{*} = \frac{\lambda_e}{\lambda} \; {}^{40}K \left(e^{\lambda t} - 1\right) \qquad (A2)$$

where e is the decay constants of ^{40}K for electron capture and is the total decay constant of ^{40}K.

The $^{40}Ar/^{39}Ar$ ratio of a given sample can be represented by combining the above two equations:

$$\frac{^{40}Ar^{*}}{^{39}Ar} = \frac{\lambda e}{\lambda} \frac{^{40}K}{^{39}K} \frac{1}{\Delta T} \frac{e^{\lambda t} - 1}{\int Q(\varepsilon)\sigma(\varepsilon)d\varepsilon} \quad \text{(A3)}$$

In this equation, the most difficult parameters to determine are the neutron flux density and the capture cross sections because the energy spectrum of the incident neutrons and the cross sections of ^{39}K for capture of neutrons of varying energies are not known. For these reasons, the parameter J is defined as follows:

$$J = \frac{\lambda}{\lambda e} \frac{^{39}K}{^{40}K} \Delta T \int Q(E)\sigma(\varepsilon)\, d\varepsilon \quad \text{(A4)}$$

and can be simply calculated from the $^{40}Ar^*/^{39}Ar$ ratio of a sample of known age that was irradiated with the unknown samples. With the known age of the monitor (t_m), J is calculated by substitution of A4 into A3 and rearranging giving:

$$J = \frac{e^{\lambda t_m} - 1}{^{40}Ar^*/^{39}Ar}$$

The parameter J can then be substituted into equation (1) and solved for t to yield the age of the sample:

$$t = \frac{1}{\lambda} \ln\left(\frac{^{40}Ar^*}{^{39}Ar} J + 1\right)$$

Irradiation

The desired nuclear reaction, $^{39}K(n,p)^{39}Ar$, requires fast neutrons to proceed, so the best irradiation conditions are those with high fast neutron flux relative to lower energy neutrons. In most reactors, the greatest fast/thermal flux ratio is present in the core. The two reactors used to irradiate samples in this study are the TRIGA reactor of the U.S. Geological Survey, in Denver, Colorado, and an experimental reactor at the University of Michigan. In both reactors, it was possible to use the core

facility for irradiation. For more information on the TRIGA reactor, see Dalrymple and others, (1980).

To determine or check correction factors for interfering isotopes produced by nuclear interactions during irradiation, CaF_2 and K_2SO_4 are included in the irradiation package. Measurements of the irradiated CaF_2 yield conversion factors for the two reactors:

TRIGA

$$(^{36}Ar/^{37}Ar)_{Ca} = .000264$$
$$(^{39}Ar/^{37}Ar)_{Ca} = .000673$$

MICHIGAN

$$(^{36}Ar/^{37}Ar)_{Ca} = .000286$$
$$(^{39}Ar/^{37}Ar)_{Ca} = .000751$$

Measurements of the irradiated K_2SO_4 yield conversion factors for the two reactors:

TRIGA

$$(^{40}Ar/^{39}Ar)_{K} = .005$$

MICHIGAN

$$(^{40}Ar/^{39}Ar)_{K} = .0382$$

These values were used to correct the measured isotopic

ratios before an age was calculated for an individual sample.

FLUX MONITOR

As previously described, to determine the age of an unknown sample it is necessary to include, with the irradiation package, a sample of known K-Ar age. It is best if the standard is of similar age to the unknown so that the $^{40}Ar/^{39}Ar$ ratios are similar. Ideally, it is also desireable to include a standard with a similar composition as the unknown and to ensure homogeneity of the standard, it should have an evenly-distributed ^{40}Ar concentration. In this study, the GA1550 biotite standard was used as a flux monitor for all the unknowns. This standard has been used at the Australian National University K-Ar laboratory by McDougall and Roksandic (1974) and has a uniform concentration of radiogenic ^{40}Ar (Tetley, 1978). This same standard has been successfully used as a flux monitor for biotite, muscovite, feldspar and hornblende samples.

Ar Extraction and Purification

The general method of extracting Ar from minerals has been described by many workers (e.g., Lanphere and Dalrymple, 1971). For the purposes of this study, the extraction and purification technique is described in general terms. The equipment used in this study is one of a kind, and has several features which make it, in certain

respects, the finest available. For specific design features, contact Dr. T. M. Harrison, State University of New York at Albany.

The sample to be analyzed is dropped into a previously outgassed, machined Mo crucible. The crucible is located in the center of a doubley shielded furnace with a high vacuum space (10^{-8} - 10^{-9} torr) between the interior and exterior portions of the furnace. The entire extraction line and sample portion of the furnace is also joined to a high vacuum pumping system which routinely reaches pressures lower than 5 x 10^{-8} torr. During extraction, gasses evolved are immobilized on an activated charcoal finger which is externally cooled with liquid N_2. When the 10 to 20 minute heating cycle is completed, the gas is allowed to interact with an ion pump which removes hydrogen from the system. The ion pump is then isolated from the system by a high vacuum valve. The liquid N_2 is removed from the finger to allow all the gas to interact with a Ti - Zr getter pump. This pump sorbs the remaining active gases (O_2, N_2, and remaining H_2) leaving the clean rare gasses for analysis in the mass spectrometer.

The background of Ar (blank) produced in this extraction system was checked several times during the period of research and was consistantly below 4 x 10^{-14}.

MASS SPECTROMETRY

Isotope analyses of Ar from samples were preformed using a mass spectrometer with a 60 degree sector and a radius of curvature of 11.4 cm (4.5 in). An electro- magnet fitted to the standard source-collector-flight tube assembly allows rapid peak hopping. An electrometer is used to detect the signal received from the Faraday cup and an automatic peak hopping device is used to focus the desired mass on the colector. The data acquisition system is fully automated and allows calculation of an age within minutes of an analysis. Data are reduced on an IBM pc.

MINERAL SEPARATIONS

Rock samples were crushed by jaw and roller crushers then sieved to various size fractions between 35 and 200 mesh. The crushed samples were then observed under a binocular, reflected light microscope in order to choose the size fractions most suitable for analysis. The coarsest grained sample, with euhedral grains and the least number of composites, was selected for the final steps of the separation proceedure.

The sample was then transfered to a 1000 ml beaker and washed, first with water, then with acetone. After drying, the powder was put into separation funnels containing methaline iodide (D=3.3). The heavy liquid was variably

diluted with acetone until the mineral of interest could be isolated from the other phases in the sample.

The Franz magnetic separator was used in conjunction with heavy liquids to complete the separation.

Each sample was hand picked under the reflected light microscope to obtain the purest sample possible.